MODELING FUTURE SEA LEVEL RISE FROM MELTING GLACIERS

A

THESIS

Presented to the Faculty

of the University of Alaska Fairbanks

in Partial Fulfillment of the Requirements

for the Degree of

DOCTOR OF PHILOSOPHY

By

Valentina Radić, M.S.

Fairbanks, Alaska

August 2008

MODELING FUTURE SEA LEVEL RISE FROM MELTING GLACIERS

By

Valentina Radić

RECOMMENDED: _____

_____

_____

_____

Advisory Committee Chair

_____

Chair, Department of Geology and Geophysics

APPROVED: _____

Dean, College of Natural Science and Mathematics

_____

Dean of the Graduate School

July 30, 2008

Date

Abstract

Melting mountain glaciers and ice caps (MG&IC) are the second largest contributor to rising sea level after thermal expansion of the oceans and are likely to remain the dominant glaciological contributor to rising sea level in the 21st century. The aim of this work is to project 21st century volume changes of all MG&IC and to provide systematic analysis of uncertainties originating from different sources in the calculation. I provide an ensemble of 21st century volume projections for all MG&IC from the World Glacier Inventory by modeling the surface mass balance coupled with volume-area-length scaling and forced with temperature and precipitation scenarios from four Global Climate Models (GCMs). By upscaling the volume projections through a regionally differentiated approach to all MG&IC outside Greenland and Antarctica (514,380 km^2) I estimated total volume loss for the time period 2001-2100 to range from 0.039 to 0.150 m sea level equivalent. While three GCMs agree that Alaskan glaciers are the main contributors to the projected sea level rise, one GCM projected the largest total volume loss mainly due to Arctic MG&IC. The uncertainties in the projections are addressed by a series of sensitivity tests applied in the methodology for assessment of global volume changes and on individual case studies for particular glaciers. Special emphasis is put on the uncertainties in volume-area scaling. For both, individual and global assessments of volume changes, the choice of GCM forcing glacier models is shown to be the largest source of quantified uncertainties in the projections. Another major source of uncertainty is the temperature forcing in the mass balance model depending on the quality of climate reanalysis products (ERA-40) in order to simulate the local temperatures on a mountain glacier or ice cap. Other uncertainties in the methods are associated with volume-area-length scaling as a tool for deriving glacier initial volumes and glacier geometry changes in the volume projections. Nevertheless, the lack of more detailed knowledge of global ice volume constrains the estimates of the potential and projected sea level rise from melting MG&IC. Any progress in this field is limited without a more complete glacier inventory database.

Table of Contents

Page

Signature page i
Title Page ii
Abstract iii
Table of Contents iv
List of Figures viii
List of Tables x
List of Appendices xi
Acknowledgements xii

Chapter 1: Introduction 1
1.1 Sea level rise – a review 1
1.2 Cryospheric contributions to sea level rise 7
1.2.1 Contribution to sea level rise from the Greenland and Antarctic ice sheets 8
1.2.2 Contribution to sea level rise from mountain glaciers and ice caps 10
1.3 Thesis objectives 19
1.4 References 21

Chapter 2: Projections of 21st century sea level rise from the melt of mountain glaciers and ice caps 29
2.1 Abstract 29
2.2 Introduction 29
2.3 Data and Methods 32
2.3.1 Glacier data 33
2.3.2 Climate data 35
2.3.3 Mass balance model 36
2.3.4 Modeling mass balance for 1961-1990 38
2.3.5 Modeling future volume changes of glaciers and ice caps 45
2.4 Results and Discussion 51
2.4.1 Volume projections for MG&IC from WGI 51
2.4.2 Regional and global volume projection for 2001-2100 53

Page

2.4.3 Uncertainties 56
2.5 Conclusions 60
2.6 References 62
Appendix 2.A 66

Chapter 3: Modeling future glacier mass balance and volume changes using ERA40-reanalysis and climate models – A sensitivity study at Storglaciären, Sweden 73
3.1 Abstract 73
3.2 Introduction 74
3.3 Study site 75
3.4 Data 76
3.4.1 Mass balance of Storglaciären 76
3.4.2 Meteorological observations 76
3.4.3 Reanalysis data: ERA-40 77
3.4.4 Regional climate model: RCA3 78
3.4.5 General circulation models 79
3.5 Methods 79
3.5.1 Validation of temperature and precipitation from ERA-40 80
3.5.2 Mass balance model 81
3.5.3 Future runs of mass balance model 82
3.6 Results and discussion 88
3.6.1 Validation of ERA-40 temperature 88
3.6.2 Validation of ERA-40 precipitation 88
3.6.3 Calibration of the mass balance model 90
3.6.4 Mass balance and volume projections until 2100 92
3.6 Conclusions 98
3.7 References 100

Chapter 4: Volume-area scaling vs flowline modelling in glacier volume projections 104

Page

4.1 Abstract 104
4.2 Introduction 104
4.3 Theory of volume-area scaling 106
4.4 Methods 107
4.4.1 The flowline model 107
4.4.2 Set of synthetic steady-state glaciers 108
4.4.3 Model-derived volume-area relationships 109
4.4.4 Volume projections using volume-area scaling 110
4.5 Results and discussion 112
4.5.1 Volume-area relationship in steady state 112
4.5.2 Volume-area relationship in non-steady state 112
4.5.3 Volume evolutions: sensitivity experiments 114
4.6 Conclusions 119
4.7 References 119

Chapter 5: Analysis of scaling methods in deriving future volume evolutions of valley glaciers 122
5.1 Abstract 122
5.2 Introduction 122
5.3 Methods 124
5.3.1 Investigated glaciers and data 125
5.3.2 Volume evolutions from the ice-flow model 126
5.3.3 Volume evolutions from the scaling methods 132
5.3.4 Sensitivity experiments 137
5.4 Results and discussion 138
5.4.1 Scaling methods 138
5.4.2 Sensitivity to scaling exponents 141
5.4.3 Sensitivity to scaling constants 142
5.4.4 Mass balance/thickness feedback 144
5.5 Conclusions 146
5.6 References 147

Page

Chapter 6: Conclusions **151**

6.1 References 154

List of Figures

Page

2.1 Flow chart of the methodology 33
2.2 Mask of grid-based glacierized area on 1°×1° resolution. 34
2.3 Example for area-altitude distribution 42
2.4 Grid-based (1°×1°) modeled mean specific mass balance for 1961-1990 44
2.5 (a) Size distribution of MG&IC from WGI 45
2.6 Upscaling (a) number of MG&IC, (b) glacierized area, (c) glacierized volume and (d) volume changes 49
2.7 Histogram of regional volume changes for 1961-1990. 50
2.8 21st century volume projections 52
2.9 Projections of annual (a) mean temperature and (b) precipitation from four GCMs. 53
2.10 Projected volume changes and their sea level contribution for 2001-2100 54
2.11 Total volume change in SLE for 16 regions for 21st century 55
2.12 Histogram of root mean square (RMS) errors between the modeled and observed mean specific winter, summer and annual mass balance 57

3.1 Study area including the meteorological stations. 77
3.2 Temperature seasonal cycles averaged over 1961-2001 from ERA-40 and six GCMs. 84
3.3 Monthly sums of precipitation from ERA-40 reanalysis and Ritsem. 84
3.4 Annual time series of (a) temperature and (b) precipitation, derived from downscaling RCA3. 85
3.5 Daily air temperatures averaged over the period 1965-2001 from ERA-40 and Tarfala 89
3.6 Monthly lapse rates derived from ERA-40 and Tarfala station temperatures. 89
3.7 Measured and modeled (a) summer mass balance, b_s, (b) winter mass balance, b_w, and (c) net mass balance, b_n 92
3.8 Volume projections for Storglaciären in the 21st century 93

Page

3.9 Volume projections for Storglaciären in the 21st century, derived from method VII of the mass balance model. 96
3.10 Running 20-year relative changes of (a) net mass balance, *db*, (b) air temperature, *dT*, and (c) precipitation, *dP*. 97
3.11 Static mass balance sensitivity due to (a) temperature change, *db/dT*, and (b) precipitation change, *db/dP* 98

4.1 Mass balance profile 109
4.2 Log-log plot of volume *V* vs area *A* for 37 synthetic glaciers in steady state 112
4.3 Surface area evolution derived from the flowline model 113
4.4 Log-log plot of volume vs area for 24 volume (area) evolutions 114
4.5 Normalized volume evolutions of the largest test glacier 116
4.6 Evolution of area-averaged mass balance (a, c) and normalized glacier volume (b, d) derived from the flowline model and from the scaling methods 118

5.1 Contour maps of the investigated glaciers based on topographic maps 125
5.2 Reference mass balance profiles 130
5.3 Results of the dynamic calibration for four glaciers 131
5.4 Observed (solid line) and modeled (dashed line) surface elevations and bed along the flowline. 132
5.5 Modeled area-elevation distribution 136
5.6 Future volume evolutions (normalized by initial volume at t=0) for six glaciers 139
5.7 Same as Figure 5.6 except that absolute volumes are shown 143
5.8 Same as Figure 5.7 except that volumes are normalized 144

List of Tables

Page

1.1 Estimates of the various contributions to the global sea level rise for 1961-2003 and 1993-2003. 6

1.2 Estimates of recent changes (losses) in global glacier volumes 13

2.1 GCMs whose temperature and precipitation scenarios are used to force the mass balance model 35

2.2 Mass balance model parameters 40

2.3 Total glacierized area, modeled mean specific mass balance for 1961-1990 44

2.4 Regional glacier volume changes for 1961-1990 51

2.5 Projected total volume change in SLE for 2001-2100, for MG&IC from WGI 53

2.6 Total volume changes in SLE for 2001-2100 for 16 regions and all four GCMs 55

2.7 Mean specific mass balance for 1961-1990 derived from the 'reference' parameter set of the mass balance model and three sensitivity tests 58

2.8 Total volume change over 2001-2100 in SLE for six different cases of upscaling 60

2.A-1 44 glaciers with observed seasonal mass balance profiles ($\geq$ 4 years), location, and observational period of mass balance profiles. 66

2.A-2 Total volume change over 1961-1990 in SLE for five different cases of upscaling 70

2.A-3 Volume change in SLE over 2001-2100 for MG&IC from WGI (ΔV_{WGI}) and total volume changes from five different cases of upscaling 71

3.1 Gridded climate data sets 79

3.2 Explained variance (r^2) between the measured summer mass balances, b_s and positive degree-day sums, $\Sigma a_i T_i$ 91

3.3 Annual, winter (DJF) and summer (JJA) trends in the climate models for the grid point nearest to Storglaciären 95

5.1 Observational time periods used in the flowline model for the six glaciers 129

Page

5.2 Differences between 100-year volume changes projected from the flowline model and those obtained from the scaling method 145

List of Appendices

Appendix 2.A 66

Acknowledgements

I believe I am one of a few who can share the experience, or should I say privilege, of starting a PhD program at one continent and completing it at another. I had the enriching experience of living in two different cultures with two different styles of lives in just four years. None of this would have been possible without one truly amazing person who is to be 'blamed' for opening the door into the world of science. This person is *Regine Hock*, my supervisor, who will probably never forget my first 'discovery' in glaciology when I proudly revealed "Regine, glaciers move!" *Regine*, thank you for recognizing and believing in my potential (despite that revelation) and for motivating me from the very beginning with all your shared knowledge, amazing enthusiasm and support. Most of all, thank you for teaching me the rules of the game that scientists play.

I thank all the personnel at INK, Stockholm University, with whom I have worked during the first three years, to the administrative and technical staff whose help was offered at any time, and to my fellow graduate students for their friendship. In particular: *Mattias de Woul*, for welcoming me as a member of the team, for many insights into Swedish society, and for the occasions when you were a true 'non-Swede' (considered a Swedish compliment). *Mark Dyurgerov*, for your amazing ability to put things into broad perspective, no matter how complex they look on a small scale. It has been a pleasure having you in our glaciology team! *John Hulth*, for all the problems in statistics that kept my neurons alerted. *Tim Johnsen*, for all the laughs and the attempts to pronounce Swedish words properly. Tack så mycket! *Steffen Holzkämper*, for being the best neighbor in the corridor. *Hernán De Angelis*, for our long discussions ending with attempts to discover the meaning of life while practicing Argentinean and Croatian traditions of indulging ourselves in a good wine after dinner.

I thank my co-supervisor *Johannes Oerlemans* for all the enlightened discussions, advice, and insight into glacier dynamics during my visits to Utrecht University. I am also thankful to all personnel of the Ice and Climate group at Utrecht University who welcomed me and made me feel as a full member of their academic group. Particularly, I am grateful to *Carleen Tijm-Reijmer, Wouter Greuell, Roderik van de Wal*, and all graduate students.

Moving from Stockholm University to the University of Alaska Fairbanks, from a 'city-girl' lifestyle to a challenging and in many aspects tough life on the last frontier, I found myself overwhelmed with hospitality and friendliness of so many Alaskans. I wish to thank all of you who welcomed me and shared your time, thoughts, knowledge, experience, and laughs with me. I express my gratitude to GI personnel and graduate students for always being friendly and for creating a highly stimulating working atmosphere. Special thanks to: *Keith Echlemeyer, Martin Truffer, Craig Lingle, Carl Benson* ("Good night and good luck!"), *Sandy Zirnheld, By Valentine, Chris Larsen, Laura LeBlanc, Indrani Dass, David Podrasky, Doug Christensen, Ed Bueler, Matt Nolan*, and *Michael Whalen*. I would like to thank my committee members *Uma Bhatt* and *Jing Zhang* for their guidance and support. *Will Harrison*, thank you for having your office door always open for me (literally) and for your consistent readiness to start a scientific discussion that either left me enlightened or in new wanderings. Special thanks to so many individuals at the Physics Department and the Department of Geology and Geophysics, particularly *Mary* and *Robert Parsons, Bill Witte*, and *June Champlin* for your friendliness and support during my TA months. All my TA colleagues from Fall Semester 2007, thanks to your friendship and all the laughs (and we had quite some stories to share) the Alaskan winter was less dark. *Jason Amundson*, thank you for being 'the ears and the voice' on the other side of my office cubicle. Thanks to you I started accepting whatever life brings with a unique word of wisdom: 'sure'.

Throughout my graduate studies many individuals provided me with helpful insights, necessary data input, comments on manuscripts and useful advice. In this regard, I express my gratitude to: *Anthony Arendt, Tómas Jóhannesson, Roger Braithwaite, Edward Hanna, Al Rasmussen, Georg Kaser, Per Kålberg, Erik Kjellström, Carsten Maas, Reza Entezarolmahdi, Patrick Samuelsson, Sarah Raper, Veijo Pohjola, Nedjeljka and Mark Žagar, Zoran Pasarić, Branko Grisogono, Xiangdong Zhang*, and *Deliang Chen*.

Memories of my years in Stockholm carry the fingerprints of many people who shared and let me share my life with them. Croatians that I have met in Katolska Domkyrkan, thank you for always being welcoming, friendly, and ready to join voices in song. In particular: *Marinko* and *4M*, for your genuine goodness, sincere friendship, help in need, all the created songs, and delicious *Marija*'s cuisine. *Ivana Novak*, for being such a determined person, encouraging me to seek more in life. *Melita*, for all of our conversations that bordered between chit-chat and deep

philosophizing. *Ivan*, for you friendship and for enriching my senses with great Macedonian music. *P. Stjepan/Željko*, for your hospitality and for introducing me to the best pizzeria in Stockholm.

Life in Stockholm would not have had the same flavor without the student group at St. Eugenia. Many people passed through that group that left everlasting mark on my life for which I am thankful. *P. Klaus*, you are to take all the credit! *Francesco, Sam, Barbara, Olaf, Tomislav, Memma, Agnieszka, Alberto, Max, Ilaria, Johnathan*, and *Carol*, thank you for your friendship and for the memories of 'pearl days' that we shared. *Joe*, we had an unforgettable and crazy time wherever our feet stepped!

Thousands of thanks to:
The members of *Stockholms Stamningsförening* group, tack så jette mycket!
Per and *Emma*, for your warm friendship and support.
Mišo, for 'opening my eyes' about many things in Sweden and for being a living proof that dreams do come true if we work on it.
Mirta, for being a special person and a true friend. When ever I passed Bromma station I always smiled.
Dirk-Sytze, for so many shared adventures, all the encouragement and support, and for making me feel special.
My fellow toastmasters at *Tundra Talkers*, for welcoming me and for all your support.
Bindu and *Amani*, for your warm friendship, insights into Indian culture and all the delicious (but hot!) cuisine.
Pierre, for you undisputable originality. Fairbanks is not the same without you!
Dale, for your sincerity and true goodness. The world has its true handy-man!
Chris Petrich, for sharing with me so many things that are usually taken for granted - without them the essence of life would be lost.

Finally, I wish to thank my family and friends at home in Croatia who have supported me during my stay in Sweden and Alaska, followed me in their thoughts, emailed me frequently, and made me feel important and appreciated every time I came home.
Dragi moji roditelji, neizmjerno vam hvala na vašoj gotovo nadljudskoj podršci u svemu.

Chapter 1

Introduction

"*The rising sea will reclaim our ground*
nothing but water will abound
our people forced to leave for higher ground."

from "Our People on the Reef" by *Jane Resture* (2005)

Trends in global climate warming and sea level rise are observed during the last 100-years which both, according to global climate models, will continue in the future [*IPCC*, 2007]. State-of-the-art knowledge on climate, ocean and land processes identifies melting mountain glaciers and ice caps, after ocean thermal expansion, as the currently second major contributor to sea level rise. However, both the observations and models on sea level changes carry a variety of uncertainties. In this section, by following the question-answer concept, I will briefly present the importance of global sea level change for society, the current state of knowledge of sea level changes in response to climate change and the attempts to project future sea level changes until 2100 including discussion on related uncertainties. Since the aim of this Thesis is to project the 21st century sea level rise from the melt of mountain glaciers and ice caps the emphasis in this review is put on modeling glacier volume changes, their contribution to sea level rise and the assessment of uncertainties.

1.1 Sea level rise – a review

Why do we care about sea level change?

In 1990, the near-coastal population (area within 100 km horizontally and 100 m vertically of the shoreline) was 1.2 billion people, meaning that 23% of the world's population lives in an area with three times the global-mean density [*Small and Nicholls*, 2003]. Human settlements are also preferentially located close to the world's shoreline, including most of the largest cities, which means that the world's economy is also concentrated in the coastal zone [*Nordhaus*, 2006]. Thus, sea level rise has a major impact on coastal cities, deltaic lowlands, small islands, and coastal ecosystems. The potential threat has triggered studies on impacts and responses to sea-level rise

which are focused on a range of direct and indirect socio-economic impacts such as loss of land and buildings, loss of tourist amenities, increasing flood risk, impact on variety of commercial infrastructure, coastal process plants and offshore oil and gas production. In practice, existing studies have focused on a sub-set of natural system effects (inundation, flood and storm damage, wetland loss, erosion, saltwater intrusion etc.) while the treatment of adaptation to climate change has been limited or even ignored. Also, the cost of protecting against sea-level rise may have been underestimated, especially for deltas and small islands [*McLean et al.,* 2001].

Globally averaged sea level is an integrator of changes in the Earth's heat budget. Thus, precise estimates of the global mean sea level change provide strong constraints on climate model simulations [*Mitchum et al.,* 2006]. From a scientific point of view this is very important because climate models at present provide the only insight we have concerning how the Earth system might evolve in coming decades in response to increasing greenhouse gases.

What do we know from the paleo/historical record about global sea level changes?

The geological indicators of past sea level are usually not sufficiently precise to enable fluctuations of sub-meter amplitude to be observed [*IPCC,* 2001]. It is important that the areas, which provide proxy data on sea level rise, are tectonically stable and that no barriers or other shoreline features caused changes in the local conditions. Such areas are: Mediterranean (including archeological data and biological indicators of sea level change, e.g. *Laborel et al.,* [1994]; *Morhange et al.,* [1996]), the Baltic Sea (fresh-to-marine transitions, e.g. *Eronen et al.,* [1995]) and stable tropical islands and continental margins (coral formations, e.g. *Chappell,* [1982]). The results from these areas indicate that for the past 3,000 to 6,000 years oscillations in global sea level on time-scales of 100 to 1,000 years are unlikely to have exceeded 0.3 to 0.5 m. However, global sea level rose by about 120 m after the end of the last ice age (approximately 21,000 years ago), as a result of loss of mass from the ice sheets, and stabilized between 3,000 and 2,000 years ago. Sea level indicators suggest that global sea level did not change significantly from then until the late 19th century [*IPCC,* 2007].

What do recent global sea level observations show and can we trust them?

Tide gauges, which measure the radial position of the surface of the ocean with respect to the crust, particularly highlight the impact of the solid Earth on sea-level estimation. On the time

scale of a century, motion of the Earth's surface can be the same order of magnitude as motion of the sea surface (~0.1 m) and locally can exceed this by a significant amount. Thus, the problem of the impact of sea-level variations requires consideration of the land motion. Land motion corrections from tide gauge records have relied primarily on models of glacial isostatic adjustment (GIA), [e.g., *Peltier*, 2001], however, no corrections due to other land motions are considered. *IPCC* [2007] summarized the global sea level trends for the 20th century obtained from tide gauge data with GIA correction studies as 1.7 ± 0.5 mm yr^{-1}, while the assessment for 1961-2003 is 1.8 ± 0.5 mm yr^{-1}. *Domingues et al.*, [2008] derived new estimates for the period 1961-2003 with a trend of 1.6 ± 0.2 mm yr^{-1}. However, the global coverage in tide gauges still suffers from scarcity of data, especially for the Southern Hemisphere, while the models for GIA correction still need improvement.

Since 1992, global mean sea level can be computed at 10-day intervals by averaging the altimetric measurements from the satellites over the area of coverage (66°S to 66°N) [*Nerem and Mitchum,* 2001]. The emergence of global altimeter datasets and reconstructions of upper ocean heat content based on historic hydrographic data provided insight into spatial patterns associated with inter-annual and lower frequency sea level variations [*Cabanes et al.*, 2001]. The dominant sea level signal at these time scales is associated with ocean volume redistribution, and not the ocean's volume change, meaning that the redistribution signal needs to be removed from the trends at each tide gauge station. *Cabanes et al.* [2001] suggested that the under-sampling problem of tide gauges could lead to overestimation of the global sea level trend, although the magnitude of this effect has been questioned by *Miller and Douglas* [2004]. The current best estimate of average rate of global sea level rise from satellite altimetry over 1993-2003 is 3.1 ± 0.7 mm yr^{-1} [*IPCC*, 2007]. However, the error in the instrumental calibration dominates the error budget. *Domingues et al.* [2008] noted that sea level estimated from satellite altimeter observations follows the tide gauge estimate closely up to 1999 and then begins to diverge, implying a higher rate of rise. It is still unclear why the tide gauge and satellite estimates diverge.

How do we explain the observed global sea level change?

The observation of sea level change contains information on land movements, mass redistribution or geoid changes, and changes in ocean volume or distribution of water within the ocean basins. The changes in the ocean volume are affected by the changes in ocean density (steric sea level

change, where thermosteric is due to temperature changes and halosteric is due to salinity changes) and the influx of water from the continents (eustatic sea level rise). This influx is more likely due to melting of the mountain glaciers and polar ice than due to changes in terrestrial water storage. The studies on steric sea level rise and those on contribution from terrestrial water storage are briefly presented here while the cryospheric contribution will be presented separately and with more details later.

Ishii et al. [2006] estimated a linear trend of 0.36 ± 0.06 mm yr^{-1} rise in thermosteric sea level considering heat content in the 0-700 m layer in the period 1955-2003. Consideration of a deeper ocean layer, 0-3000 m, increased this estimate to 0.40 mm yr^{-1} for the period 1957-1997. An additional small halosteric component (salinity change) was estimated by *Ishii et al.* [2006] as 0.04 ± 0.01 mm yr^{-1}, consistent with the earlier estimate by *Antonov et al.* [2002]. Halosteric expansion is nearly compensated by a decrease in volume of the added freshwater when its salinity is raised (by mixing) to the mean ocean value. However, for regional changes in sea level, thermosteric and halosteric contributions can be equally important. *Domingues et al.* [2008] reported improved estimates for thermosteric sea level rise of 0.52 ± 0.08 mm yr^{-1} for 1961-2003 (0-700 m layer) which are about 50% larger than earlier estimates. For the 1993-2003 decade, the estimated 1.6 ± 0.5 mm yr^{-1} of thermosteric (0-750 m) sea level rise [*Willis et al.*, 2004] accounted for more than half of the rise in total sea level. However, *Domingues et al.* [2008] pointed out the bias in this estimate due to errors in the fall rate of expendable bathy-thermographs (XBTs), and reported a lower trend for 1993-2003 of 0.79 mm yr^{-1}. All the results indicate that there is a substantial inter-annual-to-decadal variability and regional variability, not only in the rate of ocean warming, but also in the ratio of thermosteric to total sea level change. Part of the recently observed rise (~0.5 mm yr^{-1}) may be due to the recovery of sea level after the cooling effects of the eruption of Mt. Pinatubo in 1991 [*Church et al.*, 2005].

Since the Earth's gravitational field is not sensitive to the thermal expansion of sea water, observations of the gravitational field can be used in concert with sea level change observations to separate the steric from eustatic sea level rise [*Watts and Morantine*, 1991]. However, geodetic observations of the gravitational field have significant errors due to uncertainty in the terrestrial reference frame, meaning that a 2 mm yr^{-1} error in relative velocity between the mean surface of

the Earth and the Earth system's center of mass can result in an error as large as 0.4 mm yr^{-1} in mean global sea level variation [*Blewitt et al.,* 2006].

Changes in terrestrial water storage result from climate variations, from direct human interventions in the water cycle, and from human modification of the physical characteristics of the land surface. For contribution to sea level one should consider (i) climate-driven changes of terrestrial water storage (deep ground water, lakes, lake-affected ground water, permafrost) and (ii) anthropogenic changes (artificial reservoirs, dam-affected ground water, groundwater mining, irrigation, wetland drainage, urbanization and deforestation). Order-of-magnitude estimates suggest that the permafrost thawing resulting in a decrease of stored water in the soil column and enhancing subsurface hydraulic connectivity (thus leading to more free drainage of the landscape) has the potential to be an important contributor to sea-level rise in recent years [*Lawrence and Slater*, 2005]. On the other hand, impoundment of water behind dams removes water from the ocean and lowers sea level [e.g. *Chao,* 1994]. However, it is very difficult to provide estimates of the net anthropogenic contribution, given the lack of worldwide information on each factor. Thus, *IPCC* [2007] summarized that the land contribution is either small (< 0.5 mm yr^{-1}) or is compensated for by unaccounted or underestimated contributions.

The estimated contributions to the budget of global mean sea level change and the observed rates of sea level rise are presented in Table 1.1. To summarize, the observed global mean sea level rise over 1961-2003 is 1.8 ± 0.5 mm yr^{-1}, the estimate of steric contribution is 0.42 ± 0.12 mm yr^{-1}, the contributions from terrestrial water storage are probably very small, the contribution from mountain glacier and ice caps is 0.50 ± 0.18 mm yr^{-1}, from Greenland ice sheet is 0.05 ± 0.12 mm yr^{-1} and from Antarctic ice sheet 0.14 ± 0.41 mm yr^{-1} [*IPCC*, 2007]. Thus, the sum of thermal expansion and contribution from land ice is smaller by 0.7 ± 0.7 mm yr^{-1} than the observed global average sea level rise. Even with the new estimates of *Domingues et al.* [2008], with observed sea level rise of 1.6 ± 0.2 mm yr^{-1} and steric contribution of 0.7 ± 0.1 mm yr^{-1}, the gap between observed and explained sea level rise is not closed. However, during the 1993-2003 period the observed sea level rise of 3.1 ± 0.7 mm yr^{-1} and the sum of steric and eustatic components of 2.8 ± 0.7 mm yr^{-1} show that the discrepancy between observed and explained sea level rise is smaller. Nevertheless, the increased thermal expansion in this period (1.6 ± 0.5 mm yr^{-1}) may partly reflect decadal variability rather than acceleration.

Table 1.1. Estimates of the various contributions to the global sea level rise for 1961-2003 and 1993-2003, compared with the observed rate of rise

Source	Reference	Sea level rise (mm yr^{-1})	
		1961-2003	1993-2003
Thermal expansion	*IPCC* [2007]	0.42±0.12	1.6 ± 0.5
	Domingues et al., [2008]	0.7 ± 0.1	1.0 ± 0.1
Mountain glaciers and ice caps	*IPCC* [2007]	0.50 ± 0.18	0.77 ± 0.22
Greenland ice sheet	*IPCC* [2007]	0.05 ± 0.12	0.21 ± 0.07
Antarctic ice sheet	*IPCC* [2007]	0.14 ± 0.41	0.21 ± 0.35
Sum	*IPCC* [2007]	1.1 ± 0.5	2.8 ± 0.7
Observed	*IPCC* [2007]	1.8 ± 0.5	3.1 ± 0.7
	Domingues et al., [2008]	1.6 ± 0.2	2.3 ± 0.2

How successful are the attempts to predict future global sea level changes?

High-resolution Atmosphere Ocean General Circulation Models (AOGCMs) which can reproduce detailed ocean features have been used to understand and project future sea level changes under global warming. Since climate is a profoundly nonlinear system in which variability on different time and spatial scales interact, accuracy in projected future changes depends on how well the AOGCMs incorporate processes on as many different space and time scales as possible [*Palmer*, 1999]. If greenhouse gas concentrations are on one end of the chain with climate impact on sea level rise on the other, these ends are linked through processes such as radiative forcing, atmospheric regimes and teleconnections, ocean-atmosphere-land interactions, cryospheric interactions, and biogeochemical interactions [*Palmer et al.*, 2008]. The model accuracy with which the climate impact can be determined from the underlying climate forcing is determined by the chain's weakest link. Additionally, good AOGCM performance evaluated from the present climate does not necessarily guarantee reliable predictions of future climate [*Reichler and Kim*, 2008]. The 'chain analogy' is especially applicable for sea level projection due to thermal expansion since this process can be calculated directly in AOGCMs by simulating the changes in ocean temperature. However, the contributions to sea level rise from the ice sheets and

mountain glaciers are projected by ice sheet-climate or glacier-climate coupled models. This means that processes on glacier-climate interface are currently not fully coupled in AOGCMs, but the AOGCMs output scenarios are used to force ice sheet and glacier dynamical models in order to project the volume changes. This adds additional uncertainty in future sea level projections from the cryospheric component that will be discussed later. Furthermore, the models for glacial isostatic rebound, which are used in extracting the land motion signals from tide gauge sea level observations, depend on glaciological and climate input. For terrestrial water storage land surface models are used, although their priority is to calculate fluxes from land to atmosphere for the purpose of atmospheric modeling. Thus, modeling future global sea level is a complex task which needs an interdisciplinary approach.

The history of seismicity, and future events, may contribute non-negligibly to observed sea-level trends. Besides modeling sea level changes due to climate forcing there have been efforts to combine numerical models of solid Earth deformation with large catalogues of seismic events to estimate the cumulative impacts of this seismicity on global sea level. *Melini and Piersanti* (2006) estimated a mean sea level signal at tide gauge stations of as much as 0.25 mm yr^{-1}. The signal mainly originates from very large thrust events (1960 Chile, 1964 Alaska).

IPCC [2007] projected global sea level rise between the present (1980-1990) and the end of this century (2090-2099) to range between 0.18 m to 0.59 m under various emission scenarios and a spread of AOGCMs, not including uncertainty in carbon cycle feedbacks. Sea level rise during 21^{st} century is projected to have substantial geographical variability.

1.2 Cryospheric contributions to sea level rise

This section provides a more detailed overview on assessments of cryospheric contributions to recent sea level rise and attempts to model future contributions from projected volume changes of Antarctic and Greenland ice sheets and mountain glaciers and ice caps (here defined as all ice masses outside the continuous ice sheets). The emphasis is on recent methodologies in modeling future sea level rise from the retreat of mountain glaciers and ice caps, highlighting the fields where more work is needed in order to decrease the range of uncertainties in future projections. It should be borne in mind that the ice sheets/glaciers contribution to sea level change corresponds to volume change in ice sheets/glaciers converted to the sea level equivalents (glacier volume

change divided by current ocean area of 362×10^6 km^2), thus it is assumed that all melt finds its way directly into the oceans.

1.2.1 Contribution to sea level rise from the Greenland and Antarctic ice sheets

Observations

Current techniques for measuring ice sheet mass balance include: the mass-budget approach (balancing total snow accumulation and losses by ice discharge and meltwater runoff), repeated altimetry (to estimate volume changes), and temporal changes in gravity (to infer mass changes) measured from satellites (Gravity Recovery and Climate Experiment, GRACE). Snow accumulation is estimated from stake measurements, annual layering in ice cores, sometimes with interpolation using satellite microwave measurements or shallow radar sounding [*Jacka et al.,* 2004], or from atmospheric modeling [e.g. *Bromwich et al.,* 2004]. Losses by ice discharge are the product of velocity (measured in situ or remotely) and thickness (measured by airborne radar, seismically, or from measured surface elevations assuming hydrostatic equilibrium for floating ice near grounding lines). Meltwater runoff is generally estimated from models calibrated against available surface observations [e.g. *Hanna et al.,* 2005; *Box et al.*, 2006].

Associated errors in the mass-budget of the ice sheets are difficult to assess because of high temporal and spatial variability, but they are probably ~ ± 5% for Greenland and somewhat higher (~ ± 7%) for Antarctica because of sparser data coverage. However, using satellite measurements of passive-microwave emissions to interpolate between in situ observations, *Arthern et al.* [2006] estimated substantially lower uncertainty for Antarctica. All altimetry mass-balance estimates (satellite radar and laser altimetry) carry instrumental errors in measurement of ice-sheet elevation changes, uncertainty in the rate of basal uplift by which the measurements are corrected, and the uncertainly due to changes in near-surface snow density which is used to convert thickness to mass changes. Error sources in measurements of Earth's gravity field (GRACE) include measurement errors, leakage of gravity signal from regions surrounding the ice sheets, and causes of gravity changes other than ice-sheet changes.

In Greenland, most measurements indicate substantial ice loss which has doubled in the last decade, both from increased runoff and from acceleration of outlet glaciers [*Krabill et al.*, 2000, 2004; *Velicogna and Wahr*, 2005; *Rignot and Kanagaratnam*, 2006; *Thomas et al.*, 2006]. The

period of increased ice loss overlaps with the period of higher summer temperatures and sustained local warming. However, some outlet glaciers accelerated and thinned dramatically, thus exceeding the rate of mass loss which could be explained by increasing summer melting. Increases in near-coastal melting and in ice flow velocity more than offset the increases in inland thickening due to increased snowfall in the 1990s [e.g. *Zwally et al.,* 2005; *Box et al.,* 2006]. *IPCC* [2007] reports a net loss from Greenland of 0.05 ± 0.12 mm yr^{-1} sea level equivalent (SLE) during 1961-2003, with a much larger net loss of 0.21 ± 0.07 mm yr^{-1} during 1993-2003. Inter-annual variability is very large, driven mainly by variability in summer melting, but also by sudden glacier accelerations [*Rignot and Kanagaratnam*, 2006].

In Antarctica, the agreement between different studies (e.g. with satellite radar altimetry, *Zwally et al.* [2005]; from changes in gravity, *Velicogna and Wahr* [2006]) are showing predominate mass loss along coastal sectors of the Antarctic Peninsula and West Antarctica, but thickening further inland and over most of East Antarctica [*Davis et al.,* 2005; *Zwally et al.,* 2005], with an overall balance near zero over 1961-2003. Near-coastal glacier acceleration appears to be associated with thinning, or even breakup, of floating glacier tongues and ice shelves into which the glacier flows. Associated glacier thinning progressively ungrounds more of the glacier, extending zones of thinning further and further inland. The probable cause is enhanced bottom melting of the ice shelves by warmer ocean waters. At present, the variability in flow speed of Antarctic glaciers is unknown in many places, but where known, changes are significant [e.g. *Rignot et al.,* 2004, 2005]. *IPCC* [2007] reports a net loss from Antarctic ice sheet of 0.14 ± 0.41 mm yr^{-1} SLE during 1961-2003, and 0.21 ± 0.35 mm yr^{-1} during 1993-2003.

Although both Greenland and Antarctic ice sheets are showing recent increases in mass loss, it is still not clear if the loss is anomalous or normal behavior revealed only recently because of improvements in measuring techniques. The small number of measurements, lack of agreement between techniques, and existence of systematic errors that cannot be estimated accurately preclude formal error analysis and confidence limits in the mass budgets.

Modeling

Large-scale numerical models used to predict the evolution of the Greenland and Antarctic ice sheets require time-dependent boundary conditions (surface mass balance, surface temperature,

and sea level, the latter needed to model grounding-line changes). Current ice sheet models employ grids of 20 to 40 km horizontal spacing with 10 to 30 vertical layers and include ice shelves, basal sliding and bedrock adjustment [e.g. *Huybrechts et al.*, 2004]. However, ice sheet models run for recent climate do not capture the rapid coastal flow (outlet glaciers) accelerations observed since the mid-nineties [*IPCC*, 2007]. Most of the glacier accelerations in Antarctica closely followed reduction or loss of ice shelves, which is caused by changes in basal melting or iceberg calving. Ice-shelf basal melting depends on temperature and ocean circulation within the cavity beneath. Isolation from direct wind forcing means that the main drivers of sub-ice-shelf circulation are tidal and density (thermohaline) forces, but lack of knowledge of sub-ice bathymetry does not allow the models to simulate circulation beneath the thinning ice shelves. If outlet glaciers' accelerations were to be sustained in the future these models under-predict future contributions to sea level [*Steffen et al.*, 2006].

For computational efficiency, most long simulations with comprehensive ice flow models use a simplified stress distribution, but recent changes in ice sheet margins and ice streams cannot be simulated accurately with these models, demonstrating a need for resolving the full stress configuration. Additionally, current models are not capable of simulating the increases in ice flow of slow-moving ice due to greater drainage of surface melt water into the ice sheet as observed for sites on Greenland [*Zwally et al.*, 2002; *van de Wal et al.*, 2008]. It should be noted that there is also a large uncertainty in current model predictions of the atmosphere and ocean temperature changes which drive the ice sheet changes, and this uncertainty is probably at least as large as that of the dynamic ice sheet response.

1.2.2 Contribution to sea level rise from mountain glaciers and ice caps

Observations, estimates and uncertainties for the 20th century

Estimates of global volume changes (in SLE) are based on glacier inventory data such as surface area, data on front variations, in-situ measurements of mass balance, and surface elevation changes observed by laser altimetry. The most traditional method for measuring mass budget of glaciers, or the mass balance, is the glaciological method based on snow probings and stake measurements. The mass balance over one year is the net budget between yearly accumulation on the glacier (deposition of snow by snowfall, wind, avalanches or condensation) and yearly ablation (glacier melt, wind transport of mass from the glacier, evaporation, sublimation, calving

of icebergs). Direct measurements require stake measurements of accumulation and ablation which when multiplied by the mean density of the mass gained or lost give the mass balance at the location of the stake. The mass balance of the glacier as a whole is estimated by extrapolation from a network of such stakes. Although the method is relatively simple, each point measurement carries independent error of approximately ± 50 kg m^{-2} yr^{-1} and the measurements usually do not account for internal accumulation. Internal accumulation occurs when surface meltwater percolates beneath the previous year's summer surface and refreezes there, and it can contribute up to 100% of annual net (surface plus internal) accumulation [e.g. *Bazhev*, 1980]. The process is dominant in cold and polythermal glaciers (those whose internal temperatures are below freezing at least in parts of the glacier) which form the majority of glaciers in the world, thus neglecting internal accumulation is probably the largest single bias affecting mass-balance measurements.

Calculation of the mass balance of the glacier as a whole (area-averaged net mass balance) contains errors due to spatial undersampling. On single glaciers of moderate size it is reasonable to assume that the mass balance depends only on the surface elevation. However, the networks of measurement stakes are often organized so that they capture non-random spatial variation in elevation bands. *Trabant and March* [1999] showed that typical uncertainty for elevation-band averages of mass balance is ± 200 kg m^{-2} yr^{-1}.

The geodetic method applies photogrammetry or laser/satellite altimetry, by which the glacier surface elevation is measured at two times with reference to some external datum, usually sea level. Repeated surveys with laser altimetry have been possible only in the last decade, showing high horizontal (meter-scale) and vertical (decimeter-scale) accuracy [*Arendt et al.*, 2002]. However, larger errors occur when comparing laser-altimetry elevations with elevations read from old topographic maps which may be uncertain by tens of meters. Application of satellite radar altimetry and GRACE carries the errors already mentioned for monitoring surface elevations of the ice sheets.

The observations from both the direct and geodetic methods suffer from incompleteness in spatial coverage. In addition, only ~300 (out of a total of >160,000) glaciers in the world have been subject to mass balance observations. About 40 glaciers have mass balance records longer than 20 years and ~100 glaciers have records of more than five years [*Dyurgerov and Meier,* 1997, 2005;

Dyurgerov, 2002]. Also, the observations are biased towards glaciers in maritime climates, e.g. more than 60% of long-term mass balance records are from the Alps, Scandinavia, northwestern Northern America, and parts of the Former Soviet Union. There is a serious lack of mass balance observations on very large glaciers (Arctic, Alaska, Central Asia, Patagonia Ice Fields), which may have different mass balances compared to the small and medium-size (modal size 2-4 km^2) glaciers that are commonly used for mass balance studies. Many of these under-represented glaciers are calving glaciers (in Alaska, Patagonia and high Arctic and Antarctic latitudes). Considering calving as a process which accounts for roughly two-thirds of total ablation of glaciers and ice sheets around the world [*van der Veen*, 2002] its under-representation in observations (and in modeling) is a significant source of uncertainties. Recent advances in remote sensing promise to alleviate the problem of coarse spatial coverage, however, we need to rely on the records from traditional methods for global assessment of the 20^{th} century glacier's volume changes. The observational results on the mass budget are collected and distributed by the World Glacier Monitoring Service [WGMS, *Haeberli et al.*, 2005a, b].

Another major source of systematic errors in the global assessment is our poor knowledge of glacier inventory data, i.e. data on glacier location, surface area, and volume. The inventory exists only for about 37% (~ 72,000) of all glaciers in the world, the area of individual glaciers around the Antarctic ice sheet has not been determined, and glacier area changes over time are not always reported [*Dyurgerov*, 2003].

Since data on glacier mass budget and area exist for individual glaciers one needs to find viable extrapolation methods to estimate global mass budgets and volume changes which are then converted to sea level equivalents. Having in mind all the observational errors and uncertainties mentioned above, extrapolation from a single glacier to glacierized regions with no observational data can attach even larger uncertainty in the results. A maximum distance to which single-glacier mass balance measurements yield useful information for nearby glaciers is assumed to be 600 km [*Steffen et al.*, 2006]. For estimates over regions without any nearby measurements one may use an analogy with similar regions at different longitudes, or at the same latitude in the opposite hemisphere, but there is no reliable way to determine the error of such estimates [e.g. *Dyurgerov and Meier,* 2005].

Since the mass balance database is also very limited considering the length of the records in time, especially before 1960, one must find approaches for temporal extrapolation. For example, *Meier* [1984] used a simple statistical analysis to relate short-term mass balance observed sequences with the meteorological records which are then used to estimate long-term mass balance sequences. *Dyurgerov and Meier* [1997] reconstructed mass balance records using linear regressions between poorly measured mass balances and those with long data records.

The uncertainties in the observations propagate in the assessments of the contribution of mountain glaciers and ice caps to the observed 20th century sea level rise. *IPCC* [2007] summarized the estimates for 1961-2003 to range from 0.32 to 0.68 mm yr^{-1}, and for 1993-2003 to range from 0.55 to 0.99 mm yr^{-1}. These assessments from several authors differ due to updates in inventory and mass balance data, and especially due to different estimates of the entire area of mountain glaciers and ice caps and whether or not glaciers surrounding Greenland and Antarctic ice sheets are included (Table 1.2).

Table 1.2. Estimates of recent changes (losses) in global glacier volumes expressed in sea level equivalent (SLE). The area is equivalent to the total area of mountain glaciers and ice caps (MG&IC) including or excluding those surrounding Greenland and Antarctic ice sheets

Reference	Area ($\times 10^3$ km^2)	Period	Greenland and Antarctic MG&IC	SLE (mm yr^{-1})
Thorarinsson [1940]	449	1920s-1930s	Excluded	~0.4
Meier [1984]	542	1900-1961	Excluded	0.46 ± 0.26
Ohmura [2004]	510	1967-1996	Excluded	~0.40
Cogley [2005]	572	2000-2004	Excluded	0.78 ± 0.08
Dyurgerov and Meier [2005]	785	1961-2003	Included	~0.51
Dyurgerov and Meier [2005]	785	1994-2003	Included	~0.93
Kaser et al. [2006]	546	1961-2004	Excluded	0.43±0.19
Kaser et al. [2006]	785	1961-2004	Included	0.50±0.22
Raper and Braithwaite [2006]	522	1900-2000	Excluded	0.21 to 0.30

Besides disagreements in total glacier area, the estimates of global volume changes differ in methods of calculation. *Dyurgerov and Meier* [2005] classified all the single-glacier mass

balances into 49 homogeneous regions and calculated regional mass balance averages while each mass balance series was weighted by the area of its glacier. Then the regions, weighted by their glacierized surface areas, were assigned to 13 larger regions and finally combined into 6 large glacier systems. Thus, several steps of area averaging were applied to circumvent the biases toward small and isothermal glaciers in the database. A different method, applied by *Cogley* [2005], calculates specific balance over a glacierized cell by using a spatial interpolation algorithm [*Cogley*, 2004]. At each glacierized cell in a 1°× 1° grid a two-dimensional polynomial is fitted to the single-glacier observations, and the resulting estimate of specific mass balance is multiplied by the glacierized area of the cell.

Models, projections and uncertainties for the 21st century

Since climate is the main driver of glacier behavior the 'ideal' approach for projecting glacier volume changes would be through coupled glacier-climate models. Such models require understanding processes of ice dynamics and their feedback to mass balance changes in response to climate changes. Although glacier ice flow models are highly developed and applied to several single glaciers [e.g. *Oerlemans et al.,* 1998*; Schneeberger et al.*, 2001], they are not practical for global assessment due to the lack of input data which they require, such as glacier geometry data (especially glacier bed topography and glacier thickness). Hence, projections of global volume changes need to rely on simple models with restricted data requirements. This section provides an overview of the mass balance models, climate data input, and methods used for modeling future glacier volume evolutions.

There are two main categories of the mass balance models: energy balance (reviewed in *Hock*, [2005]) and degree-day or temperature-index models (reviewed in *Hock* [2003]). The energy balance models are physically based, estimating melt as the residual in the energy balance equation, thus they require detailed meteorological input data such as net surface short-wave and long-wave radiation, snow and ice albedo, and fluxes of sensible and latent heat and heat supplied by rain. The energy components are often approximated by parameterization, i.e. a simplification of the physical processes using a function of variables that controls the required energy component [e.g. *Oerlemans and Fortuin*, 1992; *Fleming et al.*, 1997]. Thus, the energy balance models aim to represent the reality of heat exchange on the glacier surface but their usage for global assessment may be hampered due to their high data requirements. Conversely,

temperature-index models have low data requirements, main inputs are temperature and precipitation, but they lack a rigorous physical basis. A classical degree-day approach basically uses the following equation to predict melt, M:

$$M=\beta\, T_{pdd}\,, \tag{1.1}$$

where β is the degree-day factor (mm water equivalent d^{-1} K^{-1}) and T_{pdd} is the sum of all positive ($T > 0°C$) daily or monthly mean temperatures over the period of interest. The degree-day factor is a constant, which must be determined by means of field data of M and T_{pdd}. Thus, ablation in temperature-index models is completely driven by variations in temperature while the variations in other meteorological variables are neglected. However, the models generally perform well since positive degree days are shown to be good indicators of glacier melt [e.g. *Ohmura*, 2001; *Hock*, 2003]. There is a transition between temperature-index and energy balance models in order to find a balance between input data requirements, computational requirements and realistic physical representation. This transition includes a spectrum of improved temperature-index models and/or simplified energy balance models [e.g. *Jóhannesson et al.*, 1995, *Hock*, 1999; *Braithwaite and Zhang*, 2000; *Oerlemans*, 2001; *Pellicciotti et al.*, 2005]. Because degree-day models with constant degree-day factors totally neglect the effect of variations in extra-terrestrial irradiance and albedo on the mass balance, attempts to enhance these models have focused on including these effects.

All the mentioned models deal with surface ablation, while the actual effect on the mass balance is through the runoff. Thus, a more realistic approach to simulate actual glacier mass loss must include multi-layer subsurface and bulk subsurface modules in the models [e.g. *Reijmer and Hock,* 2008]. These modules deal with refreezing within the snow pack (internal accumulation), formation of superimposed ice, and snow metamorphosis (variation in snow grain size and shape and variations in snow density). In most models accumulation is treated as precipitation falling when the 2m air temperature is under a certain threshold (usually in range of 0°C to 2°C) whereas everything above that threshold is considered as rain [e.g. *Greuell and Böhm*, 1998]. Energy balance models include (re)sublimation as a contributor to mass balance through the computation of the latent heat flux, while this is impossible to compute by means of degree-day models. Additionally, models may be created to consider removal and addition of mass by action of the

wind and avalanches. Physically based models which incorporate calving as a contributor to glacier mass loss are still under development [*van der Veen*, 2002].

The performance of the mass balance models is validated by comparing modeled results with observations, which in most cases means comparison with measured mass balance series over the observational period. In most cases mass balance observations are used to calibrate the model, i.e. to tune the model's parameters in order to improve the modeled simulations of the observed record [e.g *Hock et al.,* 2007]. While this is a straightforward method with application of optimization algorithms, it has a drawback in global assessment when tuned parameters from one particular model are used for other glaciers.

Climate data are needed to calibrate and drive glacier mass balance models and thus determine glacier volume changes. Traditionally, glacier models have been forced by meteorological observations from the weather stations located on or near the glacier [e.g. *Greuell and Böhm,* 1998; *Braithwaite and Zhang*, 1999; *Hock and Holmgren*, 2005; *de Woul and Hock*, 2005]. Then, functions transferring the data from one location to another are needed. An example is the use of a constant lapse rate to convert the temperature measured at a climatic station to the near-surface temperature at the various points on the glacier. However, scarcity of meteorological weather-station data in remote glacierized areas poses constraints to such an approach and hampers larger-scale glacier modeling. To circumvent this problem for large-scale glacier modeling, especially for calibrating mass balance models, one may use gridded climatology or climate reanalysis data. Gridded climatology offers an archive of available meteorological observations from the 20th century interpolated on a world grid with fine spatial (>1°) and temporal (daily, monthly, annual, decadal) resolution (e.g. gridded climatology of Climate Research Unit, *New et al.*, [1999]). Reanalysis data are derived by processing multidecadal sequences of past meteorological observations using modern data assimilation techniques developed for numerical weather prediction (e.g. NCEP/NCAR reanalysis, www.cdc.noaa.gov/cdc/data.ncep.reanalysis.html; ERA-40 reanalysis of European Centre for Medium-Range Weather Forecast, *Simmons and Gibson* [2000]). The result is a dynamically consistent three-dimensional gridded data set which represents the best estimate of the state of the atmosphere at a certain time.

Future projections of glacier contribution to sea level rise rely, as mentioned before, on the climate projections from AOGCMs. These 3-D models of the general circulation of the atmosphere and ocean are drivers of the glacier models, meaning that the uncertainties in future AOGCM scenarios are propagated into uncertainties in future glacier's volume changes. Although future climate projection from different AOGCMs may agree on a global scale the effects of climate change will differ locally. For the impact studies, the information from global scale needs to be transferred (downscaled) to local scale [e.g. *Wilby et al.*, 1998]. The two main methods are dynamical (physically-based) and statistical (empirical) downscaling. In dynamical downscaling a regional climate model is applied to large-scale circulation using AOGCM output as boundary conditions [e.g. *Xu*, 1999]. Statistical downscaling methods rely on the existence of empirical relationships between atmospheric processes at different spatial and temporal scales. Historical climate AOGCM simulations can be downscaled by using local observations. Derived empirical relationships from historical/recent climate simulations can then be applied on the future transient AOGCM simulations [e.g. *Reichert et al.*, 2001; *Salathé*, 2005]. However, the drawback of statistical downscaling is the assumption that the empirical relationships remain unchanged in the future even if climate changes.

Recent methods for modeling future global volume changes can generally be divided into two categories: an 'indirect' approach via mass balance sensitivities to temperature and precipitation changes [e.g. *Gregory and Oerlemans*, 1998; *ACIA*, 2005] or a 'direct' approach via modeling mass balance in time [*Raper and Braithwaite*, 2006]. The concept of the 'indirect' approach relies on mass balance sensitivity, i.e. how the mean specific mass balance responds to certain change in temperature and precipitation. Then glacier volume changes can be estimated by multiplying these sensitivities by the projected temperature and precipitation changes and the glacier area. Many studies focused on determining mass balance sensitivities for the glaciers with available mass balance data and most studies concluded that glaciers in wetter or maritime climates tend to be more sensitive than sub-polar glaciers or glaciers in continental climates [e.g. *Oerlemans and Fortuin*, 1992; *Braithwaite and Zhang*, 1999; *de Woul and Hock*, 2005]. Global average mass balance sensitivity of all mountain glacier and ice caps (MG&IC) is estimated by weighting the local sensitivities by glacierized area in various regions.

Based on modeled mass balance sensitivity of 12 representative glaciers *Oerlemans and Fortuin* [1992] derived a relationship between mass balance sensitivity and annual mean precipitation, while mass balance modeling of a further 61 glaciers confirmed this relationship [*Braithwaite and Raper*, 2002]. An extension of this approach is to use regional and seasonal mass balance sensitivities to both changes in temperature and precipitation [*Oerlemans and Reichert*, 2000]. The relationship between mass balance sensitivities and climate variables enable extrapolation of mass balances sensitivities from a glacier with observed mass balances to climatically-related glaciers without mass balance observations. *Gregory and Oerlemans* [1998] applied this approach with projected temperatures from AOGCM and derived a eustatic sea level rise from glaciers to be 0.132 m and 0.182 m from two simulations for 1990-2100 period. However, this approach soon becomes inaccurate for climate changes when the glacier areas over which the mass balance sensitivities have been estimated change. Ideally, glacier area changes should be simulated by coupling the mass balance model with numerical ice flow model for each glacier individually. However, since ice flow models require input data, unknown for the vast majority of MG&IC, their application is limited on global scale. To circumvent this problem, a common way that accounts for area changes is to apply a volume-area scaling [*Bahr et al.*, 1997], which implies that the volume of a mountain glacier in a steady state is proportional to its area raised to a power. Thus by modeling the volume changes (mass balance rate) one may derive area changes via the volume-area power law relation. *Van de Wal and Wild* [2001] improved the estimations of *Gregory and Oerlemans* [1998] by applying a volume-area scaling approach and derived a eustatic sea level rise from glaciers to be 0.057 m for 2001-2070. However, under non-steady state conditions the power law relationship between glacier volume and area may change as the mass balance profile changes, [*Bahr et al.*, 1997] posing a problem in simulating future volume changes. In addition, since the scaling method indirectly assumes perfect plasticity, i.e. the assumption that dynamical changes in glacier geometry are instantaneous, it might work only for the glaciers with linear mass balance profiles and small mass balance perturbations in response to climate forcing [*Harrison*, personal communication].

To circumvent the problems occurring in the 'indirect' approaches via mass balance sensitivities, the 'direct' approach applies modeling the glacier mass balance by forcing the model with recent and future climate scenarios. *Raper and Braithwaite*, [2006] modeled glacier mass balance profiles with a model of simple ice geometry which requires assumptions about glacier and ice

cap hypsometry and predetermines the area altitude for any area and glacier's altitudinal range. This approach also applies volume-area scaling from *Bahr et al.* [1997] but tries to simulate the tendency of mass balance to reach a new equilibrium in a new climate (e.g. mass balance of a mountain glacier becomes less negative in warming climate as the glacier retreats from low-lying, high-ablation altitudes, while mass balance of an ice cap lying on a flat bed becomes more negative in warming climate as the ice cap shrinks to lower high-ablation attitudes). Applying the 'geometric' model and forcing it with temperature scenarios from two GCMs *Raper and Braithwaite* [2006] projected the sea level rise from all MG&IC outside Greenland and Antarctica to be 0.046 m and 0.051 m for 2100-2100.

All the assessments of future global volume changes rely on availability of present glacier inventory data. To date about 37% of the estimated total glacier area is inventoried and made available through the World Glacier Monitoring Service and National Snow and Ice Data Center. Although the problem of an incomplete World Glacier Inventory is recognized and addressed through Global Land Ice Measurements from Space (GLIMS, e.g. *Raup et al.,* 2007), the state-of-the-art estimates on total volume of MG&IC are derived from assumed regional glacier size distributions based on percolation theory [*Meier and Bahr*, 1996] and volume-area scaling relationships [*Bahr et al.,* 1997]. Therefore, the uncertainty range in volume projections can not be narrowed until a complete initial input data on glacier areas and volumes are made available. *IPCC* [2007] reported a range of volume projections for 21st century under different emission scenarios and different GCMs from 0.070 m to 0.170 m of sea level equivalent. Nevertheless, upper bound estimate can be even higher if the present acceleration in glacier melt due to thinning and dynamic instability of tidewater glaciers is assumed to remain constant over 21st century [*Meier et al.*, 2007]. Taking into account sparse information on tidewater glaciers with changes in ice dynamics *Meier et al.* [2007] projected total volume change from MG&IC, including those surrounding Antarctica and Greenland ice sheets, to be 0.240 m ± 0.128 m in SLE by the end of 2100.

1.3 Thesis objectives

The aim of this Thesis is to project 21st century volume changes of all mountain glacier and ice caps and to provide systematic analysis of uncertainties originating from different sources in the

method. Referring to the previous sections, the main sources of uncertainties in modeling future sea level rise from melt of the mountain glaciers and ice caps are:

- incomplete world glacier inventory data (glacier area, volume)
- lack of observational data on recent global volume changes
- uncertainties in AOGCM output which force the glacier models
- downscaling global climate projections from AOGCM to local glacier scale
- modeling glacier mass balance (surface balance, internal accumulation, calving)
- coupling mass balance with glacier geometry changes (glacier dynamics)
- spatial extrapolation of volume projections
- conversion of global volume changes to sea level changes

Chapter 2 presents the methodology and results on assessment of future global volume changes while Chapters 3, 4 and 5 present the analyses of uncertainties in volume projections based on case studies. Chapter 6 brings the results from study cases back into perspective of global volume changes and provides overall conclusions.

More specifically, in Chapter 2 I provide an ensemble of 21st century volume projections for all MG&IC from the World Glacier Inventory by modeling the surface mass balance coupled with volume-area-length scaling and forced with temperature and precipitation scenarios with A1B emission scenario from four GCMs. By upscaling the volume projections through a regionally differentiated approach to all MG&IC outside Greenland and Antarctica I estimate total volume change. I discuss uncertainties in the projections and present results from a series of sensitivity tests which are applied to parameters in the mass balance model, volume-area scaling relationship, method to account for glacier advance, and method for upscaling the volume changes.

In Chapter 3 we analyze the uncertainties in volume projections associated with the choice of glacier mass balance model and the choice of climate model. For a study site we have chosen Storglaciären, a well investigated valley glacier in Sweden, for which we calibrate a temperature-index mass balance model using ERA-40 reanalysis of temperature and precipitation. The glacier's 21st century volume changes are derived using variants of the mass balance model

forced by output from one regional and six global climate models. The results are published in the Journal of Geophysical Research.

In Chapter 4 we analyze the uncertainties in volume projections associated with the approaches to consider volume-area scaling as a practical alternative to ice-flow modeling. A one-dimensional ice flow model is applied to numerically generated synthetic glaciers in order to investigate the volume-area power-law relationships for both steady-state and non-steady state conditions. Volume projections derived from volume-area scaling are compared with those derived from the ice-flow modeling. The results are published in the Annals of Glaciology.

In Chapter 5 we expanded the analysis from Chapter 4 by comparing the volume projections derived from scaling methods and ice-flow model for 6 mountain glaciers. The ice flow model is calibrated for each glacier using historical length fluctuations. 100-year volume evolutions forced by different hypothetical mass balance perturbations are compared to those obtained from volume-area, volume-length and volume-area-length scaling. The results are in press in the Journal of Glaciology.

1.4 References

ACIA (2005), *ACIA, Impacts of a warming Arctic: Arctic climate impact assessment*, Cambridge University Press.

Antonov, J. I., S. Levitus and T. P. Boyer (2002), Steric sea level variations during 1957-1994: Importance of salinity, *J. Geophys. Res.*, *107*(C12), 8013, doi:10.1029/2001JC000964.

Arendt, A. A., K. A. Echelmeyer, W. D. Harrison, S. C. Lingle and V. B. Valentine (2002), Rapid wastage of Alaska glaciers and their contribution to rising sea level, *Science*, *297*, 382-386.

Arthern, R., D. Winebrenner and D. Vaughan (2006), Antarctic snow accumulation mapped using polarization of 4.3-cm wavelength microwave emission, *J. Geophys. Res.*, *111*, D06107, doi:10.1029/2004JD005667.

Bahr, D. B., M. F. Meier and S. D. Peckham (1997), The physical basis of glacier volume-area scaling. *J. Geophys. Res., 102*, 20355-20362.

Bazhev, A. B. (1980), Metody opredeleniya vnutrennego infil'tratsionnogo pitaniya lednikov, *Materialy Glyatsiologicheskikh Issledovaniy*, *39*, 73-81. (Methods of determining the internal infiltration accumulation of glaciers)

Blewitt, G., Z. Altamimi, J. Davis, R. Gross, C. Kuo, F. Lemoine, R. Neilan, H. P. Plag, M. Rothacher, C. K. Shum, M. G. Sideris, T. Schöne, P. Tregoning and S. Zerbini (2006), Geodetic Observations and Global Reference Frame Contributions to Understanding Sea Level Rise and Variability, Position Paper for World Climate Research Programme Workshop and a WCRP contribution to the Global Earth Observation System of Systems, UNESCO, Paris, France.

Box, J. E., D. H. Bromwich, B. A. Veenhuis, L.-S. Bai, J. C. Stroeve, J. C. Rogers, K. Steffen, T. Haran and S.-H. Wang (2006), Greenland ice sheet surface mass balance variability (1988-2004) from calibrated Polar MM5 output, *J Clim.*, *19*(12), 2783-2800.

Braithwaite, R. J. and Y. Zhang (1999), Modelling changes in glacier mass balance that may occur as a result of climate changes, *Geogr. Ann.*, *81A*(4), 489-496.

Braithwaite, R. J. and Y. Zhang (2000), Sensitivity of mass balance of five Swiss glaciers to temperature changes assessed by tuning a degree-day model, *J. Glaciol.*, *46*(152), 7-14.

Braithwaite, R. J. and S. C. B. Raper (2002), Glaciers and their contribution to sea level change, *Phys. Chem. Earth*, *27*, 1445-1454.

Bromwich, D. H., Z. Guo, L. Bai and Q.-S. Chen (2004), Modeled Antarctic precipitation. Part I: spatial and temporal variability, *J. Clim.*, *17*(3), 427-447.

Cabanes, C., A. Cazenave and C. LeProvost (2001), Sea level rise during past 40 years determined from satellite and in situ observations, *Science*, *294*, 840-842.

Chao, B. (1994), Man-made lakes and global sea level rise, *Nature*, *370*, 258.

Chappell, J. (1982), Evidence for smoothly falling sea level relative to north Queensland, Australia, during the past 6000years, *Nature*, *302*, 406-408.

Church, J. A., N. J. White and J. M. Arblaster (2005), Significant decadal-scale impact of volcanic eruptions on sea level and ocean heat content, *Nature*, *438*, 74-77.

Cogley, J. G. (2004), Greenland accumulation: an error model, *J. Geophys. Res.*, *109*(D18), D18101, doi:10.1029/2003JD004449.

Cogley, J. G. (2005), Mass and energy balances of glaciers and ice sheets, in M. G. Anderson, ed., *Encyclopedia of Hydrological Sciences*, 2555-2573.

Davis, C. H., Y. Li, J. R. McConnell, M. M. Frey and E. Hanna (2005), Snowfall-driven growth in East Antarctic ice sheet mitigates recent sea-level rise, *Science*, *308*, 1898-1901, doi:10.1126/science.1110662.

de Woul, M., and R. Hock (2005), Static mass balance of Arctic glaciers and ice cap using a degree-day approach, *Ann. Glaciol.*, 42, 217-224.

Domingues, C. M., J. A. Church, N. J. White, P. J. Gleckler, S. E. Wijffels, P. M. Barker and J. R. Dunn (2008), Improved estimates of upper-ocean warming and multi-decadal sea-level rise, *Nature*, *453*, 1090-11092, doi:10.1038/nature07080.

Dyurgerov, M. B. (2002), Glacier mass balance and regime: Data of measurements and analysis, Meier M. and R. Armstrong, eds. *INSTAAR Occasional Paper* No. 55.

Dyurgerov, M. B. (2003), Mountain and subpolar glaciers show an increase in sensitivity to climate warming and intensification of the water cycle, *J. Hydrol.*, *282*, 164-176.

Dyurgerov, M. B. and M. F. Meier (1997), Year-to-year fluctuations of global mass balance of small glaciers and their contribution to sea-level changes, *Arctic Alp. Res.*, *29*(4), 392-402.

Dyurgerov, M. B. and M. F. Meier (2005), Glaciers and the changing earth system: a 2004 snapshot, Occasional Paper 58, Institute of Arctic and Alpine Research, University of Colorado, Boulder, Colorado, 117 p.

Eronen, M., G. Glückert, O. van de Plassche, J. van der Plicht and P. Rantala (1995), Land uplift in the Olkivoto-Pyhäjärvi area, southwestern Finland, during the last 8000 years, In: *Nuclear Waste Comission of Finnish Power Companies*, Helsinki, 26 p.

Fleming, K. M., J. A. Dowdeswell, J. Oerlemans (1997), Modelling the mass balance of northwest Spitsbergen glaciers and responses to climate change, *Ann. Glaciol.*, *24*, 203-210.

Gregory, J. M. and J. Oerlemans (1998), Simulated future sea-level rise due to glacier melt based on regionally and seasonally resolved temperature shanges, *Nature*, *391*, 474-476.

Greuell, W. and R. Böhm (1998), Two-metre temperatures along melting mid-latitude glaciers and implications for the sensitivity of the mass balance variations to variations in temperature, *J. Glaciol.*, *44*(146), 9-20.

Haeberli, W., M. Zemp, M. Hoelzle, R. Frauenfelder and A. Kääb (2005a), Fluctuations of Glaciers, 1995-2000 (Vol. VIII), International Commission on Snow and Ice of International Association of Hydrological Sciences/UNESCO, Paris.

Haeberli, W., J. Noetzli, M. Zemp, S. Baumann, R. Frauenfelder and M. Hoelzle (2005b), Glacier Mass Balance Bulletin No. 8 (2002-2003), International Commission on Snow and Ice of International Association of Hydrological Sciences/UNESCO, Paris.

Hanna, E., P. Huyberchts, I. Janssens, J. Cappelen, K. Steffen and A. Stephens (2005), Runoff and mass balance of the Greenland ice sheet: 1958-2003, *J. Geophys. Res.*, *110*, D13108, doi:10.1029/2004JD005641.

Hock, R. (1999), A distributed temperature-index ice- and snowmelt model including potential direct solar radiation, *J. Glaciol.*, *45*(149), 101-111.

Hock, R. (2003), Temperature index melt modeling in mountain areas, *J. Hydrol.*, *282*, 104-115, doi:10.1016/S0022-1694(03)00257-9.

Hock, R. (2005), Glacier melt: a review of processes and their modeling, *Prog. Phys. Geog.*, *29*, 362-391.

Hock, R. and B. Holmgren (2005), A distributed energy balance model for complex topography and its application to Stoglaciären, Sweden, *J. Glaciol.*, *51*(172), 25-36.

Hock, R., V. Radić, M. de Woul (2007), Climate sensitivity of Storglaciären – An intercomparison of mass balance models using ERA-40 reanalysis and regional climate model data, *Ann. Glaciol.*, *46,* 342-348.

Huybrechts, P., J. Gregory, I. Janssens, and M. Wild (2004), Modelling Antarctic and Greenland volume changes during the 20th and 21st centuries forced by GCM time slice integrations, *Global Planet. Change, 42*, 83-105, doi:10.1016/j.gloplacha.2003.11.011.

IPCC (2001), Climate Change 2001: The Scientific Basis – Contribution of Working Group 1 to the Third Assessment Report of the Intergovernmental Panel on Climate Change, edited by J. T. Houghton *et al.*, Cambridge Univ. Press, New York, 881 pp.

IPCC (2007), Climate Change 2007: The Physical Science Basis. Contribution of Working Group 1 to the Fourth Assessment Report of the Intergovernmental Panel on Climate Change [Solomon, S. and 7 others, (eds.)], Cambridge University Press, Cambridge, UK, 996 pp.

Ishii, M., M. Kimoto, K. Sakamoto and S.-I. Iwasaki (2006), Steric sea level changes estimated from historical ocean subsurface temperature and salinity analyses, *J. Oceanogr.*, *62*(2), 155-170.

Jacka, T. H., W. Abdalati, I. Allison, F. Carsey, G. Casassa, M. Fily, M. Frezzotti, H. A.Fricker, C. Genthon, I. Goodwin, Z. Guo, G. S. Hamilton, R. C. A. Hindmarsh, C. L. Hulbe, K.C. Jezek, T. A. Scambos, C. Shuman, P. Skvarca, S. Takahashi, R.S.W. van de Wal, D. G. Vaughan, W. L. Wang, R. C. Warner, D. J. Wingham, N. W. Young and H. J. Zwally (2004), Recommendations for the collection and synthesis of Antarctic Ice Sheet mass balance data, *Global Planet. Change*, *42*(1-4), 1-15.

Jóhannesson, T., O. Sigurdsson, T. Laumann and M. Kennett (1995), Degree-day glacier mass-balance modelling with applications to glaciers in Iceland, Norway and Greenland, *J. Glaciol.*, *41*(138), 345-58.

Kaser, G., J. G. Cogley, M.B. Dyurgerov, M. F. Meier and A. Ohmura (2006), Mass balance of glaciers and ice caps: Consensus estimates for 1961–2004, *Geophys. Res. Lett.*, *33*, L19501, doi:10.1029/2006GL027511.

Krabill, W., W. Abdalati, E. Frederick, S. Manizade, C. Martin, J. Sonntag, R. Swift, R. Thomas, W. Wright and J. Yungel (2000), Greenland ice sheet: high-elevation balance and peripheral thinning, *Science*, *289*, 428-430.

Laborel, J., C. Morhange, R. Lafont, J. Le Campion, F. Laborel-Deguen and S. Sartoretto (1994), Biological evidence of sea level rise during the last 4500 years on the rocky coasts of continental southwestern France and Corsica, *Mar. Geol., 120*, 203-223.

Lawrence, D. M. and A. G. Slater (2005), A projection of severe near-surface permafrost degradation during the 21st century, *Geophys. Res. Lett., 32*, L24401, doi:10.1029/2005GL025080.

McLean, R, A. Tsyban, V. Burkett, J. O. Codignotto, D. L. Forbes, N. Mimura, R. J. Beamish and V. Ittekkot (2001), Coastal Zone and Marine Ecosystems, in: McCarthy J. J., O. F. Canziani, N. A. Leary, D. J. Dokken and K. S. White (eds.) *Climate Change 2001: Impacts, Adaptation and Vulnerability*, Cambridge University Press, Cambridge, pp. 342-380.

Meier, M. F. (1984), Contribution of small glaciers to global sea level, *Science, 226*(4681), 1418-1421.

Meier, M. F. and D. B. Bahr (1996), Counting glaciers: use of scaling methods to estimate the number and size distribution of the glaciers in the world, *CRREL Special Report,* 96-27, U.S. Army, Hanover, New Hampshire.

Meier, M. F., M. B. Dyurgerov, U. K. Rick, S. O'Neel, W. T. Pfeffer, R. S. Anderson, S. P. Anderson and A. F. Glazovsky (2007), Glaciers dominate eustatic sea-level rise in the 21st century, *Science*, doi: 10.1126/science.1143906.

Melini, D. and A. Piersanti (2006), Impact of global seismicity on sea level change assessment, *J. Geophys. Res., 111*, B03406, doi:10.1029/2004JB003576.

Miller, L. and B. Douglas (2004), Mass and volume contributions to 20th century global sea level rise, *Nature, 438*, 406-409, doi:10.1038/nature02309.

Mitchum, G. T., R. S. Nerem, A. Merrifield, T. Baker, A. Cazenave, J. Church, W. Gehrels, S. Holgate, S. Jevrejeva, E. Leuliette, L. Miller, C. Perigaud and W. Sturges (2006), 20th Century Sea-level Rise and Variability Estimates from Tide Gauges and Altimeters, Position Paper for World Climate Research Programme Workshop and a WCRP contribution to the Global Earth Observation System of Systems, UNESCO, Paris, France.

Morhange, C., J. Laborel, A. Hesnard, and A. Prone (1996), Variation of relative mean sea level during the last 4000 years on the northern shores of Lacydon, the ancient harbor of Marseille (Chantier J. Verne), *J. Coast. Res., 12*, 841–849.

Nerem, R. S. and G. T. Mitchum (2001), Observations of sea level change from satellite altimetry, in Sea Level Rise: History and Consequences, B.C. Douglas, M.S. Kearney and S.R. Leatherman eds., Acad. Press, San Diego, pp. 121-163.

New, M., M. Hulme and P. J. Jones (1999), Representing twentieth century space-time climatic variability, Part 1: Development of a 1961-1990 mean monthly terrestrial climatology, *J. Clim., 12*, 829-856.

Nordhaus, W. (2006), Geography and macroeconomics: New data and new findings, *Proc. Natl. Acad. Sci. USA*, *103*(10), 3510–3517.

Oerlemans, J. (2001), Glaciers and climate change, A. A. Balkema Publishers, Lisse. 148 pp.

Oerlemans, J. and J. P. F. Fortuin (1992), Sensitivity of glaciers and small ice caps to greenhouse warming, *Science*, *258*, 115-117.

Oerlemans, J. and B. K. Reichert (2000), Relating a glacier mass balance to meteorological data using a Seasonal Sensitivity Characteristic (SSC), *J. Glaciol.*, *46*, 1-6.

Oerlemans, J., B. Anderson, A. Hubbard. Ph. Huybrechts, T. Jóhannesson, W.H. Knap, M. Schmeits, A.P. Stroeven, R.S.W. van de Wal, J. Wallinga and Z. Zuo (1998), Modelling the response of glaciers to climate warming, *Clim. Dyn.*, *14*, 267-274.

Ohmura, A. (2001), Physical basis for the temperature-based melt-index method, *J. Appl. Meteor.*, *40*, 753-761.

Ohmura, A. (2004), Cryosphere during the twentieth century, Geophysical Monograph 150, American Geophysical Union, 239-257.

Palmer, T. N. (1999), Climate change from a nonlinear dynamical perspective, *J. Climate*, *12*, 575-591.

Palmer, T.N., F. J. Doblas-Reyes, A. Weisheimer and M. J. Rodwell (2008), Toward seamless prediction: Calibration of climate change projections using seasonal forecasts, *Bull. Amer. Meteor. Soc.*, 89, 459-470.

Peltier, W. R. (2001), Global glacial isostatic adjustment and modern instrumental records of relative sea level history, in Sea level rise: history and consequences, B.C. Douglas, M.S. Kearney and S.R. Leatherman eds., Acad. Press, San Diego, pp. 65-95.

Pellicciotti, F., B. Brock, U. Strasser, P. Burlando, M. Funk and J. Corripio (2005), An enhanced temperature-index glacier melt model including the shortwave radiation balance: development and testing for Haut Glacier d'Arolla, Switzerland, *J. Glaciol.*, *51*(175), 573-587.

Raper, S. C. B. and R. J. Braithwaite (2006), Low sea level projections from mountain glaciers and icecaps under global warming, *Nature*, *439*, 311-313, doi:10.1038/nature04448.

Raup, B. R., A. Racoviteanu, S. J. S. Khalsa, C. Helm, R. Armstrong, and Y. Arnaud (2007), The GLIMS Geospatial Glacier Database: a new tool for studying glacier change, *Global Planet. Change*, *56*, 101—110, doi:10.1016/j.gloplacha.2006.07.018.

Reichert, B. K., L. Bengtsson and J. Oerlemans (2001), Midlatitude forcing mechanisms for glacier mass balance investigated using general circulation models, *J. Clim.*, *14*(17), 3767-3784.

Reichler, Y. and J. Kim (2008), How well do coupled models simulate today's climate? *Bull. Amer. Meteor. Soc.*, *89*, 303-311.

Reijmer, C. H. and R. Hock (2008), Internal accumulation on Storglaciären, Sweden, in a multi-layer snow model coupled to a distributed energy- and mass-balance model, *J. Glaciol.*, *53*(184), 61-72.

Rignot, E. and P. Kanagarathnam (2006), Changes in the velocity structure of the Greenland ice sheet, *Science*, *311*(5763), 986-990.

Rignot, E., G. Casassa, P. Gogineni, W. Krabill, A. Rivera, and R. Thomas (2004), Accelerated ice discharge from the Antarctic Peninsula following the collapse of Larsen B ice shelf, *Geophys. Res. Lett.*, *31*(18), L18401, doi:10.1029/2004GL020697.

Rignot, E., G. Casassa, S. Gogineni, P. Kanagaratnam, W. Krabill, H. Pritchard, A. Rivera, R. Thomas, J. Turner, and D. Vaughan (2005), Recent ice loss from the Fleming and other glaciers, Wordie Bay, West Antarctic Peninsula, *Geophys. Res. Lett.*, 32(7), L07502, doi:10.1029/2004GL021947.

Salathé, E. P. (2005), Downscaling simulations of future global climate with application to hydrologic modelling, *Int. J. Climatol.*, *25*, 419-436.

Schneeberger, C., O. Albrecht, H. Blatter, M. Wild and R. Hock (2001), Modelling the response of glaciers to a doubling in atmospheric CO2: a case study of Storglaciären, northern Sweden, *Clim. Dyn.*, *17*, 825-834.

Simmons, A.J. and J. K. Gibson (2000), The ERA-40 Project Plan, ERA-40 Project Report Series, 1, ECMWF, Reading, 63 pp.

Small, C. and R. J. Nicholls (2003), A global analysis of human settlement in coastal zones, *J. Coast. Res.*, *19*(3), 584-599.

Steffen, K., R. Thomas, E. Rignot, G. Cogley, M. Dyurgerov, S. Raper and P. Huybrechts (2006), Cryospheric Contributions to Sea-level Rise and Variability, Position Paper for World Climate Research Programme Workshop and a WCRP contribution to the Global Earth Observation System of Systems, UNESCO, Paris, France.

Thomas, R., E. Frederick, W. Krabill, S. Manizade and C. Martin (2006), Progressive increase in ice loss from Greenland, *Geophys. Res. Lett.*, 2006GL026075R.

Thorarinsson, S. (1940), Present glacier shrinkage, and eustatic changes of sea-level, *Geogr. Ann.*, *22*, 131-159.

Trabant, D. and R. S. March (1999), Mass-balance measurements in Alaska and suggestions for simplified observation programs, *Geogr. Ann.*, *81A*(4), 777-789.

van der Veen, C. J. (2002), Calving glaciers, *Prog. Phys. Geog.*, *26*(1), 96-122.

van de Wal, R. S. W. and M. Wild (2001), Modelling the response of glaciers to climate change by applying volume-area scaling in combination with a high resolution GCM, *Clim. Dyn.*, *18*, 359-366.

van de Wal R. S. W., W. Boot, M. R. van den Broeke, C. J. P. P. Smeets, C. H. Reijmer, J. J. A. Donker and J. Oerlemans (2008), Large and rapid melt-induced velocity changes in the ablation zone of the Greenland ice sheet, *Science*, *321*, 111-113, doi:10.1126/science.1158540.

Velicogna, I. and J. Wahr (2005), Greenland mass balance from GRACE, *Geophys. Res. Lett.*, *32*, L18505, doi:10.1029/2005GL023955.

Velicogna, I. and J. Wahr (2006), Measurements of time-variable gravity show mass loss in Antarctica, *Science*, *311*, 1754-1756.

Watts, R. C. and M. C. Morantine (1991), Is the greenhouse gas-climate signal hiding in the deep ocean? *Climatic Change*, *18*, 3-4.

Wilby, R.L., T. M. L. Wigley, D. Conway, P. D. Jones, B. C. Hewitson, J. Main and D. S. Wilks (1998), Statistical downscaling of general circulation model output: A comparison of methods, *Water Resour. Res.*, *34*, 2995-3008.

Willis, J. K., D. Roemmich and B. Cornuelle (2004), Interannual variability in upper ocean heat content, temperature, and thermosteric expansion on global scales, *J. Geophys. Res.*, *109*, C12036, doi:10.1029/2003JC002260.

Zwally, H. J., W. Abdalati, T. Herring, K. Larson, J. Saba and K. Steffen (2002), Surface melt-induced acceleration of Greenland ice-sheet flow, *Science*, 297(5579), 218-222.

Zwally, H. J., M. B. Giovinetto, J. Li, H. G. Cornejo, M. A. Beckley, A. C. Brenner, J. L. Saba and D. Yi (2005), Mass changes of the Greenland and Antarctic ice sheets and shelves and conributions to sea-level rise: 1992-2002., *J. Glaciol.*, *51*(175), 509-527.

Xu, C.-Y. (1999), Climate change and hydrologic models: A review of existing gaps and recent research developments, *Water Resour. Manag.*, *13*, 369-382.

Chapter 2

Projections of 21st century sea level rise from the melt of mountain glaciers and ice caps

2.1 Abstract

An ensemble of 21st century volume projections for all mountain glaciers and ice caps (MG&IC) from the World Glacier Inventory is derived by modeling the surface mass balance coupled with volume-area-length scaling and forced with temperature and precipitation scenarios with A1B emission scenario from four GCMs. By upscaling the volume projections through a regionally differentiated approach to all MG&IC outside Greenland and Antarctica (514,380 km^2) we estimated total volume change to range from -0.039 m to -0.150 m of sea level equivalent for the time period 2001-2100. While three GCMs (ECHAM/MPI-OM, GFDL-CM2.0, GFDL-CM2.0) agree that Alaskan glaciers are the main contributors to the projected sea level rise, CCSM3 model projects the largest total volume loss mainly due to Arctic MG&IC. This is probably due to a greater projected polar amplification in CCSM3 than in the other three GCMs. A major source of uncertainty in the methodology is the temperature forcing in the mass balance model which depends on bias correction of ERA-40 temperatures in order to simulate the local temperatures on a mountain glacier or ice cap. Other major sources of uncertainties are the volume-area scaling in deriving initial glacier volume and upscaling the volume changes with assumptions on glacier-size distributions in each glacierized region. Our projected 21st century volume loss is probably a lower bound since no calving is modeled and no MG&IC surrounding Antarctica and Greenland are included due to a lack of glacier inventory data. Nevertheless, the large range of our projections depends on the choice of GCM emphasizing the importance of ensemble projections, especially for the Arctic.

2.2 Introduction

Modeling future glacier volume changes on a global scale contains a cascade of uncertainties starting from assumptions on initial glacier area and volume, simulation of glacier mass balance and ice dynamics, and projecting local climatic scenarios. To date about 37% of the estimated total glacier area is inventoried and made available through the World Glacier Monitoring Service (WGMS) and National Snow and Ice Data Center (NSIDC). The estimates on total volume of glaciers and mountain ice caps (MG&IC) are derived from assumed regional glacier size distributions based on percolation theory [*Meier and Bahr*, 1996] and a scaling relationship

between individual glacier volume and area [*Bahr et al.*, 1997]. Volume-area scaling implies that the volume of a mountain glacier in a steady state is proportional to its area. Although the relationship has strong physical basis [*Bahr, 1997a*; *Bahr et al.*, 1997] the constant of proportionality in the volume-area power law has originally been derived from approximately 100 glaciers [*Chen and Ohmura*, 1990; *Bahr*, 1997a] and then applied globally. This constant contributes to a large uncertainty in projected volume changes for each individual glacier and in assessments of global volume changes [*Meier et al.*, 2007]. The lack of complete glacier inventory and disagreements on estimates of total MG&IC areas make the estimates on total volumes to differ considerably. *IPCC* [2007] reported that the potential sea level equivalent of all MG&IC, excluding those surrounding Greenland and Antarctic ice sheets, is in the range from 0.15 m and 0.37 m. Including the MG&IC that surround the ice sheets the potential SLE ranges from 0.50 m to 0.72 m.

In the light of these uncertainties future global volume changes have been projected either by an 'indirect' approach via mass balance sensitivities to temperature and precipitation changes [e.g. *Gregory and Oerlemans*, 1998; *ACIA*, 2005] or a 'direct' approach via modeling mass balance in time [*Raper and Braithwaite*, 2006]. The 'indirect' approach relates mass balance sensitivities, derived for the glaciers with available mass balance observations, to temperature and precipitation changes. The established relationships are then used to extrapolate the mass balance sensitivities to all the glacierized regions with no mass balance observations. Future volume projections are derived for hypothetical changes in temperature and precipitation or for changes derived from output of General Circulation Models (GCMs) [e.g. *Gregory and Oerlemans*, 1998]. The 'direct' approach models the changes in glacier mass balance by forcing mass balance models with an output from a GCM. In both approaches, if the glacier area is kept constant in time, volume loss of an individual glacier is overestimated when compared to volume projections derived from the ice flow models [e.g. *Schneeberger et al.*, 2003; *Radić et al.*, 2007]. The most common way to account for glacier area changes in volume projections on a global scale is through the scaling relationships between glacier volume, area and length [*van de Wal and Wild*, 2001; *Raper and Braithwaite*, 2006; *Meier et al.*, 2007; *IPCC*, 2007]. *Raper et al.* [2000] applied the scaling relationship to develop a 'geometric' model which, coupled with a mass balance model, enables the glacier to reach a new equilibrium in a perturbed climate. Applying this model and forcing it with temperature scenarios from two GCMs *Raper and Braithwaite* [2006]

projected the sea level rise from all MG&IC outside Greenland and Antarctica for 21st century to be 0.046 m and 0.051 m.

Another source of uncertainty in modeling future volume changes are the mass balance models which range from full energy balance models to linear regression temperature-index models, making the projections highly sensitive to the choice of the mass balance model [e.g. *Hock et al.*, 2007]. However, since positive degree days are good indicators of surface melt [e.g. *Hock*, 2003] the degree-day models are most commonly applied for deriving regional and global estimates of recent and future mass balance [*Braithwaite et al.*, 2002; *de Woul and Hock*, 2005; *Raper and Braithwaite*, 2006]. Nevertheless, two major criticisms of the application of surface mass balance models for global volume projections are that (1) the sample of glaciers with available mass balance observations to which the models are calibrated is biased toward small glaciers, area < 10 km^2 [*Dyurgerov and Meier*, 1997] and (2) the models do not consider dynamical processes, such as calving, of maritime-terminating glaciers which account for two-thirds of total ablation of glaciers and ice sheets around the world [*van der Veen*, 2002]. Taking into account sparse information on tidewater glaciers with changes in ice dynamics *Meier et al.* [2007] estimated that worldwide glacier melt has experienced acceleration due to thinning and dynamic instability of tidewater glaciers. Assuming this acceleration to remain constant over the 21st century they projected total volume change from MG&IC, including those surrounding Antarctica and Greenland ice sheets, to be 0.240 m ± 0.128 m in SLE by the end of 2100. Assuming no acceleration of present rate of mass balance loss, the volume change in SLE would be 0.140 m ± 0.025m. Their former result appears to be much larger than the one suggested by the *IPCC* [2007], where SLE from MG&IC projected by GCMs with several emission scenarios varies between 0.070 m and 0.170 m, but in close agreement with the recent work by *Rahmstorf* [2007]. However, both *IPCC* [2007] and *Rahmstorf* [2007] recognize the lack of sufficient glaciological data and models as a large uncertainty in the estimates of future glacier melt.

Despite all the social and economical importance of future sea level rise only a few studies have been devoted to lower the ranges of uncertainties in the projection of MG&IC contribution to sea level rise. Although the problem of an incomplete World Glacier Inventory (WGI) is recognized and addressed through Global Land Ice Measurements from Space (GLIMS), methods for global assessments of glacier changes are not adequately tested for MG&IC presently available in WGI.

Projections of volume changes have been derived for samples of glaciers worldwide where each sample consists of an assumed number of glaciers and their sizes [e.g. *Raper and Braithwaite*, 2006; *Meier et al.*, 2007], without any information on their exact location, geometry, or local climate regime. In the light of these assumptions the total error in the global estimates can only be assumed and it is a common way to assume cancellation or decrease of errors in the global assessments due to large scatter of independent errors for each glacier [e.g. *Schneeberger et al.*, 2003; *Kaser et al.*, 2006]. Therefore, we find it necessary to present a comprehensive method for estimating future global volume changes which distinguishes the sources of uncertainties originating in glacier-climate modeling from those originating in assumptions about glacier size and volume distribution. Our overall goal is to project 21st century volume changes of all MG&IC for all glacierized regions excluding those which surround Greenland and Antarctic ice sheets since no inventory is available for them. Thus, we aim to (1) model individual volume changes for each MG&IC from WGI by forcing a mass balance model coupled with volume-area-length scaling with temperature and precipitation scenarios from several GCMs for the period 2001-2100, (2) upscale the volume projections to all glacierized regions outside Greenland and Antarctica using regionally differentiated approach, (3) provide systematic analysis of uncertainties originating from different sources in the method.

2.3 Data and Methods

We adopt the following overall methodology (also schematically presented in Figure 2.1):
First, we calibrate a mass balance model on glaciers with available data on seasonal mass balance profiles using gridded temperature and precipitation data. Second, we perform regression analysis between the model parameters and gridded climate variables. The resulting relationships are then applied to all MG&IC from WGI to obtain model parameters. Third, the model is used to compute global mean specific mass balance for the period 1961-1990. The model is then forced with temperature and precipitation scenarios from four GCMs in order to derive an ensemble of projections for the 21st century volume changes of all MG&IC from the WGI. Volume-area-length scaling is used to account for glacier geometry changes and their feedbacks to glacier mass balance. To provide estimates of volume changes for the MG&IC that are not included in WGI we apply glacier size distribution relations for each glacierized region and regionally upscale the projected volume changes to obtain a projection on the global scale. Finally, we apply several

sensitivity tests to provide and explain methodological uncertainties in the projected glacier volume changes and corresponding sea level change.

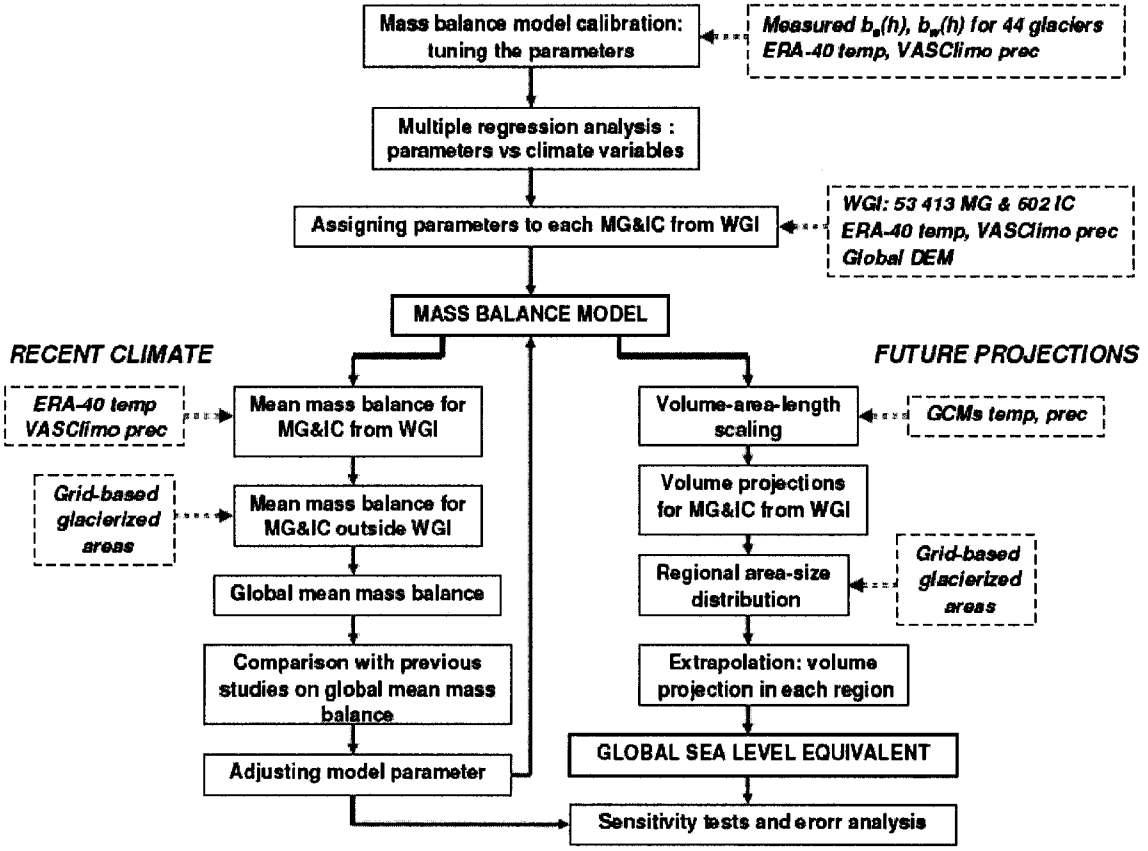

Figure 2.1. Flow chart of the methodology.

2.3.1 Glacier data

Mass balance

The degree-day mass balance model needs to be calibrated with observed seasonal mass balance profiles (mass balance vs. elevation). In total 44 glaciers worldwide were found with sufficient records of seasonal mass balance profiles for periods of ≥ 4 years. The sources of these data are: the compilation by *Dyurgerov* [2002], *Dyurgerov and Meier* [2005], World Glacier Monitoring Service (WGMS; e.g. *Haeberli et al.* [2005]), Norwegian Water Resources and Energy Directorate [e.g. *Kjøllmoen*, 2001] and *Mokievsky-Zubok et al.* [1985].

World Glacier Inventory

The National Snow and Ice Data Center (NSIDC) provides online access to information for more than 50,000 MG&IC throughout the world. The inventory entries are based upon a single observation in time. Parameters needed for our methodology include geographic location, surface area, length, and glacier elevation range (minimum and maximum elevation), and we extracted all data for MG&IC from WGI with area ≥ 0.01 km^2 resulting in 53,366 mountain glaciers (MG) and 586 ice caps (IC). We added 47 Alaskan mountain glaciers from data compiled by *Arendt et al.* [2002] and 16 Icelandic ice caps from Icelandic Inventory provided by *Sigurðsson* (personal communication). Thus, the total number from the supplemented WGI is 53,413 mountain glaciers and 602 ice caps.

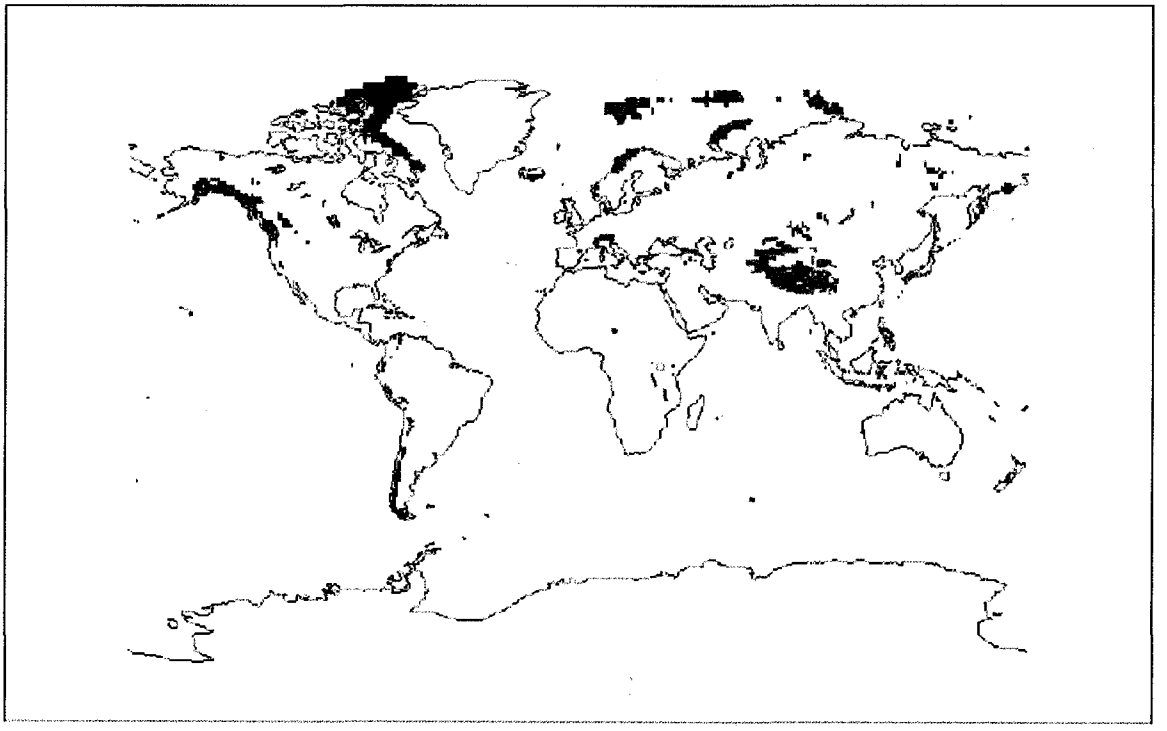

Figure 2.2. Mask of grid-based glacierized area on 1°×1° resolution. Green grid cells are glacierized according to Cogley [2003] and contain one or more MG&IC from WGI. Red grid cells contain one or more MG&IC from WGI, but are unglacierized in Cogley [2003], while blue grid cells are glacierized in Cogley [2003] but without any MG&IC from WGI.

For regional and global assessment of mass balance an additional data source is the 1° latitude/longitude gridded world glacier coverage of *Cogley* [2003]. A map of the gridded ice-mask from WGI and from *Cogley* [2003] data set is presented in Figure 2.2. If the maximum and minimum glacier elevations are not reported in WGI we use the 30-arc-second (1-km) gridded, quality-controlled global Digital Elevation Model (DEM) of the Global Land 1-km Base Elevation (GLOBE) Project (available at http://www.ngdc.noaa.gov/mgg/topo/globe.html). Maximum and minimum glacier elevations are approximated by the maximum and minimum DEM elevations in 150×150 sec grid cell centered at the closest point to glacier coordinates.

2.3.2 Climate data

The 40-year reanalysis project of the ECMWF, ERA-40, derived for the period from mid-1957 to mid-2002, covers the whole globe with spectral resolution TL159, corresponding to a grid-spacing close to 125 km (1.125°) in the horizontal with sixty levels in the vertical [*Kållberg et al.*, 2004]. We extracted 6-hourly 2m air temperature reanalysis from a bi-linearly interpolated grid of 0.5°×0.5° resolution. Since ERA-40 precipitation is not reanalyzed data we used precipitation from VASClimO Climatology which gives the monthly globally gridded data set of observed station precipitation [*Beck et al.*, 2005]. The climatology is prepared at the Global Precipitation Climatology Centre in the frame of the project VASClimO which is part of the German Climate Research Programme (DEKLIM). We extracted monthly precipitation sums from January 1951 to December 2000 on 0.5°×0.5° resolution.

Table 2.1. GCMs whose temperature and precipitation scenarios are used to force the mass balance model: First two GCMs have spectral horizontal grid: T85 is approximately 1.40° in latitude and longitude while T63 is approximately 1.87°. L refers to the number of vertical levels

	Model	Country of origin	Atmosphere resolution
1	CCSM3	United States	T85L26
2	ECHAM5/MPI-OM	Germany	T63L31
3	GFDL-CM2.0	United States	2.5° × 2.0° L24
4	UKMO-HadCM3	United Kingdom	3.75° × 2.50° L15

For future projections of glacier volume change we used time series of monthly 2m air temperature and precipitation for the 20th century historical run and the 21st century run with A1B emission scenario from four GCMs (Table 2.1). A1B is an intermediate scenario of greenhouse

forcing for which the hierarchy of models projects global average surface warming in a range from 1.7 to 4.4 °C at the end of 21st century relative to 1980-1999 [*IPCC*, 2007].

2.3.3 Mass balance model

Setup

For each elevation band on a glacier we calculate the specific mass balance rate, b, as

$$b(h) = - M(h) + C(h) + R(h), \tag{2.1}$$

where M represents ablation, C accumulation and R refreezing while h is the average altitude of the elevation band. Ablation is calculated through a degree-day model. Thus, monthly ablation, M (mm w.e.), is calculated for each elevation band as

$$M = DDF_{ice/snow}\, T_m^+\, n, \tag{2.2}$$

where $DDF_{ice/snow}$ is a degree-day factor for ice or snow (mm w.e. d^{-1} $°C^{-1}$), T_m^+ (°C) is a positive monthly mean temperature and n is a number of days in a month m. The degree-day factor for snow, DDF_{snow} is used above the equilibrium line altitude (ELA) regardless of snow cover, while below ELA we apply DDF_{ice} when the snow depth is zero. The ELA is calculated from the observed net mass balance profiles averaged over the observational period and is kept constant in time for the calibration period. Monthly snow accumulation, C (mm w.e.), is calculated for each elevation band as

$$C = a_m P_m \qquad \begin{cases} a_m = 1, T_m < T_{snow} \\ a_m = 0, T_m \geq T_{snow} \end{cases}, \tag{2.3}$$

where P is monthly precipitation (mm) which is assumed to be snow if the monthly temperature T_m (°C) is below the threshold temperature, T_{snow}, which discriminates snow from rain precipitation. Refreezing is considered through the parameterization of a superimposed-ice thickness as in *Woodward et al.* [1997]. The potential annual amount of refreezing, R (cm), is related to the annual mean air temperature, T_a (°C), as

$$R = -0.69\ T_a + 0.0096, \tag{2.4}$$

where the lower boundary for R is 0 along the whole glacier, while the upper boundary applies only in the ablation zone and is equal to the accumulated snow. Monthly melt is considered to

refreeze until the accumulated melt in one balance year exceeds the thickness of the potential refreezing, R.

The input data for the mass balance model are monthly temperatures from ERA-40 reanalysis and monthly precipitation from VASClimO Climatology. The 2m temperature from ERA-40 presents an average temperature over the grid cell at the surface altitude of the smoothed topography in the climate model. Thus there is a bias between ERA-40 2m temperature of the grid cell and the near-surface temperature on the glacier located in that grid cell. To correct this bias we apply a 'statistical lapse rate', lr_{ERA}, derived from ERA-40 altitude of a grid cell and the highest altitude of a glacier. From the highest glacier altitude, h_{max}, to the snout of the glacier we apply another lapse rate, lr, to simulate the decrease in temperature as elevation increases along the glacier surface. The temperature, T, at each elevation band in Equation (2.2) is calculated as

$$T(h) = T_{ERA} + lr_{ERA}(h_{\max} - h_{ERA}) + lr(h - h_{\max}). \tag{2.5}$$

Since the precipitation data set is based on interpolated precipitation from available weather stations it also needs correction in order to represent the precipitation on the glacier located in that grid cell. Therefore we assign a precipitation correction factor, k_P, to compute precipitation at h_{max} while from the top to the snout of the glacier we apply a precipitation gradient d_{prec} (% of precipitation increase per meter of elevation increase). Thus, the precipitation, P, at each elevation band in Equation (2.3) is calculated as

$$P(h) = k_P P_{ERA}\left[1 + d_{prec}(h - h_{\max})\right]. \tag{2.6}$$

Specific mass balance, b, is derived for each month (Equation 2.1) and integrated over the mass balance year to derive specific annual net mass balance, b_n. Winter mass balance, b_w, and summer mass balance, b_s, are integrated over the winter and summer season, respectively. The beginning of winter (summer) season for glaciers located in the northern hemisphere north of 75°N is 1 September (1 May) otherwise it is 1 October (1 May), while for glaciers in the northern hemisphere it is 1 July (1 Nov).

Calibration

There are 7 model parameters which need to be tuned: lr_{ERA}, lr, DDF_{snow}, DDF_{ice}, k_P, d_{prec} and T_{snow} and their values are expected to lie within the initial ranges listed in Table 2.2. The mass

balance model is calibrated for each glacier by tuning model parameters to yield maximum agreement between (1) modeled and observed area-averaged winter and summer mass balances, and (2) modeled and observed winter and summer mass balance profiles averaged over the period of observations. The global optimization algorithm according to *Vrugt et al.* [2003] is applied to parameter tuning in order to derive the best-fit parameter sets. Since the 44 glaciers do not experience large area changes in the reference period and since the observed area changes are not updated on a yearly basis we calculate 'reference mass balance' keeping the reported glacier area constant in time [*Elsberg et al.*, 2001].

Calibrated model parameters, correlation statistics and glacier characteristics are listed in Table 2.A-1. The median r^2 for area-averaged winter mass balance and averaged winter mass balance profile is 0.57 and 0.90, respectively, while for summer mass balance it is 0.53 and 0.98, respectively. This shows that for most glaciers the model is capable of explaining a large percent of the variance in both summer and winter mass balance. However, for two Russian glaciers, Garabashi and Kozelskiy, the model is incapable of simulating measured mass balance profiles ($r^2 < 0.1$) and therefore we exclude these two glaciers from further analysis. For our 44 glaciers the range of tuned values for the precipitation correction factor k_P is from 0.8 to 12.0, with a median value of 3.3 and mean value of 4.2. We arbitrarily assume that any k_P larger than 6 is an overestimated precipitation correction due to unrepresentative precipitation data for the glacier site. This criterion excluded an additional 7 glaciers, marked in Table 2.A-1, leaving 36 glaciers for further analysis. The mean value and standard deviation for each model parameter derived from the sample of 36 glaciers are listed in Table 2.2.

2.3.4 Modeling mass balance for 1961-1990

First a specific mass balance for each MG&IC from WGI is derived. Then we calculate the mean specific mass balance for each glacierized grid cell. Final area-weighted averaging is applied to derive global mean specific mass balance.

MG&IC from WGI

Before applying the calibrated mass balance model on 53,413 mountain glaciers and 602 ice caps from WGI model parameters need to be assigned to each MG&IC. Therefore we use the tuned model parameters on 36 glaciers and analyze their relationships to climatic variables in order to

derive functions which would then relate known climatic variables for each MG&IC to their unknown model parameters. We use the conclusions from previous studies that glaciers in wetter or maritime climate with smaller annual temperature amplitude tend to be more sensitive to temperature and precipitation changes than sub-polar or continental glaciers with drier climate and larger temperature amplitude [e.g. *Oerlemans and Fortuin*, 1992; *Braithwaite and Zhang*, 1999]. More specifically, several studies have used the relationships between mass balance sensitivities and climatic variables in order to spatially extrapolate mass balance sensitivities [e.g. *Gregory and Oerlemans*, 1998; *de Woul and Hock*, 2005]. Climate variables used in these relationships are mean annual precipitation and/or continentality index (CI) defined as the average difference between the coldest and warmest mean monthly temperature during one year [e.g. *Holmlund and Schneider*, 1997; *de Woul and Hock*, 2005]. Based on these considerations and our sample of 36 glaciers we first apply multiple regression analysis between the mass balance sensitivities to temperate and precipitation changes and two variables: CI and mean annual precipitation. Secondly, we apply multiple regressions between the model parameters and the following variables: mass balance sensitivities to temperature and precipitation change, CI, mean annual precipitation, mean glacier elevation and elevation range. The mass balance sensitivities to 1K temperature increase and 10% precipitation increase are derived from the mass balance model as

$$\frac{\Delta\overline{b_n}}{\Delta T} = \frac{\overline{b_n}(+1K) - \overline{b_n}}{1K} \tag{2.7}$$

$$\frac{\Delta\overline{b_n}}{\Delta P} = \frac{\overline{b_n}(+10\%) - \overline{b_n}}{10\%} \tag{2.8}$$

where $\overline{b_n}$ is modeled area-averaged net mass balance rate averaged over the mass balance record period while $\overline{b_n}(+1K)$ and $\overline{b_n}(+10\%)$ are modeled with uniformly perturbed temperature of +1K and precipitation of +10%, respectively. Continentality index, CI (K), and mean annual precipitation, $\overline{P_{annual}}$ (mm), are averaged over the period 1980-2000.

Modeled mass balance sensitivities to temperature and precipitation change for each glacier in the sample are listed in Table 2.A-1. The sample mean for mass balance sensitivity to temperature change of +1K and precipitation change of +10% is -0.90 m yr^{-1} and 0.24 m yr^{-1}, respectively.

These values are relatively high due to a large number of Norwegian glaciers in the sample, which are known to have high mass balance sensitivities [e.g. *de Woul and Hock*, 2005]. The resulting functions from multiple regression analysis between the mass balance sensitivities and two climate variables, CI and $\overline{P_{annual}}$, are presented in Table 2.2. The correlation is shown to be significant at the 95% confidence level. The analysis between model parameters and climatic variables shows that only three model parameters, DDF_{snow}, DDF_{ice} and k_P, have significant correlations on 95% confidence level with at least one of the following variables: mass balance sensitivities, CI, mean annual precipitation and mean glacier elevation. The resulting functions for these three model parameters are presented in Table 2.2. There is a general pattern observed in these functions: mass balance sensitivities are higher for glaciers with greater annual precipitation and lower amplitude in annual temperature cycle in agreement with the previous studies [e.g. *de Woul and Hock*, 2005]. We apply these functions to derive DDF_{snow}, DDF_{ice} and k_P for MG&IC from WGI. For the remaining model parameters we use the mean value from the sample of 36 glaciers (Table 2.2) as a first order approximation.

Besides the model parameters, we need to know glacier location (lat°, long°), surface area, and minimum and maximum glacier elevation for each MG&IC from WGI in order to apply the mass balance model. Since data on area-altitude distribution are not available, we approximate the distribution following the approach of *Raper and Braithwaite* [2006]: for mountain glaciers the area-altitude distribution is approximated with a triangle relying on the argument that observed area-altitude distribution tend to have a maximum near the mean altitude where the mass flux of ice is greatest. Thus the peak of the triangle is at the mean elevation corresponding to assumed equilibrium line altitude (ELA). Area-altitude distribution for ice caps, assuming perfect plasticity, is approximated by a parabolic shape with a circular base [*Paterson*, 1994]. The approximate area-altitude distribution for a mountain glacier and an ice cap is illustrated in Figure 2.3. As done in the calibration of the model we keep the area of each MG&IC from WGI constant in time, thus deriving 'reference mass balance' [*Elsberg et al.*, 2001].

Table 2.2. Mass balance model parameters: initial range in the optimization algorithm, mean and standard deviation from the sample of 36 glaciers, functions derived from multiple regression analysis and corresponding r^2

Parameter	Initial range	Mean	σ	Function	r^2
$lr_{ERA}\left[\frac{K}{100m}\right]$	-1.00 -0.01	-0.69	0.14	-	-
$lr\left[\frac{K}{100m}\right]$	-1.00 -0.01	-0.44	0.18	-	-
$DDF_{snow}\left[\frac{mm\ w.e.}{d\ ^\circ C}\right]$	2.00 8.00	4.92	1.54	$DDF_{snow} = -0.856 - 5.175\ \frac{\Delta\overline{b_n}}{\Delta T} - 6.804\ \frac{\Delta\overline{b_n}}{\Delta P} + 0.217\ CI - 7.5\times10^{-4}\ \overline{h}$	0.33
$DDF_{ice}\left[\frac{mm\ w.e.}{d\ ^\circ C}\right]$	4.00 12.00	7.17	1.72	$DDF_{ice} = 0.539 - 6.067\ \frac{\Delta\overline{b_n}}{\Delta T} - 6.804\ \frac{\Delta\overline{b_n}}{\Delta P} + 0.184\ CI - 4.3\times10^{-4}\ \overline{h}$	0.33
k_P	0.00 20.00	3.28	1.07	$k_P = 3.485 + 7.164\ \frac{\Delta\overline{b_n}}{\Delta P} - 1.77\times10^{-3}\ \overline{P_{annual}} - 2.32\times10^{-4}\ \overline{h}$	0.53
$d_{prec}\left[\frac{1}{100m}\right]$	0.00 0.90	0.08	0.05	-	-
$T_{snow}\left[^\circ C\right]$	0.00 2.00	1.11	0.61	-	-
$\frac{\Delta\overline{b_n}}{\Delta T}\left[\frac{m}{yr\,K}\right]$		-0.90	0.20	$\frac{\Delta\overline{b_n}}{\Delta T} = -0.980 + 0.014\ CI - 1.4\times10^{-4}\ \overline{P_{annual}}$	0.34
$\frac{\Delta\overline{b_n}}{\Delta P}\left[\frac{m}{yr\,10\%}\right]$		0.24	0.09	$\frac{\Delta\overline{b_n}}{\Delta P} = 0.053 + 0.002\ CI - 1.2\times10^{-4}\ \overline{P_{annual}}$	0.74

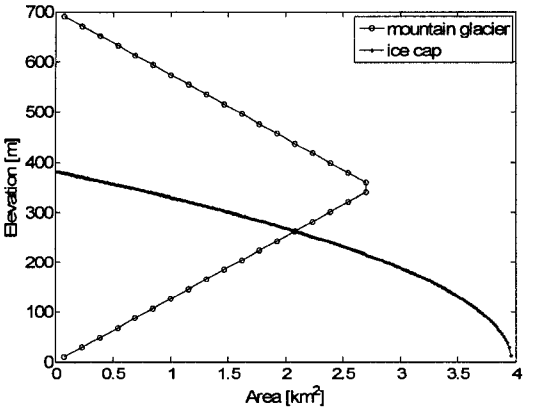

Figure 2.3. Example for area-altitude distribution of an ice cap (A=500 km^2) and a mountain glacier (A=50km^2). Spatial step along the ice cap radius is Δx=50 m, while the spatial step along the glacier elevation is Δh=20 m.

Grid-based mean specific mass balances

We use the data set of *Cogley* [2003] which provides a fraction of glacierized area on a 1°×1° global grid and the estimate of total surface area of each grid cell [*de Woul*, 2008] to derive global grid-based data of glacierized areas. We distinguish between the glacierized grid cells that contain one or more MG&IC from WGI and those without the MG&IC from WGI. For each grid cell i that contains MG&IC from WGI the specific mass balance, b_{WGI}, is derived as area-weighted average over all calculated glaciers

$$b_{WGI\,i} = \frac{\sum_{j=1}^{J} b_{i,j} A_{i,j}}{\sum_{j=1}^{J} A_{i,j}}, \tag{2.9}$$

where $b_{i,j}$ and $A_{i,j}$ are mean specific mass balance and area, for each glacier in the grid cell i, and J is the total number of the glaciers in the grid cell. For glacierized grid cells lacking MG&IC from WGI the specific mass balance is equal to modeled specific mass balance of a hypothetical glacier in the grid cell. We assume that the hypothetical glacier is located in the center of the grid cell and has a surface area of 10 km^2. The choice for surface area is arbitrary but does not influence the specific 'reference' mass balance. We derive maximum and minimum elevation for the hypothetical glacier from 30sec global DEM (GLOBE) as maximal and minimum elevation in

the grid cell. The glacier starts at the maximum elevation but the elevation range is limited to 1,520 m or the minimum elevation. The limit of 1,520 m is chosen to avoid too much discrepancy between the mean specific mass balance of the grid cells with MG&IC from WGI and without. Area-altitude distribution of the hypothetical glacier has a triangular shape in order to be consistent with the distribution for glaciers from WGI. Thus, for each hypothetical glacier we apply the mass balance model whose parameters are derived from the functions and mean values in Table 2.2.

Global mean specific mass balance

Global mean specific mass balance is derived as an area-weighted average over all the glacierized grid cells. The glacierized area for each grid cell is derived from data by *Cogley* [2003] and the total area of MG&IC from WGI. If the latter is ±20% of the former, the WGI value is assumed. Otherwise, the estimate by *Cogley* [2003] is assumed to represent the total glacierized area of the grid cell. In the case where an individual ice mass from WGI has surface area in excess of the total area of the grid cell we adopt the WGI value.

With the described methodology we obtain a grid-based global mean specific mass balance for 1961-1990 of 0.326 m yr^{-1}, which differs from the value of -0.219± 0.092 m yr^{-1} reported in *IPCC* [2007]. Since we are interested in future volume projections it is important that our modeled global mass balance for the recent climate does not have an initial offset from the previous estimates. Therefore we initialize the mass balance model, following *Raper and Braithwaite* [2006], by uniformly adjusting the model parameter lr_{ERA} to make the grid-based global mean specific mass balance approximately agree with the *IPCC* [2007] estimate. Adjustment of lr_{ERA} is chosen since the parameter, i.e. the correction of biases in ERA-40 air temperatures, is not well constrained by the calibration of the mass balance model on 36 glaciers. Results are shown in Table 2.3. The uniform adjustment of lr_{ERA} from -0.69 $K(100m)^{-1}$ to -0.52 $K(100m)^{-1}$ is needed to arrive at the global mean specific mass balance of -0.214 m yr^{-1} or, expressed in SLE, -0.305 mm yr^{-1}. Area-averaged specific mass balance for grid cells containing one or more MG&IC from WGI is -0.200 m yr^{-1}, while the remaining grid cells yielded -0.232 m yr^{-1}. A map with grid-based mean specific mass balance is presented in Figure 2.4.

Size distribution of MG&IC from WGI with corresponding area-size distribution and volume changes is illustrated in Figure 2.5. The majority of MG&IC from WGI occur in the first few size bins ($A < 3$ km^2) for which the model derived negative specific mass balance. The largest size bin, containing the ice cap from Novaya Zemlya (A=11,130 km^2) has positive specific mass balance and therefore compensates partially for the loss of volume from the small mountain glaciers. This shows the importance of modeling accurately the mass balance from very large MG&IC since they carry most of the weight in global estimates of SLE.

Table 2.3. Total glacierized area, modeled mean specific mass balance for 1961-1990 and corresponding sea level equivalent (SLE), and modeled area-weighted global mean mass balance sensitivity to temperature increase of 1K and precipitation increase of 10%

Glacierized grid cells	Area (km^2)	Mean specific mass balance (m yr^{-1})	SLE (mm yr^{-1})	$\frac{\Delta \overline{b_n}}{\Delta T}\left[\frac{m}{yr\,K}\right]$	$\frac{\Delta \overline{b_n}}{\Delta P}\left[\frac{m}{yr\,10\%}\right]$
With MG&IC from WGI	288,710	-0.200	-0.18	-0.73	0.16
Without MG&IC from WGI	225,710	-0.232	-0.13	-0.66	0.15
All	514,420	-0.214	-0.31	-0.70	0.15
IPCC [2007]	546,000	-0.219 ± 0.092	-0.33 ± 0.14		

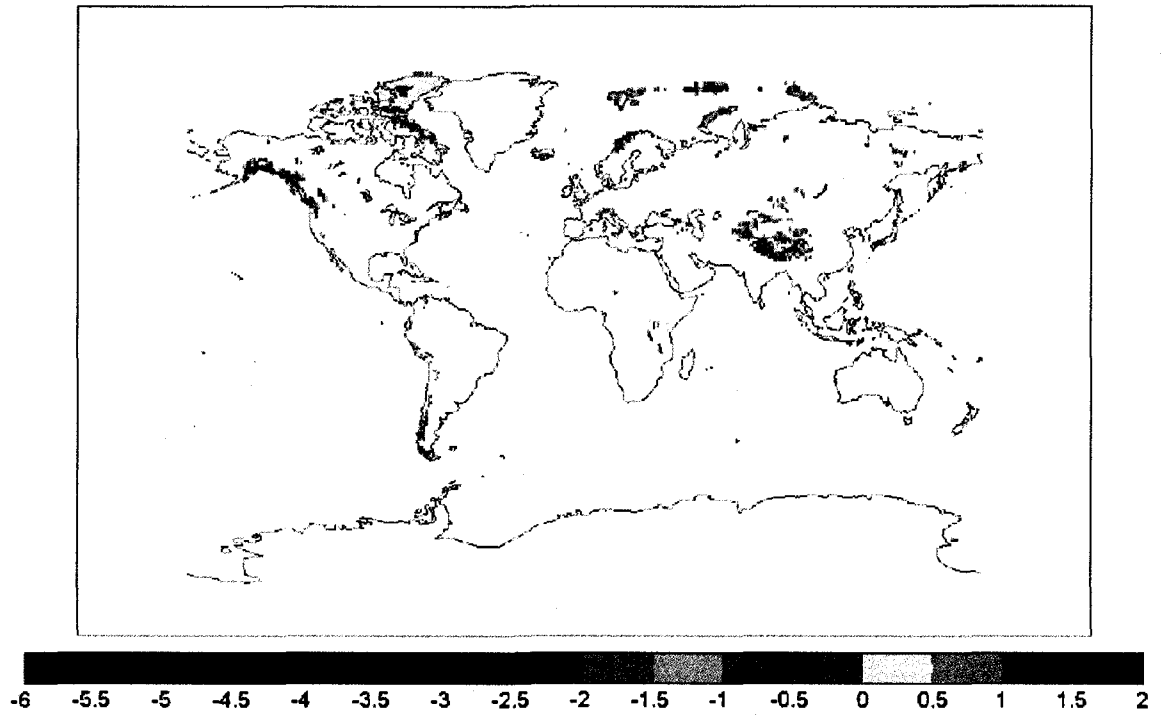

Figure 2.4. Grid-based (1°×1°) modeled mean specific mass balance for 1961-1990.

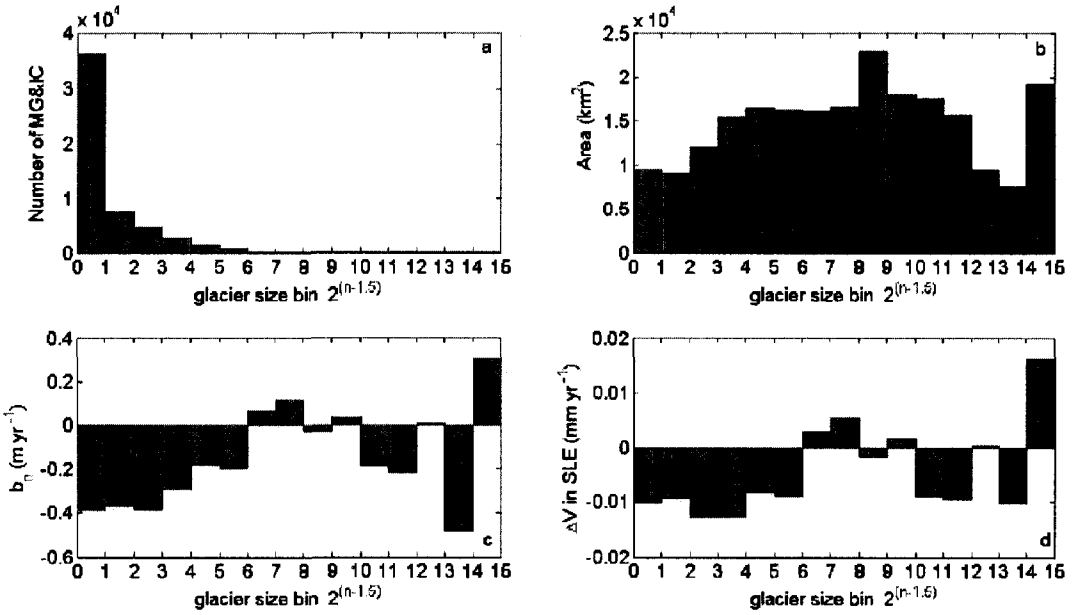

Figure 2.5. (a) Size distribution of MG&IC from WGI, (b) total area for each size bin, (c) area-weighted mean specific mass balance for each size bin, and (d) volume change in SLE for each size bin for 1961-1990.

2.3.5 Modeling future volume changes of glaciers and ice caps

Glaciers and ice caps from WGI

For future projections we force the mass balance model for each MG&IC from WGI with the temperature and precipitation simulations from four GCMs. Since GCMs are unable to represent the local subgrid-scale features and dynamics this leads to biases in the climate variables over the local scale i.e. over each glacier. We follow the methodology in *Radić and Hock* [2006] and correct the biases in temperature by adjusting the average annual temperature from GCM to match the average annual cycle from ERA-40. For precipitation, the average annual precipitation is scaled with a factor to match the average annual precipitation from VASClimO Climatology. We chose the period of 1980-1999 as a 'baseline' period over which the averages and the bias correction are derived. The bias correction is then applied over 21st century simulations.

We run the mass balance model for the period 2001-2100 and assume that the initial area for each MG&IC, i.e. at time t=2001, is equal to the area reported in WGI. We apply scaling relationships between glacier volume, area, and length [*Bahr et al.*, 1997] which, when coupled with a mass

continuity equation, provide sufficient first approximation of interrelated changes in glacier geometry and surface mass balance in glacier volume projections [*Radić et al.*, 2008]. A volume, V, of a valley glacier without calving and without hanging or discontinuous longitudinal profiles is related to its surface area, A, and its length, L, via a power law:

$$V = c_a A^{\gamma}, \tag{2.10}$$

$$V = c_l L^{q}. \tag{2.11}$$

Based on a theoretical analysis of glacier dynamics and glacier geometry and on analysis on 144 measured glaciers *Bahr et al.* [1997] derived the scaling exponents γ and q to be 1.375 and 2.2, respectively. A few estimates for the constant c_a are from *Chen and Ohmura* [1990] who found c_a=0.2055 $m^{3-2\gamma}$ for 63 mountain glaciers and from *Bahr* [1997b] who derived c_a=0.191 $m^{3-2\gamma}$ from volume and surface area for 144 glaciers. The corresponding value for c_l is missing in these studies and therefore we use c_l=4.5507 m^{3-q} derived from analysis of scaling methods in volume projections of six valley glaciers in *Radić et al.* [2008]. Following the method in *Radić et al.* [2008] we derive the volume change for each glacier from WGI and for each time step, Δt=1 year, as

$$\Delta V(t) = \sum_{i=1}^{n} b_i(t) a_i(t). \tag{2.12}$$

This is the discretized mass continuity equation with constant ice density, ρ=900 kg m^{-3}, where $b_i(t)$ is modeled annual specific mass balance of the i-th elevation band, while $a_i(t)$ is the area of the i-th band and n the total number of bands. Initial volume and length, at t=2001, are derived from scaling relationships with glacier area (c_a=0.2055 $m^{3-2\gamma}$ in Equation 2.10) while the annual length changes are derived from the annual volume changes (c_l=4.5507 m^{3-q} in Equation 2.11). Assuming a constant slope of a valley glacier the length changes are then converted to changes in glacier elevation range, allowing the glacier front to retreat or advance while keeping the maximum glacier elevation fixed in time. This approach allows the number of elevation bands, n, to change while keeping the area-altitude distribution constant. This is partially simulating the feedback between the changes in glacier area and its area-averaged mass balance thus allowing the glacier to reach a new equilibrium in different climate [e.g. *Raper et al.*, 2000; *Radić et al.*,

2007]. For each time step we derive the ELA as glacier mean elevation and therefore it can change in time due to the changes in minimum glacier elevation.

The scaling relationships for mountain glaciers are not representative for the ice caps and therefore we do not use them for future projections of the ice caps from WGI. Although many ice caps in the warming climate will disintegrate into small glaciers, to simulate this effect goes beyond our methodology. Instead, for ice caps we assume a parabolic form of thickness-length relationship as in *Paterson* [1994]:

$$H = 3.4L^{0.5}, \tag{2.13}$$

where H and L are thickness and radius in meters. Considering an ice cap with a circular plain its area and volume are determined by

$$A = \pi L^2 \tag{2.14}$$

$$V = \frac{2}{3}\pi H L^2 \tag{2.15}$$

We keep the minimum elevation of the ice caps fixed and allow for thickness changes by scaling the maximum thickness with volume at each time step according to Equation (2.15). Changes in length and area are derived from scaling the relationship with thickness, assuming parabolic area-altitude distribution (Figure 2.3). ELA is assumed constant in time.

Regional and global volume projections

We upscale the volume changes computed for the MG&IC from WGI to all MG&IC using a regionally differentiated approach. The approach requires the area-size distribution of each region due to the non-linear character of the volume-area relationships (Equation 2.10). Because many glacierized grid cells do not contain any WGI glaciers we define 16 geographical regions for which we calculate the total number of MG&IC from WGI, N_{WGI}, their total area, A_{WGI}, and size distribution. Following *Meier and Bahr* [1996] we assume that by knowing the approximate total glacierized area in each region and the approximate sizes of the largest glaciers, the numbers and size distributions of glaciers in regions can be determined. MG&IC from WGI and their areas are

distributed in size bins as shown an example for one region (Figure 2.6). From *Cogley* [2003] we derive total glacierized area in each region, A_{region}. We 'upscale' the size distribution of MG&IC from WGI by uniformly shifting the area-size distribution until the total area of the region is equal to A_{region} (Figure 2.6b). This implies adding glaciers into each size bin (Figure 2.6a). Therefore, by upscaling the size distribution we derive the total number of glaciers in each size bin and the total number of glaciers in the region, N_{total}. For some regions the total number of glaciers is given in the literature [e.g. *Williams and Ferrigno*, 1993]. Therefore, an additional criterion for the upscaling is to make N_{total} approximately agree with the reported number of glaciers in the region. We upscale the volume in each size bin by multiplying the total number of MG&IC in each bin by the mean volume of MG&IC in the bin. Here, we do not distinguish mountain glaciers from ice caps.

The next step is to upscale the projected volume changes of MG&IC from WGI based on the upscaled glacier size distribution in each region. For each size bin of each region we calculate the mean volume change of MG&IC from WGI, which is then assumed to represent the volume change for each glacier in the bin. By multiplying the mean volume change with its upscaled number of glaciers in the bin we derive total volume change in each bin and each region. The example for upscaling volume change in one region for the period 1961-1990 is shown in Figure 2.6d.

To validate our upscaling approach, we apply the approach to the 1961-1990 period and compare resulting volume changes to those derived from grid-based mean specific mass balance (Table 2.4). Figure 2.7 illustrates regional volume changes in SLE for the MG&IC from WGI, ΔV_{WGI}, total volume changes derived from the upscaling method, $\Delta V_{upscaled}$, and total volume changes derived from grid-based mean specific mass balance (Figure 2.4), $\Delta V_{grid\text{-}based}$. On the global scale results are similar, however, large discrepancies occur in Alaska, South America and especially in Arctic Canada.

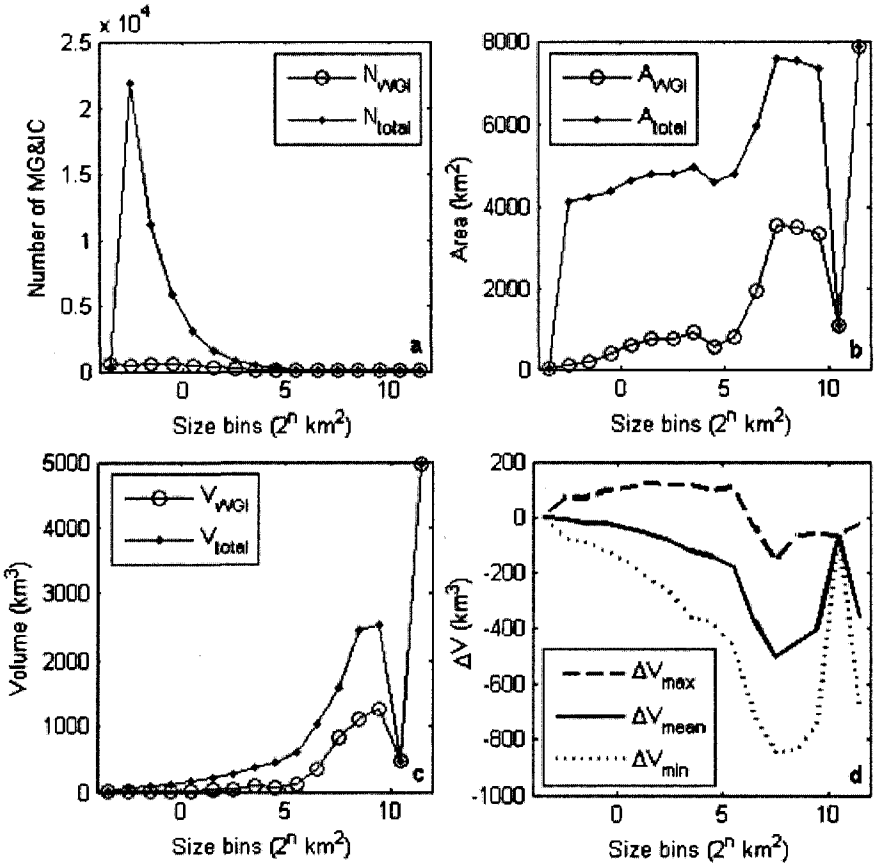

Figure 2.6. Upscaling (a) number of MG&IC, (b) glacierized area, (c) glacierized volume and (d) volume changes in Alaska for 1961-1990. In figure (d) ΔV_{mean} corresponds to the upscaling which assumes that mean volume change of MG&IC from WGI in each size bin is the representative volume change for the whole bin, while for ΔV_{max} the representative volume change in the bin is: mean volume change + standard deviation of volume changes in each bin, and for ΔV_{min} the representative is: mean - standard deviation.

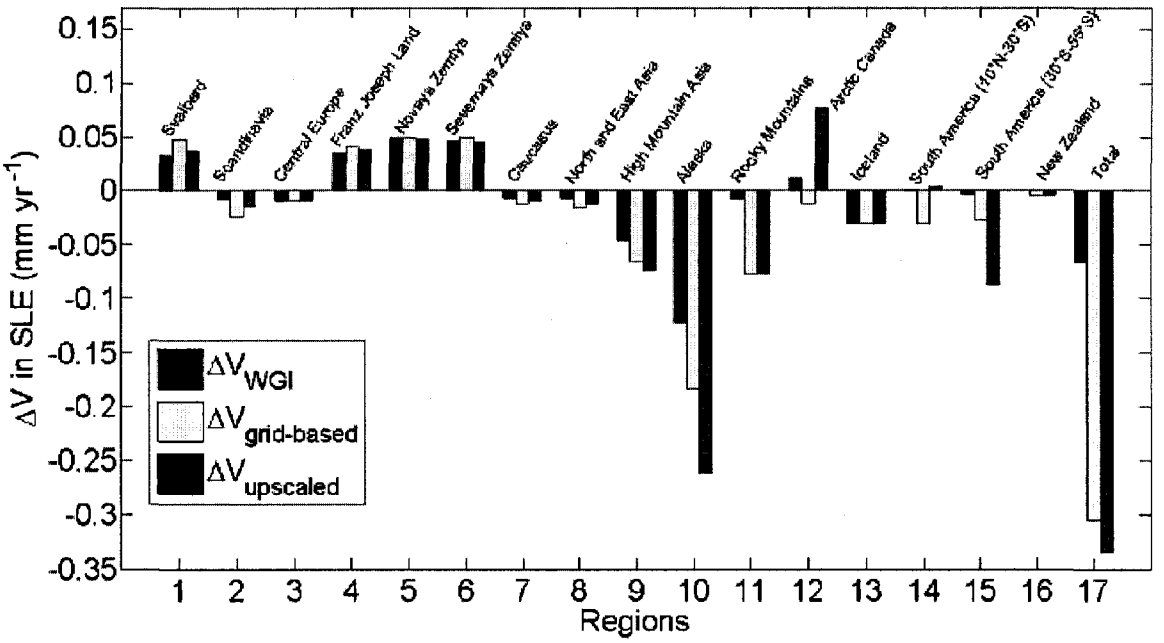

Figure 2.7. Histogram of regional volume changes for 1961-1990 expressed in sea level equivalent (SLE). ΔV_{WGI} is volume change of MG&IC from WGI in each region, $\Delta V_{grid\text{-}based}$ is total volume change derived from grid-based mean specific mass balances, and $\Delta V_{upscaled}$ is total volume change derived from the upscaling method.

Table 2.4. Regional glacier volume changes for 1961-1990. A_{WGI}, N_{WGI}, and V_{WGI} are total area, number, and volume of MG&IC from WGI in each region, while A_{total}, N_{total} *and* V_{total} are their upscaled values for each region. ΔV_{WGI} is volume change of MG&IC from WGI in each region, $\Delta V_{upscaled}$ is total volume change derived from the upscaling method for each region and $\Delta V_{grid\text{-}based}$ is total volume change derived from grid-based mean specific mass balances (Figure 2.4)

#	Region	A_{WGI}	A_{total}	N_{WGI}	N_{total}	V_{WGI}	V_{total}	ΔV_{WGI}	$\Delta V_{upscaled}$	$\Delta V_{grid\text{-}based}$
		(km^2)				(km^3)		in SLE ($mm\ yr^{-1}$)		
1	Svalbard	25760	33380	372	1628	7717	8479	0.032	0.036	0.047
2	Scandinavia	1337	2680	1171	1932	92	179	-0.008	-0.014	-0.023
3	Central Europe	2759	2760	2886	2538	187	187	-0.010	-0.009	-0.010
4	Franz Joseph Land	12518	14090	701	1384	2086	2120	0.035	0.037	0.040
5	Novaya Zemlya	22062	22060	654	657	8511	8511	0.048	0.047	0.048
6	Severnaya Zemlya	18260	18310	220	282	5578	5580	0.046	0.044	0.049
7	Caucasus	1392	2210	1510	2430	88	130	-0.007	-0.010	-0.012
8	North and East Asia	2036	3690	2562	3872	117	192	-0.007	-0.012	-0.016
9	High Mountain Asia	70847	118670	33505	75201	6828	11350	-0.046	-0.075	-0.065
10	Alaska (131°W-155°W)	26338	78610	3059	45621	10383	17117	-0.122	-0.262	-0.183
11	Rocky Mountains (109°W-130°W)	1823	21690	3056	17405	118	1178	-0.008	-0.077	-0.078
12	Arctic Canada	24085	147060	1272	31024	6035	23802	0.012	0.077	-0.012
13	Iceland	10879	11000	16	56	4880	4892	-0.030	-0.030	-0.030
14	South America (10°N-30°S)	1223	7250	1776	4117	57	374	0.001	0.004	-0.031
15	South America (30°S-55°S)	1229	29760	887	6889	98	2596	-0.003	-0.087	-0.026
16	New Zealand	94	1160	240	2062	4	48	0.000	-0.004	-0.004
	Total	222642	514380	53887	197098	52780	86734	-0.066	-0.335	-0.305
	Total in SLE (mm)					131	216	-2.0	-10.1	-9.1

2.4 Results and Discussion

2.4.1 Volume projections for MG&IC from WGI

The mass balance model is run with temperature and precipitation scenarios from four GCMs on 53,413 mountain glaciers and 602 ice caps from WGI. Total area for MG&IC from WGI are 173,120 km^2 and 49,554 km^2, respectively, while their potential SLE is 0.086 m and 0.045 m. Future volume evolutions for all MG&IC from WGI are presented in Figure 2.8 and their total volume changes are listed in Table 2.5. Since all four GCMs unanimously project an increase in annual mean temperatures averaged over all the glacierized area, the projected volume change, ΔV_{WGI}, is negative for each GCM. However, CCSM3 projects the largest total volume change in SLE, ΔV_{WGI}=-0.089 m while the results from other three GCMs are closely clustered around ΔV_{WGI} =-0.023 m. The causes for these differences are in 21st century temperature and precipitation scenarios. Figure 2.9 illustrates annual temperature and precipitation averaged over

all grid cells containing MG&IC from WGI for all four GCMs. Although the biases in annual cycle of temperature are corrected for each GCM, CCSM3 projects consistently higher annual surface temperatures for the first half of 21st than the other three GCMs. A possible cause for the lowest volume losses ΔV_{WGI} =-0.018, projected from GFDL, are relatively lower annual temperatures combined with larger maximum values of annual precipitation.

Projected volume loss for MG&IC from WGI is dominated by the volume loss from the mountain glaciers (Table 2.5). The ice caps from WGI contribute considerably less to sea level rise than the WGI mountain glaciers. In fact, projections only for the ice caps with the scenarios from GFDL and MPI are slightly positive. A possible explanation is that all the GCMs project greater warming over the mountain glacier regions compared with the ice cap regions. This is in agreement with the findings of *Raper and Braithwaite* [2006] who used only temperature scenarios from two GCMs. Nevertheless, most of the ice caps from WGI are from Svalbard, Franz Joseph Land, Novaya Zemlya and Severnaya Zemlya, which are the regions with modeled gain of ice mass in the reference period 1961-1990 (Figure 2.7). This shows high sensitivity of regional volume changes to model parameter, lr_{ERA}, which is uniformly adjusted to match the global specific mass balance to previous estimates. In this case, the MG&IC from Arctic regions might have unrepresentative degree-day model parameters due to biases in ERA-40 surface temperatures, which are not adequately corrected with uniformly adjusted lr_{ERA}.

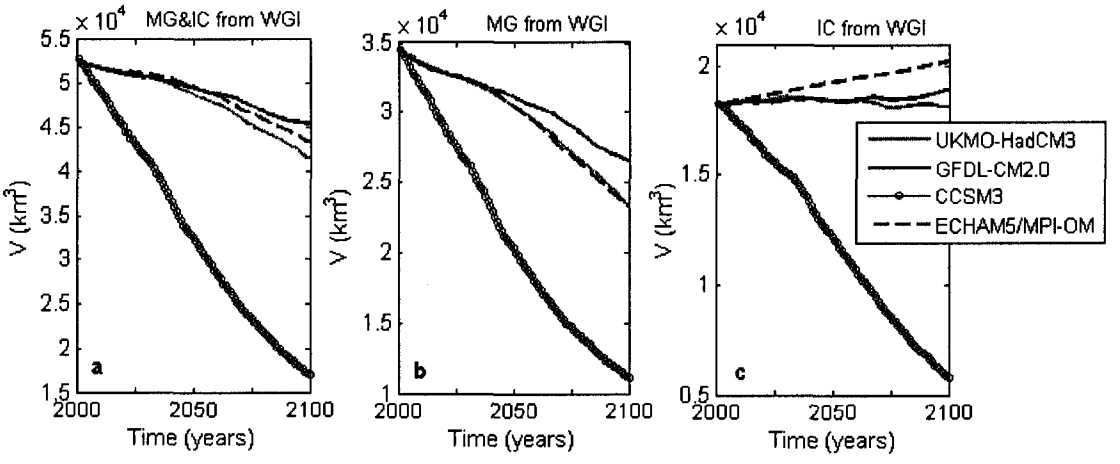

Figure 2.8. 21st century volume projections for (a) mountain glacier and ice caps (MG&IC) from World Glacier Inventory (WGI), (b) MG from WGI and (c) IC from WGI derived from temperature and precipitation scenarios from four GCMs.

Table 2.5. Projected total volume change in SLE for 2001-2100, for MG&IC from WGI, derived from temperature and precipitation scenarios from four GCMs

Model	ΔV_{WGI} in SLE (mm) 2001-2100		
	MG&IC	MG	IC
UKMO-HadCM3	-28	-28	0
GFDL-CM2.0	-18	-19	1
CCSM3	-89	-58	-31
ECHAM5/MPI-OM	-23	-28	5

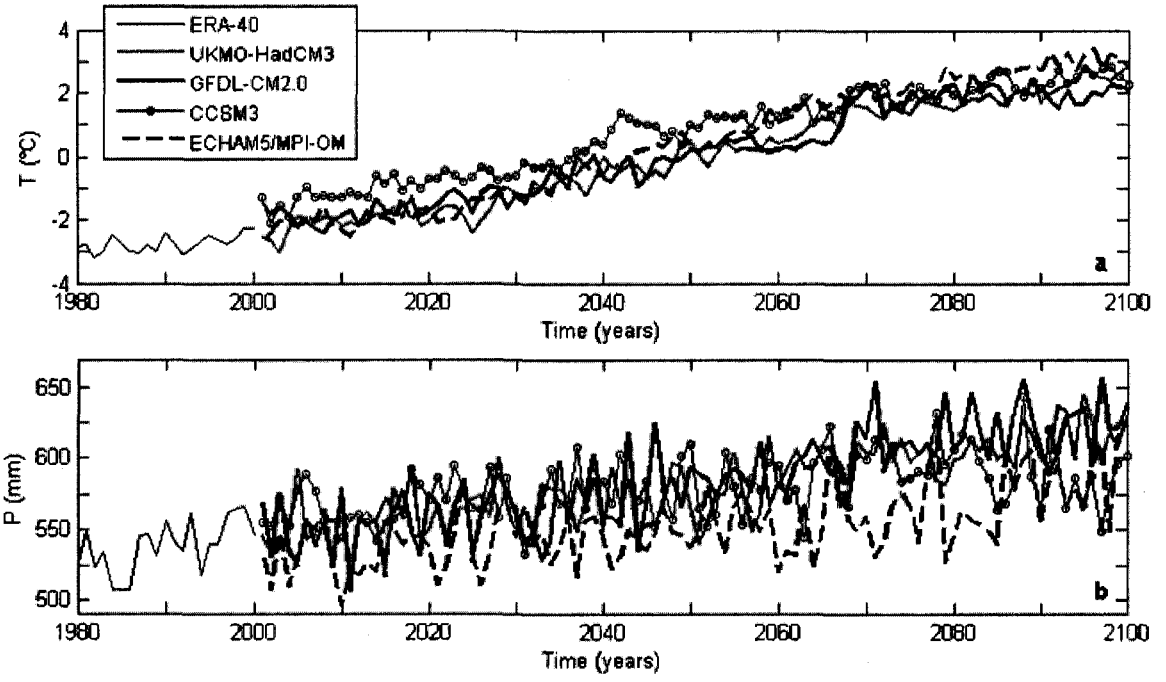

Figure 2.9. Projections of annual (a) mean temperature and (b) precipitation from four GCMs averaged over all the grid cells containing MG&IC from WGI.

2.4.2 Regional and global volume projection for 2001-2100

Global volume evolution in time and contribution to sea level rise are presented in Figure 2.10. Total regional and global volume changes over 21st century from temperature and precipitation scenarios of four GCMs are shown in Table 2.6. Upscaling the volume changes from all WGI glaciers using CCSM3 projections yields the largest global volume change over 2001-2100 period, $\Delta V_{upscaled}$ = -0.150 m in SLE while the results from the other three GCMs range from -

0.039 m to -0.060 m. All GCM forcings yield the major sea level contributions from Alaska, Arctic Canada, Iceland, Himalaya, Svalbard and South America. However, the relative contributions of each region to the global estimate vary within the GCMs (Figure 2.11). Alaskan glaciers are the largest contributors to global volume change according to three GCMs, yielding 45% to 52% of projected volume change. However, for CCSM3 the largest contributor is Arctic Canada (36%) with the volume loss of -0.054 m which itself exceeds the total volume loss projected from ECHAM5/MPI-OM and GFDL-CM2.0. In fact, all the Arctic regions north of 70°N (Arctic Canada, Svalbard, Franz Joseph Land, Novaya Zemlya, and Severnaya Zemlya) have larger volume losses in the projections from CCSM3 than in other three GCMs (Table 2.6). This caused the modeled future SLE from CCSM3 to be up to three times larger than in other GCMs. Thus, the future volume projections are particularly sensitive to temperature and precipitation scenarios for the Arctic meaning that any disagreements in the scenarios for the Arctic climate will have strong impacts on the estimates of global volume loss.

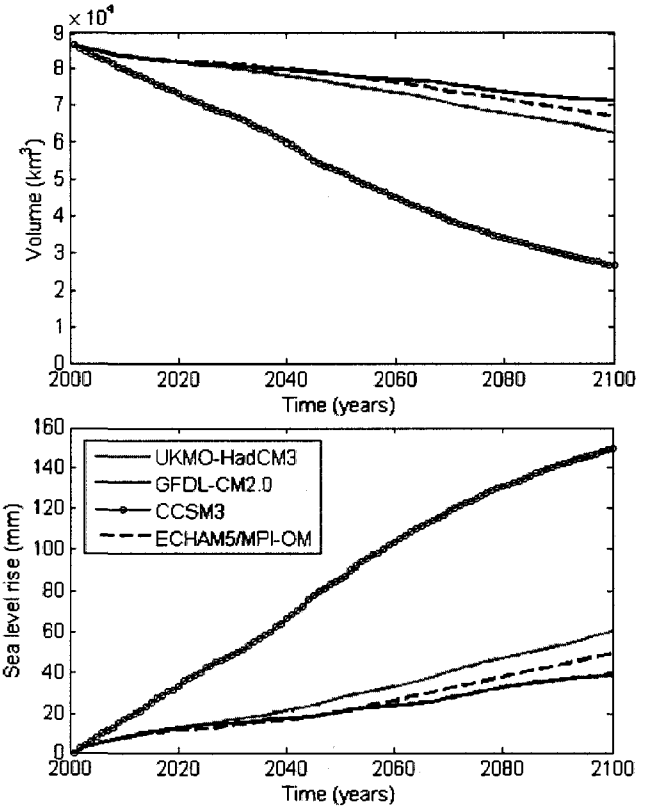

Figure 2.10. Projected volume changes and their sea level contribution for 2001-2100, derived from temperature and precipitation scenarios from four GCMs.

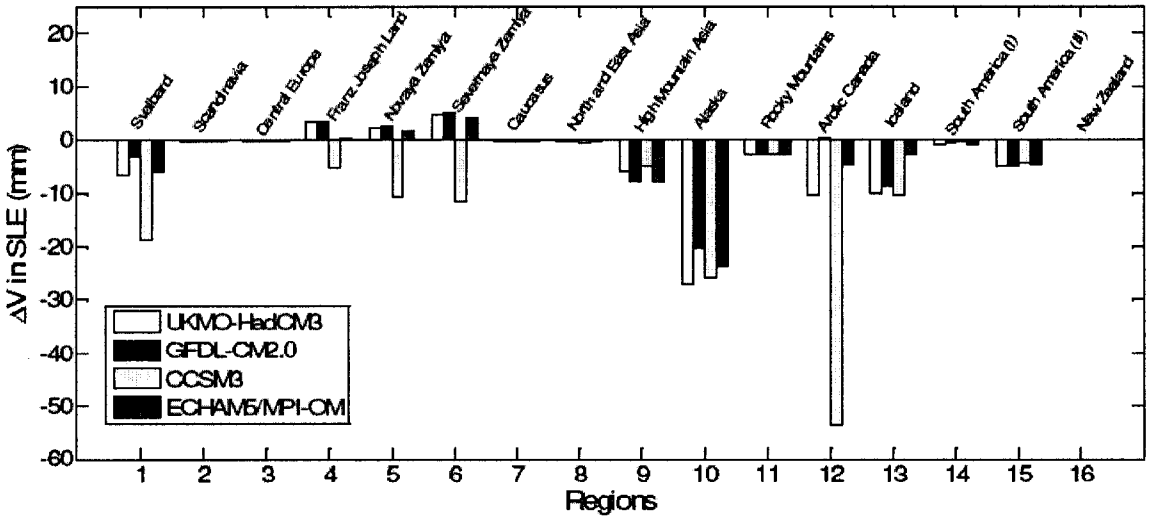

Figure 2.11. Total volume change in SLE for 16 regions for 21st century based on temperature and precipitation projections of four GCMs.

Table 2.6. Total volume changes in SLE for 2001-2100 for 16 regions and all four GCMs

#	Region	$\Delta V_{upscaled}$ in SLE (mm) 2001-2100			
		UKMO-HadCM3	GFDL-CM2.0	CCSM3	ECHAM5/MPI-OM
1	Svalbard	-6.7	-3.2	-18.6	-5.8
2	Scandinavia	-0.4	-0.4	-0.4	-0.4
3	Central Europe	-0.4	-0.4	-0.4	-0.4
4	Franz Joseph Land	3.5	3.6	-5.3	0.3
5	Novaya Zemlya	2.2	2.5	-10.6	1.5
6	Severnaya Zemlya	4.6	4.9	-11.3	4.2
7	Caucasus	-0.3	-0.3	-0.3	-0.3
8	North and East Asia	-0.4	-0.4	-0.5	-0.4
9	High Mountain Asia	-6.0	-7.7	-4.9	-8.0
10	Alaska (131°W-155°W)	-27.1	-20.1	-25.8	-23.7
11	Rocky Mountains (109°W-130°W)	-2.9	-2.8	-2.9	-2.9
12	Arctic Canada	-10.3	0.3	-53.6	-4.7
13	Iceland	-9.9	-8.7	-10.3	-2.8
14	South America (10°N-30°S)	-0.8	-0.5	-0.4	-0.8
15	South America (30°S-55°S)	-5.0	-4.9	-4.4	-4.6
16	New Zealand	-0.1	-0.1	-0.1	-0.1
	Total	-60.2	-38.5	-149.8	-49.0

2.4.3 Uncertainties

Here we discuss uncertainties and present results from a series of sensitivity tests that are applied to model parameters, scaling constant in volume-area relationship, method to account for glacier advance, and method for upscaling the volume changes.

Mass balance modeling

The mass balance model simulates surface mass balance, meaning that no calving is accounted for. Thus, the projected volume changes are probably a lower bound, however, no validation can be provided due to unavailability of data on a global scale. Secondly, the calibration of the model with 36 glaciers showed that the model explains approximately 50% of the variance in area-average seasonal mass balance. Thus, the modeled mass balance for all MG&IC from WGI has at least 50% unexplained variance. However, the performance of the degree-day model is insufficient for glaciers whose melt is not governed by positive degree-days as in the case of tropical glaciers [e.g. *Wagnon et al.*, 1999]. Except the biases in modeled simulation of measured mass balance another source of uncertainties are the values of the model parameters, which are approximated by a sample mean or by the functions in Table 2.2. Even if the model has a systematic bias due to the small sample of glaciers, the scarcity of observations constrains validation and assessment of this bias. Additionally, our assumption is that the derived relationships between the model parameters and climate variables will not change in the future. However, this may not hold in changing climate, meaning that functions in Table 2.2 should depend on time.

Keeping these uncertainties in mind we investigate the sensitivity of the mass balance model to the choice of parameter values in the sample of 36 glaciers with mass balance data in order to identify parameters to which the global projections are sensitive. First, 7 experiments are carried out where each of the model parameters is assigned to have the mean value of all 36 glaciers (Table 2.2) instead of the value optimized for each glacier. The sensitivity test consists of running the model with the optimized values for six parameters and the mean value for one parameter. The results are presented in Figure 2.12 as RMS error between the modeled and observed mean specific winter, summer and annual mass balances averaged over the observation period for all 36 glaciers. The highest RMS error occurs when the model is run with the mean value for lr_{ERA}, while the other parameters have their optimized values. This error is largest for the summer mass

balance. Next two parameters to which the modeled mass balance is highly sensitive are DDF_{snow}, which is also largest for summer mass balance, and the precipitation correction factor, k_P, largest for winter mass balance. Sensitivity to DDF_{ice} is lower than DDF_{snow} due to the boundary conditions attributed to DDF_{ice} ($1.25DDF_{snow} < DDF_{ice} < 2DDF_{snow}$).

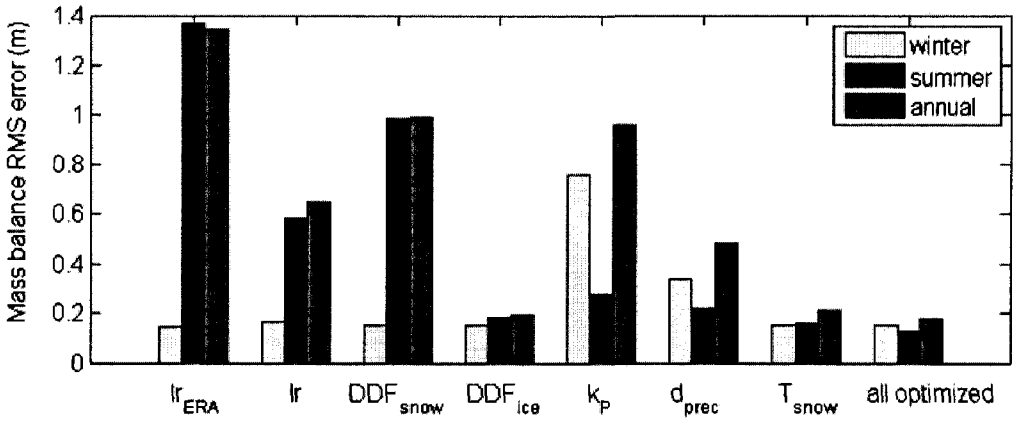

Figure 2.12. Histogram of root mean square (RMS) errors between the modeled and observed mean specific winter, summer and annual mass balance averaged over the observation period for all 36 glaciers. In each sensitivity test one parameter, labeled on the x-axis, is assigned the mean value of all 36 glaciers while the remaining 6 parameters have their optimized value for each glacier.

Since the model is shown to be highly sensitive to the value of lr_{ERA} in the sample of 36 glaciers we analyze how a small perturbation of ±0.02 K(100m)$^{-1}$ influences the estimate of global mass balance for 1961-1990. Global specific mass balance with lr_{ERA}=-0.54 K(100m)$^{-1}$ and -0.50 K(100m)$^{-1}$ is equal to -0.419 m yr^{-1} and -0.195 m yr^{-1}, respectively (Table 2.7). Thus, perturbing lr_{ERA} by ±4% from its original value resulted in deviation of global mean specific mass balance of ±0.09 m yr^{-1} or ±0.1 mm yr^{-1} SLE, making the projected global estimates highly sensitive to the choice of the correction factor for ERA-40 temperatures. An improvement from globally uniform adjustment of lr_{ERA} is to adjust the parameter region by region and validate the result with available mass balance observations in the region. However, necessary observations are not available for each region. We apply one more sensitivity test which consists of estimating global mass balance with the model parameters which all have mean values from the sample of 36

glaciers (Table 2.2), instead of applying functions for DDF_{snow}, DDF_{ice} and k_P as in the original method. Global specific mass balance changed from -0.214 m yr^{-1} to -0.331 m yr^{-1} (Table 2.7).

Table 2.7. Mean specific mass balance for 1961-1990 derived from the 'reference' parameter set of the mass balance model and three sensitivity tests. lr_{ERA} is changed from its 'reference' value -0.0052 K m^{-1} to -0.0050 K m^{-1} (test 1) and to -0.0054 K m^{-1} (test 2). In test 3, DDF_{snow}, DDF_{ice} and k_P have mean values from the sample of 36 glaciers (Table 2.2), instead of applying the functions in Table 2.2

Glacierized grid cells	Mean specific mass balance (m yr^{-1}) for 1961-1990			
	'reference'	test 1	test 2	test 3
With MG&IC from WGI	-0.200	-0.285	-0.120	-0.345
Without MG&IC from WGI	-0.232	-0.309	-0.159	-0.313
All	-0.214	-0.295	-0.137	-0.331
All in SLE (mm yr^{-1})	-0.31	-0.42	-0.19	-0.47

Initial glacier volume

To derive total initial volume and volume change of MG from WGI we have used volume-area-length scaling (Equations 2.10 and 2.11). One uncertainty source is our assumption that WGI provided initial area for the year t=2001, however, the entries are based upon a single observation during the last several decades. Another source of uncertainty is the volume-area scaling relationship, especially the uncertainty in the scaling constant c_a whose value is originally derived from regression analysis on 63 mountain glaciers [*Chen and Ohmura*, 1990]. To investigate how sensitive the results are to changes in c_a we perturb the scaling constant by ± 10% treating the estimates with c_a=0.2055 $m^{3-2\gamma}$ as the reference. The sensitivity test is applied on the projections with ECHAM4/MPI model. The results show that total initial volume (volume at t=2001) of MG from WGI derived with c_a=0.2261 $m^{3-2\gamma}$ and c_a=0.1850 $m^{3-2\gamma}$ in volume-area scaling changed from 86 mm SLE to 94 mm and 77 mm, respectively. Total volume change of all the MG from WGI for the period 2001-2100 changed from -26 mm SLE to -28 mm and -24 mm, respectively.

Volume evolutions

The scaling method coupled with the mass balance model assumes perfect plasticity, i.e. the assumption that dynamical changes in glacier geometry are instantaneous. *Radić et al.* [2008]

showed that for 6 glaciers with a uniform negative mass balance scenario of -0.015 m yr^{-1}, 100-year volume evolutions derived from volume-length scaling agree well with evolutions from a 1-D ice flow model. However, this validation is performed only on 6 glaciers with small negative mass balance scenarios. Therefore, the uncertainty in volume projections of MG&IC derived from the scaling method is not quantified, especially for ice masses with positive mass balance rates and for ice caps. Additionally, while the scaling method constrains the volume loss such that the total loss can not exceed the initial volume, it does not apply any constraints to the volume gain, i.e. the boundaries to the advancement of the mountain glacier or ice cap due to positive annual mass balances. Since in reality the advancement of the glacier and ice cap has boundaries determined by the landscape (e.g. land-sea margin) we approximate these boundaries by assuming that the projected volume gain of a mountain glacier or ice cap can not be larger than four times the initial volume. To test how sensitive the projections are to this assumption we derive the volume projections for MG&IC from WGI without this boundary condition. The projected 21st century volume change decreased by ~5 mm SLE for all GCMs.

Upscaling the volume changes

So far we have analyzed the uncertainties in modeling the volume changes of all MG&IC from WGI. Those uncertainties will propagate in the estimates of globally upscaled volume changes depending on the upscaling algorithm. However, the upscaling method itself has its assumptions and intrinsic uncertainties. In the upscaling method we have assumed that the mean volume change of MG&IC from WGI in the size bin of each regional distribution is the representative volume change for all the MG&IC in the bin. Now we consider two alternatives for the representative volume change: (1) mean volume change of MG&IC from WGI ± its standard deviation in the bin, and (2) maximum and minimum volume change found in each bin. First we apply this upscaling to derive the regional volume changes for the reference period 1961-1990 and compare them with the regional volume changes derived from the grid-based specific mass balances (Figure 2.4). The results are presented in Table 2.2. For most regions the original upscaling method yielded the volume changes which are in good agreement with the results from the grid-based mass balances. However, for some regions (e.g. Scandinavia, Caucasus, North-East Asia and Arctic Canada) the volume changes from alternative upscaling methods agree better with the estimates from grid-based specific mass balance. The estimates that give the best match to grid-based estimates are marked in Table 2.A-2 and we refer to them as the 'best

upscaling approximations'. However, we emphasize that the method with the 'best upscaling approximations' for the period 1961-1990 might not hold in the future climate. The same upscaling methods are then applied on future projections of regional volume changes (Table 2.A-3) and the results for total volume changes are presented in Table 2.8. The last column in Table 2.8 corresponds to the global volume change derived from the 'best upscaling approximations' for each region. The results show that future projections of global volume changes are highly sensitive to the choices of the upscaling methods. Results from the 'best upscaling approximations' show that the global volume loss for 21st century is larger than the loss derived from the original upscaling method. The 'best upscaling approximations' increase the volume loss by 4 mm to 15 mm depending on which GCM is used. This reflects the complexity in upscaling volume changes due to the nonlinearity of glacier response to climate forcing, sensitivity to climatic scenarios in each region, and many degrees of freedom for choosing the upscaling method.

Table 2.8. Total volume change over 2001-2100 in SLE for six different cases of upscaling: b_n corresponds to the upscaling which assumes that mean volume change of MG&IC from WGI in each size bin is the representative volume change for the whole bin, while for b_n-σ the representative volume changes in the bin is: mean volume change + standard deviation of volume changes in each bin, and for b_n+σ the representative is: mean - standard deviation. For $min(b_n)$ and $max(b_n)$ the representative volume change is the minimum and the maximum volume change in each size bin. *bn'* is the 'best upscaling approximation'

Model	$\Delta V_{upscaled}$ in SLE (mm) 2001-2100					
	b_n	b_n-σ	b_n+σ	$min(b_n)$	$max(b_n)$	b_n'
UKMO-HadCM3	-60.2	-119.2	14.1	-135.4	51.1	-75.8
GFDL-CM2.0	-38.5	-93.4	30.4	-111.1	57.0	-48.4
CCSM3	-149.8	-192.0	-77.9	-193.8	-53.7	-153.6
ECHAM5/MPI-OM	-49.0	-107.4	24.1	-123.8	60.5	-60.4

2.5 Conclusions

We provided an ensemble of 21st century volume projections for all mountain glaciers and ice caps (MG&IC) from the World Glacier Inventory (WGI) by modeling the surface mass balance coupled with volume-area-length scaling and forced with temperature and precipitation scenarios

with A1B emission scenario from four GCMs. Results showed that total volume change in SLE of 53,413 mountain glaciers and 602 ice caps, with initial total area of 222,642 km^2 and volume 52,780 km^3, is in the range of -0.018 m to -0.089 m, depending on which GCM is applied. By upscaling the volume projections through a regionally differentiated approach to all MG&IC outside Greenland and Antarctica (514,380 km^2) we estimated total volume change to be in the range of -0.039 m to -0.150 m for the time period 2001-2100. The lower estimate agrees with the previous estimates from *Raper and Braithwaite* [2006] that applied only temperature scenarios from two GCMs with A1B emission scenarios. However, CCSM3 model opens the possibility for more dramatic glacier melt. While three GCMs agreed that Alaskan glaciers are the main contributors to the projected sea level rise (followed by MG&IC from Iceland, Svalbard, Himalaya, and Patagonia), CCSM3 model projected the largest total volume loss mainly due to Arctic MG&IC (Canadian Arctic, Svalbard, Severnaya Zemlya, Novaya Zemlya, and Franz Joseph Land). This is probably due to increased projected polar amplification in CCSM3 than in the other three GCMs.

The mass balance model was calibrated on 36 glaciers with available mass balance observations and the functions between climate variables and model parameters were derived. By this we achieved a certain amount of confidence in the model parameters that are applied to all MG&IC from WGI. However, a major source of uncertainty in the methodology is the temperature forcing in the mass balance model, which depends on bias correction of ERA-40 temperatures in order to simulate the local temperatures on a mountain glacier or ice cap. By perturbing the 'statistical lapse rate', lr_{ERA}, by ±0.02 $K(100m)^{-1}$ the global specific mass-balance for the period 1961-1990 changes by ±0.1 mm yr^{-1} of SLE. Correction of ERA-40 temperatures should be applied regionally instead of globally, however, the lack of available data on mass-balance hampers adjustment of lr_{ERA} region by region. Other major sources of uncertainties are the volume-area scaling in deriving initial glacier volume and upscaling the volume changes with assumptions on glacier-size distributions in each glacierized region. Our projected 21st volume loss is probably a lower bound since no calving is modeled. Nevertheless, the large range of our projections depends on the choice of GCM emphasizing the importance of ensemble projections. This is especially the case for the Arctic regions whose mountain glaciers and ice caps are major potential contributors to global sea level rise while climate projections from GCM contain large uncertainties due to the complex feedback mechanism.

We emphasize that our estimates are for only those MG&IC that lie outside of Greenland and Antarctica. Therefore, the question on how to account for the huge number of MG&IC that are peripheral to the large ice sheets still remains open. Our projection of total volume change is possibly a very low bound, not accounting for ~50% or more of the total area of MG&IC that may now be, or will be, contributing to sea level rise.

2.6 References

ACIA (2005), *Impacts of a Warming Arctic: Arctic Climate Impact Assessment*, Cambridge University Press.

Arendt, A. A., K. A. Echelmeyer, W. D. Harrison, S. C. Lingle and V. B. Valentine (2002), Rapid wastage of Alaska glaciers and their contribution to rising sea level, *Science*, *297*, 382-386.

Bahr, D. B. (1997a), Width and length scaling of glaciers, *J. Glaciol.*, *43*(145), 557-562.

Bahr, D. B. (1997b), Global distributions of glacier properties: A stochastic scaling paradigm, *Water Resour. Res.*, *33*(7), 1669-1679.

Bahr, D. B., M. F. Meier and S. D. Peckham (1997), The physical basis of glacier volume-area scaling, *J. Geophys. Res.*, *102*(B9), 20355-20362.

Beck, C., J. Grieser and B. Rudolf (2005), A New Monthly Precipitation Climatology for the Global Land Areas for the Period 1951 to 2000, Climate Status Report 2004, pp. 181 - 190, German Weather Service, Offenbach, Germany.

Braithwaite, R. J. and Y. Zhang (1999), Modelling changes in glacier mass balance that may occur as a result of climate changes, *Geogr. Ann.*, *81A*(4), 489-496.

Braithwaite, R. J., Y. Zhang and S.C.B. Raper (2002), Temperature sensitivity of the mass balance of mountain glaciers and ice caps as a climatological characteristic, *Z. Gletscherk. Glazialgeol.*, *38*(1), 35-61.

Chen, J. and A. Ohmura (1990), Estimation of Alpine glacier water resources and their change since the 1870's. International Association of Hydrological Science Publication 193 (Symposium at Lausanne 1990 – Hydrology in Mountainous Regions. I – Hydrological Measurements; the Water Cycle) 127-135.

Cogley, J. G. (2003), GGHYDRO - Global Hydrographic Data, Release 2.3, Trent Technical Note 2003-1, Department of Geography, Trent University, Peterborough, Ontario, Canada.

de Woul M. (2008), Response of glaciers to climate change: Mass balance sensitivity, sea level rise and runoff, Doctoral dissertation, Department of Physical Geography and Quaternary Geology, Stockholm University.

de Woul, M. and R. Hock (2005), Static mass balance sensitivity of Arctic glaciers and ice caps using a degree-day approach, *Ann. Glaciol., 42*, 217-224.

Dyurgerov M. B. (2002), Glacier mass balance and regime: Data of measurements and analysis, Meier M. and R. Armstrong, eds. *INSTAAR Occasional Paper* No. 55.

Dyurgerov M. B. and M. F. Meier (1997), Year-to-year fluctuations of global mass balance of small glaciers and their contribution to sea-level changes, *Arctic Alp. Res., 29*(4), 392-402.

Dyurgerov M. B. and M. F. Meier (2005), Glaciers and the Changing Earth System: a 2004 Snapshot, Occasional Paper 58, Institute of Arctic and Alpine Research, University of Colorado, Boulder, Colorado, 117 p.

Elsberg, D. H., W. H. Harrison, K. A. Echelmeyer and R. M. Krimmel, (2001), Quantifying the effects of climate and surface change on glacier mass balance, *J. Glaciol., 47*(159), 649-658.

Gregory J. M. and J. Oerlemans (1998), Simulated future sea-level rise due to glacier melt based on regionally and seasonally resolved temperature changes, *Nature, 391*, 474-476.

Haeberli, W., M. Zemp, M. Hoelzle, R. Frauenfelder and A. Kääb (2005), Fluctuations of Glaciers, 1995-2000 (Vol. VIII), International Commission on Snow and Ice of International Association of Hydrological Sciences/UNESCO, Paris. [http://www.geo.unizh.ch/wgms.]

Hock R. (2003), Temperature index melt modeling in mountain areas, *J. Hydrol., 282,* 104-115, doi:10.1016/S0022-1694(03)00257-9.

Hock R., V. Radić, M. de Woul (2007), Climate sensitivity of Storglaciären – An intercomparison of mass balance models using ERA-40 reanalysis and regional climate model data, *Ann. Glaciol.*, 46, 342-348.

Holmlund, P. and T. Schneider (1997), The effect on continentality on glacier response and mass balance, *Ann. Glaciol., 24*, 272-276.

IPCC, (2007), Climate Change 2007: The Physical Science Basis. Contribution of working Group I to the Fourth Assessment Report of the Intergovernmental Panel on Climate Change [Solomon, S. and 7 others, (eds.)], Cambridge University Press, Cambridge, UK, 996 pp.

Kållberg, P. W., A. J. Simmons, S. M. Uppala, and M. Fuentes (2004), The ERA-40 Archive, *ERA-40 Project Report Series, 17*, ECMWF, Reading, 31 pp.

Kaser, G., J. G. Cogley, M.B. Dyurgerov, M. F. Meier and A. Ohmura (2006), Mass balance of glaciers and ice caps: Consensus estimates for 1961–2004, *Geophys. Res. Lett.*, **33**, L19501, doi:10.1029/2006GL027511.

Kjøllmoen, B. (ed.) (2001), *Glaciological investigations in Norway in 2000*, Report No. 2, ISSN 1502-3540, 122p.

Meier, M. F. and D. B. Bahr (1996), Counting glaciers: use of scaling methods to estimate the number and size distribution of the glaciers in the world, *CRREL Special Report,* 96-27, U.S. Army, Hanover, New Hampshire.

Meier, M. F., M. B. Dyurgerov, U. K. Rick, S. O'Neel, W. T. Pfeffer, R. S. Anderson, S. P. Anderson and A. F. Glazovsky (2007), Glaciers dominate eustatic eea-level rise in the 21st century, *Science*, doi:10.1126/science.1143906.

Mokievsky-Zubok, O., Ommanney, O. S. J. and J. Power (1985), NHRI Glacier Mass Balance 1964-1984 (Cordillera and Arctic) Glacier Section, Surface Water Division, National Hydrology Research Institute, Environment Canada.

Oerlemans J. and J. P. F. Fortuin (1992), Sensitivity of glaciers and small ice caps to greenhouse warming, *Science, 258,* 115-117.

Paterson, W. S. B. (1994), The physics of glaciers, Third edition, Oxford, etc., Elsevier.

Radić, V. and R. Hock (2006), Modelling mass balance and future evolution of glaciers using ERA-40 and climate models – A sensitivity study at Storglaciären, Sweden, *J. Geophys. Res., 111*, F03003, doi:10.1029/2005JF000440.

Radić, V., R. Hock and J. Oerlemans (2007), Volume-area scaling vs flowline modelling in glacier volume projections. *Ann. Glaciol., 46*, 234-240.

Radić V., R. Hock and J. Oerlemans (2008), Analysis of scaling methods in deriving future volume evolutions of valley glaciers, *J. Glaciol.,54*(187), *in press.*

Rahmstorf, S. (2007), A semi-empirical approach to projecting future sea-level rise, Science, *315*, 368-270, doi: 10.1126/science.1135456.

Raper, S. C. B. and R. J. Braithwaite (2006), Low sea level rise in projections from mountain glaciers and icecaps under global warming, *Nature, 439*, 311-313, doi:10.1038/nature04448.

Raper, S. C. B., O. Brown and R. J. Braithwaite, (2000), A geometric glacier model for sea-level change calculations, *J. Glaciol., 46*(154), 357-368.

Schneeberger, C., H. Blatter, A. Abe-Ouchi and M. Wild (2003), Modelling changes in the mass balance of glaciers of the northern hemisphere for a transient 2 x CO2 scenario, *J. Hydrol., 282*, 145-163.

van der Veen C. J. (2002), Calving glaciers, *Prog. Phys. Geog., 26*(1), 96-122.

van de Wal, R. S. W. and M. Wild (2001), Modelling the response of glaciers to climate change by applying volume-area scaling in combination with a high resolution GCM, *Climate Dyn. 18*, 359-366.

Vrugt, J.A., H.V. Gupta, W. Bouten and S. Sorooshian (2003), A shuffled complex evolution metropolis algorithm for optimization and uncertainty assessment of hydrological model parameters, *Water Resourc. Res.*, *39*(8), SWC11-SWC116.

Wagnon, P., P. Ribstein, G. Kaser and P. Berton (1999), Energy balance and runoff seasonality of a Bolivian glacier, *Global Planet. Change*, *22*, 49-58.

Williams, R. S., Jr., and Ferrigno, J. G., editors (1993), Satellite image atlas of glaciers of the world: U.S. Geological Survey Professional Paper 1386-E (Glaciers of Europe), 164 p. ISBN 0-067-71455-7.

Woodward, J., M. Sharp and A. Arendt (1997), The influence of superimposed-ice formation on the sensitivity of glacier mass balance to climate change, *Ann. Glaciol.*, *24*, 186-190.

Appendix 2.A

Table 2.A-1: 44 glaciers with observed seasonal mass balance profiles (≥ 4 years), location, and observational period of mass balance profiles. 8 glaciers which are excluded in multiple regression analysis are marked with grey color band

#	Glacier	Country	Lat	Lon	Observed seasons
1	Abramov	Kirghizstan	39.67°N	71.50°E	67/68, 70/71-82/83, 84/85-93/94
2	Ålfotbreen	Norway	61.75°N	5.67°E	63/64-96/97
3	Austdalsbreen	Norway	61.80°N	7.35°E	91/92-00/01
4	Austre Brøggerbreen	Norway	78.83°N	11.50°E	89/90-90/91, 92/93-94/95
5	Austre Okstindbreen	Norway	66.23°N	14.37°E	89/90-95/96
6	Bench	Canada	51.43°N	124.92°W	80/81-84/85
7	Blåisen	Norway	68.33°N	17.85°E	63/64-67/68
8	Bondhusbreen	Norway	60.03°N	6.33°E	76/77-80/81
9	Bridge	Canada	50.82°N	123.57°W	76/77-84/85
10	Djankuat	Russia	43.20°N	42.77°E	67/68-94/95
11	Engabreen	Norway	66.67°N	13.85°E	70/71-82/83, 84/85-00/01
12	Garabashi	Russia	43.30°N	42.47°E	85/86-94/95
13	Golubina	Kirghizstan	42.45°N	74.50°E	80/81-89/90
14	Gråsubreen	Norway	61.65°N	8.60°E	64/65-00/01
15	Hansebreen	Norway	61.75°N	5.68°E	85/86-86/87, 90/91-95/96
16	Hellstugubreen	Norway	61.57°N	8.43°E	64/65-96/97
17	Høgtuvbreen	Norway	66.45°N	13.65°E	70/71-76/77
18	Jostefonn	Norway	61.42°N	6.58°E	95/96-99/00
19	Kongsvegen	Svalbard	78.77°N	12.68°E	64/65-68/69, 70/71-00/01
20	Nordenskiöldbreen	Norway	78.13°N	15.45°E	68/69-69/70, 70/71-71/72
21	Nordmannsbreen	Norway	61.73°N	7.33°E	63/64-00/01
22	Nuolja	Sweden	68.05°N	18.55°E	89/90-94/95
23	Nigardsbreen	Norway	61.72°N	7.13°E	63/64-82/83, 84/85-00/01
24	Peyto	Canada	51.67°N	116.58°W	65/66-89/90, 93/94-94/95
25	Place	Canada	50.43°N	122.60°W	64/65-73/74, 80/81-88/89, 93/94-94/95
26	Ram River	Canada	51.85°N	116.18°W	65/66-68/69, 70/71-73/74
27	Rembesdalskåka	Norway	60.53°N	7.37°E	66/67-72/73, 84/85-00/01
28	Riukojietna	Sweden	68.08°N	18.08°E	85/86-87/88, 89/90, 95/96-96/97, 98/99-00/01
29	Sentinel	Canada	49.90°N	122.98°W	65/66-73/74, 80/81-88/89
30	South Cascade	USA	48.37°N	121.05°W	64/65-79/80
31	Storbreen	Norway	61.57°N	8.13°E	89/90-00/01
32	Storglaciären	Sweden	67.92°N	18.58°E	80/81-00/01
33	Storsteinfjellbreen	Norway	68.22°N	17.92°E	90/91-94/95
34	Svartisheibreen	Norway	66.58°N	13.75°E	87/88-93/94
35	Sykora	Canada	50.87°N	123.58°W	80/81-84/85
36	Trollbergdalsbreen	Norway	66.72°N	14.45°E	72/73-73/74, 89/90-93/94
37	Tsentralniy Tuyuksu	Kazakhstan	43.00°N	77.10°E	64/65-89/90
38	Tunsbergdalsbreen	Norway	61.60°N	7.05°E	65/66-71/72
39	Vermuntgletscher	Austria	46.85°N	10.13°E	90/91-94/95
40	Vestre Memurubre	Norway	61.53°N	8.50°E	67/68-71/72
41	Woolsey	Canada	51.12°N	118.05°W	65/66-71/72, 73/74
42	Zavisha	Canada	50.80°N	123.42°W	77/78, 80/81-84/85
43	Helm	Canada	50.00°N	123.00°W	85/86-88/89
44	Tiedemann	Canada	51.33°N	125.05°W	80/81-84/85

Table 2.A-1: Continued from previous page: 44 glaciers with number of elevation bands, maximum and minimum elevation, surface area and model parameters (lr_{ERA}, lr, DDF_{snow}, DDF_{ice}). 8 glaciers which are excluded in multiple regression analysis are marked with grey color band

#	# years	# elev	h_{max} [m]	h_{min} [m]	area [km2]	lr_{ERA} [K/100m]	lr [K/100m]	DDF_{snow} [mm/(°C d)]	DDF_{ice} [mm/(°C d)]
1	24	10	4650	3750	32.50	-0.69	-0.53	4.5	8.2
2	34	8	1325	975	4.46	-0.55	-0.69	3.8	5.4
3	10	11	1728	1225	11.86	-0.67	-0.44	3.2	6.3
4	5	11	575	75	6.12	-0.52	-0.33	7.2	9.0
5	7	10	1675	765	14.01	-0.77	-0.57	7.1	8.8
6	5	15	2850	1450	10.51	-0.66	-0.21	6.6	8.3
7	5	7	1175	875	2.18	-0.72	-0.59	3.9	4.9
8	5	13	1620	475	10.47	-0.82	-0.36	7.7	10.7
9	9	8	2250	1550	48.44	-0.93	-0.27	5.5	6.9
10	28	9	3550	2750	2.90	-0.64	-0.30	7.1	10.5
11	30	14	1550	250	37.93	-0.53	-0.43	3.9	6.2
12	12	14	4800	3350	4.47	-0.60	-0.71	2.8	4.0
13	10	22	4325	3275	6.28	-0.59	-0.33	4.6	8.5
14	37	8	2225	1875	2.34	-0.75	-0.65	6.3	8.3
15	8	9	1310	937	3.32	-0.75	-0.72	5.2	6.5
16	33	13	2075	1475	3.09	-0.60	-0.41	3.1	6.2
17	7	12	1155	620	2.60	-0.66	-0.26	6.2	7.8
18	5	8	1610	980	3.81	-0.84	-0.42	5.5	8.0
19	8	11	1975	940	1.80	-0.27	-0.11	4.5	5.6
20	10	6	950	450	2.97	-0.75	-0.41	4.1	5.8
21	8	7	3900	2500	36.63	-0.42	-0.41	3.9	6.3
22	9	23	1770	1350	83.91	-0.64	-0.58	4.2	5.8
23	37	15	1850	450	46.63	-0.75	-0.47	5.5	6.9
24	27	9	2950	2150	13.05	-0.84	-0.81	3.9	4.9
25	21	8	2550	1850	3.79	-0.69	-0.53	2.4	4.9
26	8	6	3010	2580	1.83	-0.77	-0.18	6.3	9.7
27	24	15	1825	1125	17.18	-0.54	-0.33	2.9	5.8
28	9	15	1450	1170	4.62	-0.50	-0.24	2.6	5.2
29	18	4	1950	1650	1.57	-1.00	-0.60	5.3	8.2
30	16	6	2200	1700	1.74	-0.73	-0.94	2.5	5.0
31	12	13	2075	1475	5.20	-0.70	-0.44	4.9	8.5
32	21	30	1730	1150	3.40	-0.67	-0.32	6.1	7.7
33	5	18	1825	985	6.03	-0.64	-0.43	4.7	5.9
34	7	14	1410	785	5.48	-0.67	-0.38	6.0	9.8
35	5	14	2750	1450	25.35	-0.97	-0.57	7.0	8.8
36	7	8	1275	925	1.79	-0.77	-0.39	5.5	6.9
37	26	8	4160	3450	3.05	-0.60	-0.38	5.9	7.5
38	7	15	1915	570	47.18	-0.73	-0.27	5.9	8.6
39	5	7	3150	2550	2.24	-0.56	-0.56	3.7	7.0
40	5	14	2215	1586	9.03	-0.72	-0.30	6.3	10.2
41	8	8	2635	1960	3.89	-0.85	-0.42	5.1	6.5
42	6	5	2450	2050	6.49	-0.58	-0.38	2.5	4.0
43	4	4	2150	1850	2.25	-0.69	-0.10	3.0	5.9
44	5	11	3350	2350	34.87	-0.34	-0.34	4.5	5.7

Table 2.A-1: Continued from previous page: 44 glaciers with model parameters (k_P, d_{prec}, T_{snow}), mass balance sensitivities to temperature and precipitation change, continentality index (CI), annual sum of precipitation and mean glacier elevation

#	k_P	d_{prec} [1/100m]	T_{snow} [°C]	db/dT [m/(K yr)]	db/dP [m/(10%yr)]	CI [K]	P_{annual} [mm]	h_{mean} [m]
1	11.0	0.105	0.84	-0.72	0.00	21.6	252	4200
2	2.6	0.000	1.82	-1.11	0.40	13.6	2383	1150
3	3.1	0.114	1.01	-0.69	0.23	16.2	1399	1476.5
4	2.6	0.000	0.77	-0.96	0.07	14.7	363	325
5	2.5	0.072	0.97	-0.87	0.22	19.2	1561	1220
6	3.5	0.051	1.02	-0.97	0.17	19.0	1066	2150
7	4.6	0.153	1.72	-0.62	0.16	19.8	820	1025
8	1.8	0.105	0.81	-1.23	0.26	16.4	2440	1047.5
9	2.8	0.104	0.44	-0.99	0.18	19.8	1093	1900
10	4.8	0.066	2.00	-1.36	0.30	22.7	996	3150
11	3.2	0.080	0.61	-0.80	0.33	18.2	2010	900
12	0.8	0.407	0.56	-0.34	0.00	22.9	1189	4075
13	5.6	0.122	1.16	-0.71	0.10	23.7	399	3800
14	3.4	0.069	0.03	-0.79	0.12	18.1	517	2050
15	2.6	0.039	0.49	-1.21	0.35	13.6	2383	1123.5
16	3.7	0.094	1.50	-0.70	0.17	18.1	644	1775
17	2.9	0.078	1.20	-1.16	0.33	17.5	1959	887.5
18	3.3	0.038	0.48	-0.97	0.31	15.5	1578	1295
19	1.6	0.156	0.00	-1.06	0.31	15.9	1578	1295
20	2.2	0.000	0.00	-1.06	0.31	15.9	1578	1295
21	2.2	0.000	0.00	-1.06	0.31	15.9	1578	1295
22	2.2	0.000	0.00	-1.06	0.31	15.9	1578	1295
23	2.9	0.047	1.97	-0.91	0.30	16.3	1399	1150
24	3.2	0.062	0.49	-0.63	0.15	23.3	753	2550
25	1.9	0.071	0.90	-0.79	0.27	19.6	1689	2200
26	4.3	0.173	0.57	-0.81	0.13	23.3	605	2795
27	3.7	0.122	1.88	-0.65	0.26	18.2	1125	1475
28	3.6	0.120	0.86	-0.77	0.21	21.2	703	1310
29	1.9	0.183	0.86	-1.09	0.42	17.9	3004	1800
30	2.1	0.000	1.44	-0.87	0.35	19.1	1713	1950
31	6.0	0.096	1.23	-0.87	0.22	17.8	644	1775
32	12.0	0.152	0.02	-0.81	0.24	22.1	547	440
33	4.9	0.074	1.76	-0.57	0.19	21.2	820	1405
34	2.6	0.050	2.00	-1.05	0.36	18.2	2010	1097.5
35	3.0	0.054	0.04	-0.78	0.20	19.8	1093	2100
36	2.7	0.088	2.00	-0.82	0.27	18.7	1679	1100
37	5.6	0.128	1.48	-0.77	0.14	22.9	574	3805
38	3.3	0.059	0.53	-1.06	0.25	16.3	1399	1242.5
39	1.8	0.005	1.34	-1.06	0.18	18.2	1041	2850
40	6.2	0.076	0.04	-0.96	0.15	18.1	517	1900
41	3.5	0.065	0.70	-0.80	0.28	23.5	1275	2297.5
42	3.4	0.095	2.00	-0.68	0.21	19.8	901	2250
43	2.4	0.241	0.00	-1.29	0.19	17.9	1689	2000
44	2.8	0.091	1.69	-0.92	0.18	19.0	1335	2850

Table 2.A-1: Continued from previous page: 44 glaciers with correlation statistics between modeled and measured mass balance (r^2 and root mean square error, RMSE). 8 glaciers which are excluded in multiple regression analysis are marked with grey color band

#	r^2 (b profiles)			r^2 (area-average b)			RMSE of b profiles (m)			RMSE of area-average b		
	b_w	b_s	b_n	b_w	b_s	b_n	b_w	b_s	b_n	b_w	b_s	b_n
1	0.98	0.98	0.99	0.47	0.59	0.63	0.03	0.05	0.10	0.08	0.18	0.24
2	0.78	1.00	0.97	0.79	0.46	0.75	0.05	0.01	0.08	0.35	0.26	0.51
3	0.81	0.99	0.95	0.88	0.68	0.87	0.08	0.05	0.13	0.05	0.09	0.12
4	0.87	0.88	0.89	0.43	0.00	0.18	0.01	0.05	0.07	0.33	0.31	1.12
5	0.78	0.98	0.95	0.87	0.36	0.49	0.12	0.07	0.36	0.06	0.20	0.30
6	0.88	0.88	0.88	0.52	0.57	0.91	0.08	0.21	0.55	0.04	0.58	0.45
7	0.91	0.97	0.99	0.90	0.40	0.69	0.02	0.01	0.02	0.03	0.25	0.37
8	0.97	1.00	0.99	0.87	0.09	0.47	0.05	0.05	0.12	0.15	1.19	1.50
9	0.99	1.00	1.00	0.75	0.40	0.57	0.02	0.04	0.01	0.03	0.35	0.32
10	0.98	0.98	0.98	0.10	0.46	0.17	0.41	0.08	0.35	0.59	0.53	1.13
11	0.98	0.98	0.99	0.76	0.56	0.80	0.05	0.13	0.20	0.16	0.25	0.25
12	0.01	0.98	0.70	0.00	0.60	0.34	0.99	0.03	1.07	1.26	0.03	1.24
13	0.31	0.98	0.93	0.74	0.53	0.57	0.13	0.06	0.29	0.01	0.25	0.34
14	0.63	0.99	0.77	0.25	0.76	0.61	0.05	0.13	0.34	0.05	0.11	0.20
15	0.41	1.00	0.92	0.92	0.26	0.62	0.16	0.04	0.20	0.14	0.35	0.64
16	0.95	1.00	0.99	0.44	0.63	0.59	0.02	0.02	0.03	0.05	0.09	0.16
17	0.89	0.97	0.95	0.92	0.61	0.59	0.04	0.02	0.10	0.11	0.39	0.50
18	0.73	0.94	0.89	0.96	0.53	0.93	0.08	0.28	0.37	0.11	0.24	0.11
19	0.80	0.10	0.17	0.70	0.55	0.08	0.28	3.38	2.99	0.40	0.34	0.83
20	0.98	1.00	0.99	0.45	0.44	0.36	0.01	0.01	0.02	0.14	0.13	0.20
21	0.67	0.97	0.96	0.87	0.75	0.53	0.02	0.11	0.16	0.06	0.24	0.45
22	0.69	0.99	0.88	0.33	0.67	0.56	0.12	0.00	0.15	0.13	0.05	0.12
23	0.95	0.99	1.00	0.59	0.40	0.56	0.07	0.22	0.33	0.20	0.31	0.50
24	1.00	0.96	0.97	0.37	0.27	0.21	0.04	0.12	0.12	0.06	0.18	0.29
25	0.96	0.98	0.98	0.29	0.46	0.34	0.01	0.07	0.11	0.12	0.17	0.47
26	0.95	0.94	0.94	0.51	0.93	0.87	0.04	0.04	0.08	0.02	0.16	0.15
27	0.95	1.00	1.00	0.53	0.51	0.45	0.08	0.06	0.01	0.33	0.20	0.71
28	0.05	0.96	0.95	0.92	0.36	0.41	0.03	0.03	0.02	0.01	0.24	0.25
29	0.96	1.00	0.99	0.31	0.34	0.36	0.94	0.36	2.24	0.54	0.36	0.73
30	0.60	0.98	0.92	0.85	0.29	0.79	0.26	0.06	0.46	0.11	0.20	0.35
31	0.95	1.00	0.99	0.83	0.71	0.74	0.01	0.03	0.06	0.05	0.17	0.30
32	0.71	0.99	0.90	0.58	0.75	0.58	0.21	0.02	0.29	0.11	0.19	0.21
33	0.93	0.98	0.97	0.96	0.26	0.88	0.02	0.02	0.07	0.02	0.06	0.07
34	0.54	0.95	0.85	0.92	0.87	0.94	0.18	0.05	0.41	0.08	0.14	0.20
35	0.97	0.97	0.99	0.88	0.79	0.88	0.02	0.67	0.64	0.02	0.59	0.54
36	0.48	0.99	0.93	0.90	0.58	0.84	0.16	0.13	0.06	0.05	0.15	0.11
37	0.23	0.98	0.94	0.06	0.03	0.07	0.46	0.05	0.78	0.05	0.78	0.79
38	0.99	1.00	1.00	0.46	0.28	0.41	0.01	0.02	0.02	0.34	0.42	1.01
39	0.00	0.96	0.95	0.14	0.82	0.66	0.03	0.13	0.11	0.09	0.13	0.22
40	0.65	0.97	0.98	0.57	0.89	0.82	0.02	0.03	0.02	0.08	0.25	0.25
41	0.98	0.99	0.99	0.42	0.36	0.42	0.01	0.05	0.06	0.15	0.38	0.60
42	0.94	0.97	0.98	0.27	0.66	0.41	0.03	0.02	0.07	0.10	0.23	0.38
43	0.99	0.97	0.99	0.05	0.11	0.03	0.24	0.15	0.16	0.42	0.94	1.50
44	0.93	0.96	0.96	0.90	0.95	0.93	0.07	0.10	0.20	0.02	0.05	0.09

Table 2.A-2: Total volume change over 1961-1990 in SLE for five different cases of upscaling: b_n corresponds to the upscaling which assumes that mean volume change of MG&IC from WGI in each size bin is the representative volume change for the whole bin, while for b_n-σ the representative volume changes in the bin is: mean volume change + standard deviation of volume changes in each bin, and for b_n+σ the representative is: mean - standard deviation. For $min(b_n)$ and $max(b_n)$ the representative volume change is the minimum and the maximum volume change in each size bin. Marked values present the closest match to estimated volume changes from grid-based mean specific mass balances, $\Delta V_{grid\text{-}based}$ (Figure 2.4)

#	Region	$\Delta V_{grid\text{-}based}$ SLE (mm yr^{-1})	$\Delta V_{upscaled}$ in SLE (mm yr^{-1})				
			b_n	b_n-σ	b_n+σ	$min(b_n)$	$max(b_n)$
1	Svalbard	0.047	0.036	0.011	0.061	-0.021	0.073
2	Scandinavia	-0.023	-0.014	-0.015	-0.011	-0.015	-0.008
3	Central Europe	-0.010	-0.009	-0.014	-0.003	-0.014	0.005
4	Franz Joseph Land	0.040	0.037	0.029	0.045	0.023	0.054
5	Novaya Zemlya	0.048	0.047	0.037	0.057	0.026	0.063
6	Severnaya Zemlya	0.049	0.044	0.038	0.049	0.037	0.051
7	Caucasus	-0.012	-0.010	-0.011	-0.006	-0.011	-0.001
8	North and East Asia	-0.016	-0.012	-0.015	-0.006	-0.015	0.009
9	High Mountain Asia	-0.065	-0.075	-0.428	0.298	-0.673	0.991
10	Alaska (131°W-155°W)	-0.183	-0.267	-0.557	0.043	-0.655	0.208
11	Rocky Mountains (109°W-130°W)	-0.078	-0.077	-0.097	-0.036	-0.097	0.033
12	Arctic Canada	-0.012	0.077	0.054	0.121	-0.079	0.172
13	Iceland	-0.030	-0.030	-0.034	-0.026	-0.033	-0.025
14	South America (10°N-30°S)	-0.031	0.004	-0.011	0.018	-0.022	0.026
15	South America (30°S-55°S)	-0.026	-0.087	-0.188	0.018	-0.199	0.080
16	New Zealand	-0.004	-0.004	-0.004	-0.003	-0.004	-0.003
	Total	-0.305	-0.335	-1.224	0.620	-1.752	1.728

Table 2.A-3: Volume change in SLE over 2001-2100 for MG&IC from WGI (ΔV_{WGI}) and total volume changes from five different cases of upscaling: b_n corresponds to the upscaling which assumes that mean volume change of MG&IC from WGI in each size bin is the representative volume change for the whole bin, while for b_n-σ the representative volume changes in the bin is: mean volume change + standard deviation of volume changes in each bin, and for b_n+σ the representative is: mean - standard deviation. For $min(b_n)$ and $max(b_n)$ the representative volume change is the minimum and the maximum volume change in each size bin. *bn'* is the 'best upscaling approximation'

#	Region	UKMO-HadCM3							GFDL-CM2.0						
		ΔV_{WGI}	$\Delta V_{upscaled}$ in SLE (mm) 2001-2100						ΔV_{WGI}	$\Delta V_{upscaled}$ in SLE (mm) 2001-2100					
		SLE (mm)	b_n	b_n-σ	b_n+σ	min(b_n)	max(b_n)	b_n'	SLE (mm)	b_n	b_n-σ	b_n+σ	min(b_n)	max(b_n)	b_n'
1	Svalbard	-5.7	-6.7	-10.6	-2.5	-12.4	-0.1	-6.7	-2.5	-3.2	-7.1	0.6	-9.9	2.7	-3.2
2	Scandinavia	-0.2	-0.4	-0.4	-0.3	-0.4	-0.3	-0.4	-0.2	-0.4	-0.4	-0.3	-0.4	-0.3	-0.4
3	Central Europe	-0.5	-0.4	-0.5	-0.3	-0.5	-0.3	-0.4	-0.5	-0.4	-0.4	-0.3	-0.5	-0.2	-0.4
4	Franz Joseph Land	3.4	3.5	1.6	5.0	-0.1	5.4	3.5	3.5	3.6	1.6	4.7	-0.1	5.5	3.6
5	Novaya Zemlya	2.2	2.2	0.3	4.2	-1.1	5.3	2.2	2.5	2.5	0.4	4.5	-1.2	5.7	2.5
6	Severnaya Zemlya	4.9	4.6	3.7	5.4	3.2	5.7	5.4	5.2	4.9	4.1	5.6	3.7	5.9	5.6
7	Caucasus	-0.2	-0.3	-0.3	-0.2	-0.3	-0.2	-0.3	-0.2	-0.3	-0.3	-0.2	-0.3	-0.2	-0.3
8	North and East Asia	-0.2	-0.4	-0.5	-0.3	-0.5	0.3	-0.5	-0.2	-0.4	-0.5	-0.2	-0.5	0.3	-0.5
9	High Mountain Asia	-3.5	-6.0	-25.0	20.8	-25.7	27.3	-6.0	-4.7	-7.7	-25.6	19.1	-26.0	23.6	-7.7
10	Alaska (131°W-155°W)	-15.6	-27.1	-40.3	-9.1	-40.7	-0.1	-27.1	-11.9	-20.1	-36.1	-1.2	-36.8	3.9	-20.1
11	Rocky Mountains (109°W-130°W)	-0.3	-2.9	-2.9	-2.1	-2.9	-1.5	-2.9	-0.3	-2.8	-2.9	-2.0	-2.9	-1.0	-2.8
12	Arctic Canada	-2.3	-10.3	-26.7	6.1	-36.5	16.7	-26.7	-0.1	0.3	-9.9	10.5	-20.0	17.2	-9.9
13	Iceland	-9.9	-9.9	-10.0	-9.4	-10.0	-9.3	-9.9	-8.7	-8.7	-8.9	-8.3	-8.9	-8.3	-8.7
14	South America (10°N-30°S)	-0.1	-0.8	-0.9	-0.6	-0.9	0.0	-0.9	-0.1	-0.5	-0.8	0.2	-0.9	0.6	-0.9
15	South America (30°S-55°S)	-0.2	-5.0	-6.5	-2.3	-6.4	2.1	-5.0	-0.2	-4.9	-6.4	-2.3	-6.3	1.7	-4.9
16	New Zealand	0.0	-0.1	-0.1	-0.1	-0.1	-0.1	-0.1	0.0	-0.1	-0.1	-0.1	-0.1	-0.1	-0.1
	Total	-28.3	-60.2	-119.2	14.1	-135.4	51.1	-75.8	-18.4	-38.5	-93.4	30.4	-111.1	57.0	-48.4

Table 2.A-3: Continued from previous page

#	Region	ΔV_{WGI}	CCSM3 $\Delta V_{upscaled}$ in SLE (mm) 2001-2100				
		SLE (mm)	b_n	$b_n-\sigma$	$b_n+\sigma$	$\min(b_n)$	$\max(b_n)$
1	Svalbard	-18.3	-18.6	-19.2	-14.3	-19.2	-13.6
2	Scandinavia	-0.2	-0.4	-0.4	-0.3	-0.4	-0.3
3	Central Europe	-0.5	-0.4	-0.5	-0.3	-0.5	-0.2
4	Franz Joseph Land	-5.2	-5.3	-5.3	-3.9	-5.3	-3.6
5	Novaya Zemlya	-10.9	-10.6	-11.0	-9.2	-11.0	-8.8
6	Severnaya Zemlya	-12.0	-11.3	-12.3	-9.8	-12.4	-9.6
7	Caucasus	-0.2	-0.3	-0.3	-0.2	-0.3	-0.2
8	North and East Asia	-0.3	-0.5	-0.5	-0.3	-0.5	-0.2
9	High Mountain Asia	-2.7	-4.9	-24.8	22.0	-25.5	27.3
10	Alaska (131°W-155°W)	-14.8	-25.8	-38.8	-8.3	-39.1	-0.1
11	Rocky Mountains (109°W-130°W)	-0.3	-2.9	-2.9	-2.1	-2.9	-0.8
12	Arctic Canada	-13.1	-53.6	-58.5	-40.0	-59.2	-35.6
13	Iceland	-10.3	-10.3	-10.3	-9.8	-10.3	-9.8
14	South America (10°N-30°S)	-0.1	-0.4	-0.8	0.2	-0.9	0.6
15	South America (30°S-55°S)	-0.2	-4.4	-6.3	-1.4	-6.2	1.4
16	New Zealand	0.0	-0.1	-0.1	-0.1	-0.1	-0.1
	Total	-89.1	-149.8	-192.0	-77.9	-193.8	-53.7

		ECHAM5/MPI-OM					
	ΔV_{WGI}	$\Delta V_{upscaled}$ in SLE (mm) 2001-2100					
b_n'	SLE (mm)	b_n	$b_n-\sigma$	$b_n+\sigma$	min(b_n)	max(b_n)	b_n'
-18.6	-4.9	-5.8	-10.8	-0.6	-13.8	2.2	-5.8
-0.4	-0.2	-0.4	-0.4	-0.3	-0.4	-0.3	-0.4
-0.4	-0.5	-0.4	-0.4	-0.3	-0.5	-0.1	-0.4
-5.3	0.3	0.3	-2.2	2.7	-2.9	4.2	0.3
-10.6	1.4	1.5	-1.5	4.4	-2.1	5.8	1.5
-9.8	4.5	4.2	3.0	5.4	2.3	5.8	5.4
-0.3	-0.2	-0.3	-0.3	-0.2	-0.3	-0.2	-0.3
-0.5	-0.3	-0.4	-0.5	-0.3	-0.5	0.1	-0.5
-4.9	-4.9	-8.0	-24.8	16.5	-25.5	25.4	-8.0
-25.8	-14.2	-23.7	-38.9	-4.4	-39.3	1.7	-23.7
-2.9	-0.3	-2.9	-2.9	-2.0	-2.9	-0.5	-2.9
-58.5	-1.0	-4.7	-17.1	7.7	-27.4	16.8	-17.1
-10.3	-2.7	-2.8	-3.0	-2.5	-3.0	-2.5	-2.8
-0.9	-0.1	-0.8	-0.9	-0.5	-0.9	0.0	-0.9
-4.4	-0.2	-4.6	-6.5	-1.5	-6.4	2.1	-4.6
-0.1	0.0	-0.1	-0.1	-0.1	-0.1	-0.1	-0.1
-153.6	-23.3	-49.0	-107.4	24.1	-123.8	60.5	-60.4

Chapter 3

Modeling future glacier mass balance and volume changes using ERA40-reanalysis and climate models – A sensitivity study at Storglaciären, Sweden[1]

3.1 Abstract

Modeling the response of glaciers to future climate change is important for predicting changes in global sea-level rise and local water resources. We compute the mass balance and volume evolution of Storglaciären, a small valley glacier in Sweden, until 2100, using a temperature-index mass balance model. We focus on the sensitivity of results to the choice of climate model and variants of adjusting ERA-40 temperatures to local conditions. ERA-40 temperature and precipitation series from 1961-2001 are validated and used both as input to the mass balance model and for statistical downscaling of one regional and six global climate models (GCMs). Future volume projections are computed using area-volume scaling and constant glacier area. ERA-40 data correlates well with observations and captures observed inter-annual variability of temperature and precipitation. The mass balance model driven by several variants of ERA-40 input performs similarly well regardless of temporal resolution of the input series (daily or monthly). The model explains ~70% of variance of measured mass balance when the input temperatures are reduced by the lapse rate that maximizes model performance. Fitting ERA-40 temperatures to observations close to the glacier does not improve the performance of the model, leading us to conclude that ERA-40 can be used for mass balance modeling independent of meteorological observations. Projected future volume series show a loss of 50-90% of the initial volume by 2100. The differences in volume projections vary by 40% of the initial volume for six different GCMs input to mass balance model, while each volume projection varies by 20% depending on whether volume-area scaling or constant area is used and by 10% depending on details in the mass balance model used. The correction of biases in the seasonal temperature cycle of the GCMs with respect to the ERA-40 data is crucial for deriving realistic volume evolution. Static mass balance sensitivities to temperature and precipitation change in the 21st century are -0.48 m a^{-1} K^{-1} and 0.025 m a^{-1} per % increase, respectively.

---

[1]Published as Radić V. and R. Hock (2006), Modelling future glacier mass balance and volume changes using ERA40-reanalysis and climate models –A sensitivity study at Storglaciären, Sweden. *J. Geophys. Res.*, *111*, F03003, doi:10.1029/2005JF000440.

3.2 Introduction

Glaciers have generally retreated during the last century with notably accelerated mass losses in recent years [*Dyurgerov and Meier*, 2000; *Meier et al.*, 2003]. Further glacier wastage will have major implications on all spatial scales, ranging from local effects on river runoff [*Hock et al.*, 2005] to global effects through melt water contribution to sea-level rise [e.g. *Church et al.*, 2001; *Arendt et al.*, 2002]. Modeling the response of glaciers to future climate change therefore has major societal implications. Traditionally, glacier models have been forced by meteorological observations in the vicinity of the glaciers [e.g., *Schneeberger et al.*, 2001; *Adalgeirsdottir et al.*, 2006], but scarcity of meteorological data in remote glacierized areas poses serious constraints to such an approach and hampers larger-scale glacier modeling.

Climate reanalysis products can be very useful for investigating climatic patterns of largely inaccessible regions, thus circumventing the need for direct meteorological measurements. Reanalyses are derived by processing multi-decadal sequences of past meteorological observations using modern data assimilation techniques developed for numerical weather prediction. The result is a dynamically consistent three-dimensional gridded data set that represents the best estimate of the state of the atmosphere at a certain time. Therefore, it should be superior to the gridded climatology of the Climate Research Unit (CRU) which is derived from interpolation of observations [*New at al.*, 1999], and has been used in mass balance modeling [*Raper and Braithwaite*, 2006]. Reanalyses products are as yet little exploited in glacier monitoring. *Hanna et al.* [2001], *Reichert et al.* [2001] and *Rasmussen et al.* [2004] have used NCEP/NCAR reanalysis or the 15-year reanalysis (ERA-15, 1979-1993) by the European Centre for Medium-Range Weather Forecast (ECMWF) to estimate present glacier mass balance, or have used them to downscale the output from Global Climate Models (GCMs) in order to model future mass balance changes. Recently, ECMWF completed the ERA-40 project, which produced a global reanalysis of the state of the atmosphere, land and surface over the period of mid-1957 to mid-2002 [*Simmons and Gibson*, 2000; *Kållberg et al.*, 2004]. This 'second-generation' ECMWF reanalysis, ERA-40, opens a new potential in glacier-climate modeling [e.g., *Velicogna et al.*, 2005].

In this study we estimate the mass balance and volume changes of Storglaciären, a small valley glacier in northern Sweden, for the 21st century using climate scenarios derived from one

Regional Climate Model (RCM) and six GCMs downscaled by means of ERA-40 data. Storglaciären is chosen as the best case since it is a well investigated glacier with a wealth of available data. Specifically, it has the longest detailed mass balance record in the world [*Holmlund et al.*, 2005]. We use a simple mass balance model based on air temperature and precipitation data and apply volume-area scaling [*Bahr et al.*, 1997] for the volume change computations.

The specific goals are (1) to validate the ERA-40 data in the study area and to explore the potential to use ERA-40 data in mass balance modeling, (2) to investigate the sensitivity of the results to variations in the input of the mass balance model, such as variations caused by using monthly or daily input data, using different calibration periods, and applying different downscaling methods for the ERA-40 data, (3) to investigate the sensitivity of mass balance and volume predictions to the choice of the GCM, and (4) to derive the mass balance sensitivities for the 21st century. Hence, this study focuses on sensitivity analyses, addressing uncertainties in the modeling of the response of glaciers to climate change. We present a methodology to use daily or monthly ERA-40 data and statistically downscaled monthly GCM-output for glacier predictions which, due to its modest data requirements, may be suitable to predict future glacier wastage on large spatial scales.

3.3 Study site

Storglaciären (67.90°N, 18.57°E) has a length of 3 km and an area of approximately 3.1 km^2, ranging from 1130 m to 1720 m a.s.l. in altitude. The average and maximum ice thicknesses are 95 m and 250 m, respectively. The glacier is temperate with a perennial cold (<0°C) surface layer in the ablation area reaching up to 60 m in depth [*Pettersson et al.*, 2004]. Storglaciären is located along a strong climate gradient with a maritime climate in the west and a more continental climate towards the east, due to a dominant wind direction from the west and the effect of topography. The glacier has been intensively studied for several decades. Glacio-meteorological studies have revealed that the turbulent fluxes contribute on average 40-60% of the energy available for melt [*Hock and Holmgren*, 1996; 2005]. The mean annual air temperature (1965-2003) at Tarfala Research Station (67.92°N, 18.60°E, 1130 m a.s.l.) located ~1 km from the glacier is -3.7°C, and summer temperature (June – August) is 5.7°C, while annual precipitation is estimated to amount roughly to 1000 mm.

The glacier has retreated considerably since the beginning of 20th century when its front reached the maximum in response to cooling during the 19th century [*Holmlund*, 1987]. The retreat was interrupted by periods of higher winter precipitation in the mid-1970s which translated into a complete halt in the retreat during the 1980s. A period of significantly enhanced winter precipitation between the late 1980s and mid-1990s caused positive mass balances and mass gain but no change in terminus position. Studies of glacier-climate coupling show that the net balance of Storglaciären is well correlated with the summer temperature at the Tarfala Research Station [*Holmlund*, 1987].

3.4 Data

Our study is based on various data sets including the mass balance record of Storglaciären, daily temperature data from Tarfala Research Station, daily temperature and precipitation data from four additional meteorological stations up to 80 km away from the glacier, daily temperature and precipitation analyses from ERA-40 and a RCM from several grid points close to the glacier for the period 1958-2001 and 1961-2100, respectively, and monthly temperature and precipitation data from the grid point closest to Storglaciären from six GCMs for the period 1961 to 2100. These data sets are briefly described below.

3.4.1 Mass balance of Storglaciären

A detailed mass balance program was initiated in 1945 and revised with time. Since 1966 winter mass balance has been computed from snow probings on a regular 100 x 100 m grid and several density pits. Ablation stakes at a density of about 20 per km^2 are used for the summer balance. Winter and summer data have been extrapolated to five topography maps generated at 10 year intervals to yield area-averaged mass balances [*Holmlund et al.*, 2005]. Since 1969, according to available maps, the glacier area change is less than 1%. Mean winter, summer and net balances (in water equivalent) for the period 1945/46 -2003/2004 are +1.43, -1.66, and -0.23 m a^{-1}, respectively.

3.4.2 Meteorological observations

Daily temperature and precipitation data were available from Tarfala Research Station (67.92°N, 18.58°E, 1135 m asl) for the period 1965 to date and from four additional weather stations run by the Swedish Meteorological and Hydrological Institute (SMHI) but for shorter time periods (Figure 3.1): Ritsem (67.73°N, 17.47°E, 524 m asl., 1981-2002), Riksgränsen (68.43°N, 18.13°E,

508 m asl., 1961-2002), Abisko (68.36°N, 18.82°E, 388 m asl., 1966-2001) and Nikkaluokta (67.85°N, 19.02°E, 468 m asl., 1966-1975).

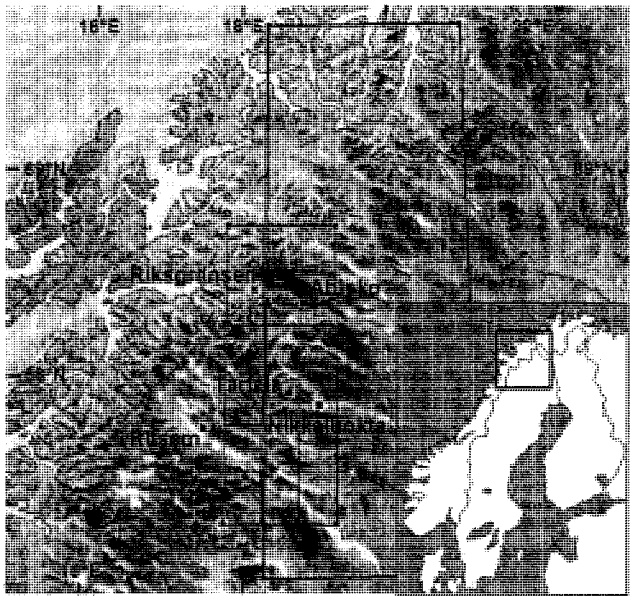

Figure 3.1. Study area including the meteorological stations used for validation of ERA-40 data. Storglaciären is located ~1 km south-west of Tarfala. Nine grid cells with the resolution of 0.5°x0.5° (~50 km^2) correspond to ERA-40 gridded data, while the large grid cell for comparison shows the grid cell used from the GCM with highest resolution (ECHAM/OPYC3, 2.8°x2.8°).

3.4.3 Reanalysis data: ERA-40

The 40-year reanalysis project of the ECMWF, ERA-40, uses the ECMWF numerical weather forecast model to produce gridded analyses of the state of the atmosphere with a 6-hour time interval. Through data assimilation, meteorological observations along with data from satellites and information from a previous model forecast are input into a short-range weather forecast model. This is integrated forward and combined with observational data for the corresponding period. ERA-40 is derived for the period of mid-1957 to mid-2002 and it covers the whole globe with spectral resolution T_L159, corresponding to a grid-spacing close to 125 km (1.125°) in the horizontal and with sixty levels in the vertical [*Källberg et al.*, 2004]. Until 1967 almost no observations from Scandinavia were included in the ERA-40 assimilation, which resulted in an underestimation of the observed warming trend over that region for the period 1958-2001. The

overall observing system improved at the end of 1978 when more satellite temperature and humidity observations became available to include in the analysis. As a result, the accuracy of medium-range forecasts initiated from the ERA-40 analysis improved from 1979 onwards [*Simmons et al.*, 2004]. In comparison with the NCEP/NCAR reanalysis, ERA-40 monthly temperatures show better agreement in trends and variability to the CRU climatology based on observations [*Simmons et al.*, 2004].

We retrieved 6-hourly 2 m air temperature and precipitation ERA-40 data from a bi-linearly interpolated grid (0.5° x 0.5°) for the area containing Storglaciären, forming 3 x 3 grid cells with the grid cell containing Storglaciären in the center (Figure 3.1). The data represent averages over a grid cell. Daily temperature of each grid cell is calculated as the average of the 6-hourly temperature. Daily precipitation is based on the forecasted fields. Since the forecast is affected by spin-up effects, the most reliable technique to derive daily precipitation is to use the 24h forecasts that are started every 12 hours [*Martin*, 2004]. We subtract the precipitation accumulated in 12 hours for each run from the precipitation accumulated in 24 hours for the same run. Precipitation derived for 00-12 h and 12-24 h time intervals is then summed to provide daily precipitation.

3.4.4 Regional climate model: RCA3

Predictions of temperature and precipitation are derived from the regional climate model RCA3 of the Rossby Centre of the Swedish Meteorological and Hydrological Institute [Kjellström et al., 2005]. It runs with a resolution of about 50 km grid spacing on an area of roughly 5000 x 5000 km^2 with Scandinavia in focus for the time period of 1961-2100. The lateral boundaries are given by output of the General Circulation Model ECHAM4/OPYC3, and runs are forced by A2 and B2 emission scenarios from IPCC (2001).

We retrieved 3-hour temperature and precipitation data for 1961 to 2100 from the runs with B2 emission scenarios for the grid points covering the study area (66-70°N, 16-20°E). The B2 emission scenario represents a modest scenario among the large suite of available emission scenarios. We chose the B2 run since it has widely been used in climate impact studies [e.g., *Oerlemans et al.*, 2005]. Daily data were calculated as the arithmetical averages of 3-hour temperatures and as the sum of 3-hour precipitation values.

3.4.5 General circulation models

Time series of monthly temperature and precipitation as predicted by six GCMs (ECHAM/OPYC3, HADCM3, CSIRO-Mk2, GFDL-R30, CGCM2, CCSR/NIES) were downloaded from the IPCC Data Distribution Centre (http://ipcc-ddc.cru.uea.ac.uk/). As for the RCA data, we use the predictions based on the B2 emission scenario (IPCC, 2001). Downloaded data series span from 1961 to 2100. For each model only the data from the output grid point nearest to Storglaciären was considered in further analysis. More details about the gridded climate data sets are given in Table 3.1.

Table 3.1. Gridded climate data sets used in this study including horizontal resolution, and the elevation and coordinates of the grid point closest to Storglaciären

Data set	Model	Resolution	Elevation (m asl)	Coordinates
Reanalysis	ERA-40	0.5° x 0.5°	509	68.50°N 18.00°E
Regional climate model	RCA3	0.5° x 0.5°	990	68.00°N 18.40°E
Global Climate Model (GCM)	HADCM3	3.75° x 2.5°	527	67.50°N 18.75°E
	CSIRO-Mk2	5.6° x 3.2°	325	68.50°N 16.88°E
	GFDL-R30	3.75° x 2.2°	190	68.20°N 18.75°E
	CGCM2	3.75° x 3.7°	134	68.65°N 18.75°E
	CCSR/NIES	5.6° x 5.5°	22	69.21°N 16.88°E
	ECHAM/OPYC3	2.8° x 2.8°	334	68.37°N 19.69°E

3.5 Methods

We adopt the following overall methodology: First we evaluate the ERA-40 data using meteorological observations, and we derive transfer functions to convert the grid point ERA-40 data to observations. Second, the ERA-40 data are used to calibrate a temperature-index mass balance model where air temperature is related to summer mass balance and precipitation is related to winter mass balance. We compare the performance of nine approaches differing in the temporal resolution of the input data and manipulation of the ERA-40 temperature data. We also investigate the stability of regression coefficients when using different time periods. Third, time series of temperature and precipitation until 2100 are downscaled from RCA3 and the GCMs using ERA-40 data, and then used as input to the mass balance model for projections of mass

balance and volume changes of Storglaciären in the coming century. We run eight variants of the calibrated mass balance model with the RCA3-derived climate scenario to study the sensitivity of the mass balance model. The variant with highest performance is then run with climate forcing derived from six GCMs in order to investigate the sensitivity of results to the choice of the climate model. We also compare the impact of using predictions based upon volume-area scaling vs predictions assuming constant glacier area. Finally, static sensitivities for 21st century are computed from the RCA3-run.

3.5.1 Validation of temperature and precipitation from ERA-40

Linear regression analysis is applied in order to investigate the correlation between the ERA-40 data and the observational data on daily, monthly and seasonal time scales. We use temperature data from Tarfala Research Station (1965-2002) since it is located in the immediate vicinity of Storglaciären. Ritsem's data (1981-2002) are used for validation of precipitation, since year-around precipitation data are not available from Tarfala, and Ritsem's data has been shown to correlate best with Storglaciären's winter balance compared to data from other surrounding stations [*de Woul and Hock*, 2005].

In order to analyze inter-annual variability of temperature and precipitation without being affected by systematic bias, time series of the temperature and precipitation ratio, R, between two consecutive years are estimated as follows:

$$R = \frac{X(t)}{X(t+1)}, \tag{3.1}$$

where t is the time index of the year, R equals R_{OBS} (R_{ERA}) when X corresponds to 3-month averaged observational (ERA-40) data. Correlations between R_{OBS} and R_{ERA} are then used as indicators of correlation of inter-annual variability between ERA-40 and observational data. The function $F(t)$ expressed as:

$$F(t) = \frac{R_{ERA}(t)}{R_{OBS}(t)} \tag{3.2}$$

indicates high inter-annual similarity if $F(t)$ values are near unity.

Since the gridded and the measured data refer to different elevations, temperature differences between ERA-40 and the observations from Tarfala station and three additional meteorological stations (Riksgränsen, Abisko and Nikkaluokta, Figure 3.1) were analyzed in order to adjust ERA-40 temperature to local conditions.

3.5.2 Mass balance model

Melt has been found to correlate well with air temperature [e.g. *Krenke and Khodakov*, 1966; *Braithwaite,* 1984; *Vallon et al.*, 1998] forming the base for most mass balance models [*Hock,* 2003]. We use a simple degree-day approach following *de Woul and Hock* [2005]:

$$b_s = \alpha_s \sum_{i=t_1}^{t_2} a_i T_i + \beta_s, \qquad \begin{cases} a_i = 1, T_i > 0 \\ a_i = 0, T_i \le 0 \end{cases} \tag{3.3}$$

$$b_w = \alpha_w \sum_{i=t_1}^{t_2} a_i P_i + \beta_w, \qquad \begin{cases} a_i = 1, T_i < 0 \\ a_i = 0, T_i \ge 0 \end{cases} \tag{3.4}$$

where α and β are the coefficients derived from linear regression between measured summer mass balances (b_s) and positive degree-day sums ($\Sigma a_i T_i$) over the entire mass balance year, and between measured winter mass balances (b_w) and annual sums of daily/monthly precipitation ($\Sigma a_i P_i$) with negative air temperatures. The mass balance year is defined from 1 October to 31 September. The model needs calibration based on seasonal mass balance data, thus hampering direct transferability to other glaciers.

We aim to show if and how much ERA-40 needs to be adjusted before being used in the model. Therefore, the model performance, i.e. the percentage of the explained variance of measured mass balance by the modeled one, is tested according to nine variants of the model input. Variants differ in the temporal resolution of the input data (seasonal, daily or monthly averages) and in the method by which ERA-40 temperatures are adjusted (downscaled) prior to model input. In methods I-III T_i is taken from ERA-40 without any adjustments, while in methods IV-IX temperatures are adjusted by different types of lapse rates to represent local conditions. The following input variants are used:

I. $\Sigma a_i T_i$ is equal to the sum of mean June, July and August temperatures ($T_{Jun}+T_{Jul}+T_{Aug}$), while $\Sigma a_i P_i$ is the sum of precipitation from all months except June, July and August

II. T_i is monthly mean temperature and P_i is monthly precipitation sum

III. T_i is daily temperature and P_i is daily precipitation sum.

IV. T_i is daily temperature which is adjusted in two steps: first by adjusting ERA-40 temperatures using the monthly variable lapse rate derived from validation of ERA-40 with Tarfala temperature data. By this ERA-40 temperatures are fit to the observations. The second step is further reduction of the temperature by the lapse rate (between Tarfala elevation and Storglaciären's equilibrium line altitude =1468 m) that maximizes correlation between degree-day sums ($\Sigma a_i T_i$) and b_s. P_i is daily precipitation sum.

V. as (IV), but T_i and P_i are monthly data

VI. T_i is daily temperature lowered by the lapse rate that maximizes correlation between degree-day sums ($\Sigma a_i T_i$) and b_s. Hence observational data are not needed. P_i is daily precipitation sum.

VII. as (VI), but T_i and P_i are monthly data

VIII. T_i is monthly temperature lowered by the average lapse rate derived from the temperature and altitude difference between ERA-40 and four meteorological stations. P_i is monthly precipitation sum.

IX. T_i is synthetic temperature data derived from the monthly data from (V) applying a normal distribution of daily temperatures from (IV). The normal distribution is derived for each month of each year and the method is used only for calibration of summer mass balance. Winter mass balance is not modeled for this case.

A set of coefficients α and β was determined by regression analysis for each of the methods. To investigate the stability of coefficients with time, regression analysis was performed for three different time periods: 1965/66-1980/81, 1980/81-2001/02 and 1965/66-2000/01. Net mass balance is derived as the sum of the winter mass balance and (negative) summer mass balance.

3.5.3 Future runs of mass balance model

Climate forcing

Direct use of meteorological output from climate models is currently not applicable for impact studies, as climate models are unable to represent local subgrid-scale features and dynamics

[*Giorgi et al.*, 2001] which leads to biases in both temperature and precipitation. Since the degree-day model is particularly sensitive to the seasonal distribution of temperature, such differences will strongly affect the mass balance simulations. Also, the direct use of coarse GCM grid points naturally results in a poor representation of the local climate, especially for precipitation, which is highly dependent on the local orographic conditions. Therefore, downscaling techniques need to be applied to the climate model output [*Wilby et al.*, 1998; *Giorgi et al.*, 2001]. Downscaling methods generally use observations as a reference climate [*Salathé*, 2005]. We use ERA-40 because these data are the input to the mass balance model. We apply a simple statistical downscaling method, referred to as 'local scaling' [*Widmann et al.*, 2003; *Salathé*, 2005], which for temperature can be thought as a lapse rate correction due to elevation difference of the local grid point relative to the climate model grid. Downscaled series were produced for RCA3 and each GCM for the period 2001 to 2100 by correcting the monthly climate model output series by the averaged difference over a baseline period prior to 2001 between climate model and ERA-40 for each month. Hence, the average seasonal cycle from ERA-40 is used as a reference by which the seasonal cycle from the climate model is 'corrected'. Future temperature time series (T_i) were calculated by:

$$T_i(t) = T_{i,c}(t) + (\overline{T_{i,ERA}} - \overline{T_{i,c}}), \qquad i = 1,\ldots,12 \tag{3.5}$$

where $T_{i,c}$ is monthly temperature for the i-th month from the climate model output from t = 2001 to 2100, $\overline{T_{i,c}}$ and $\overline{T_{i,ERA}}$ are mean temperature from climate model and ERA-40, respectively, for the i-th month averaged over a chosen baseline period. Five different baseline periods are chosen for comparison: 1961-2001, 1971-2001, 1981-2001, 1991-2001 and 2000-2001.

As an example, Figure 3.2 shows the seasonal cycles for ERA-40 temperatures averaged over the 1961-2001 period compared with those modeled by the six GCMs. Although overall patterns are reproduced well, some models have strong seasonal biases. CSIRO and CCSR/NIES have the temperature maximum shifted by one month combined with subdued seasonality, probably since the grid cell used contains large ocean percentage due to coarse horizontal resolution.

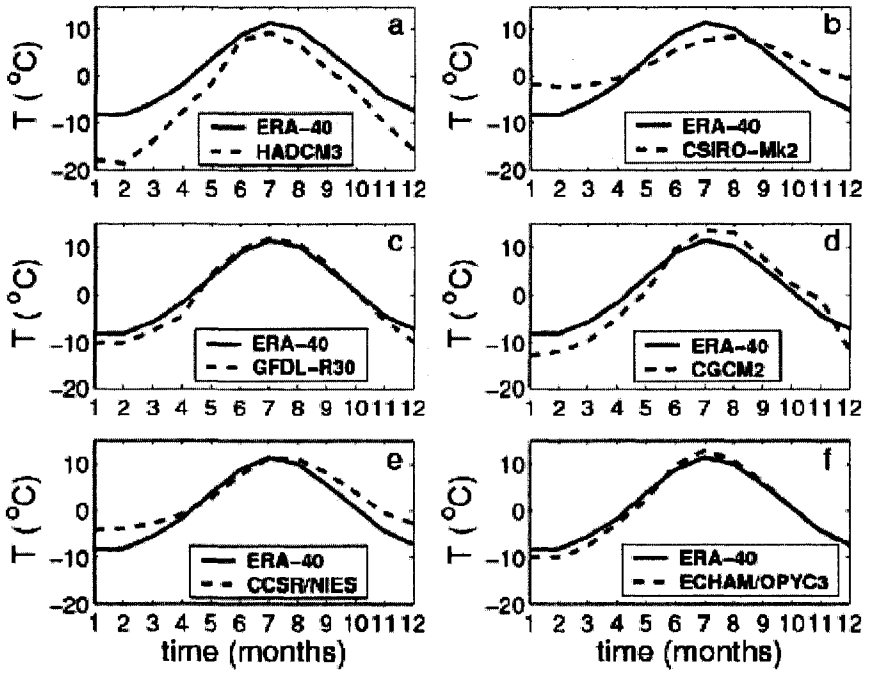

Figure 3.2. Temperature seasonal cycles averaged over 1961-2001 from ERA-40 and six GCMs, compared before the statistical downscaling is applied to the output of GCMs.

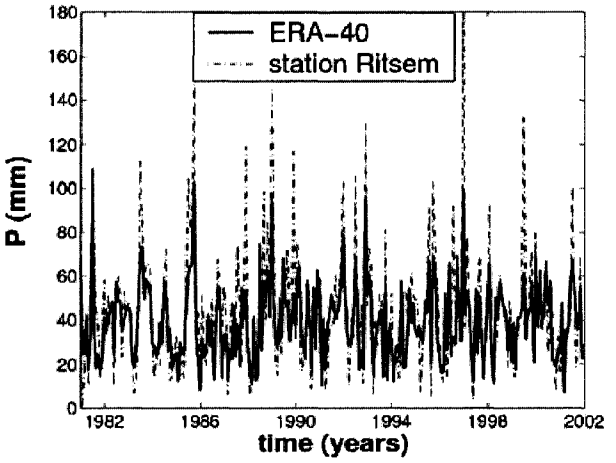

Figure 3.3. Monthly sums of precipitation from ERA-40 reanalysis and Ritsem.

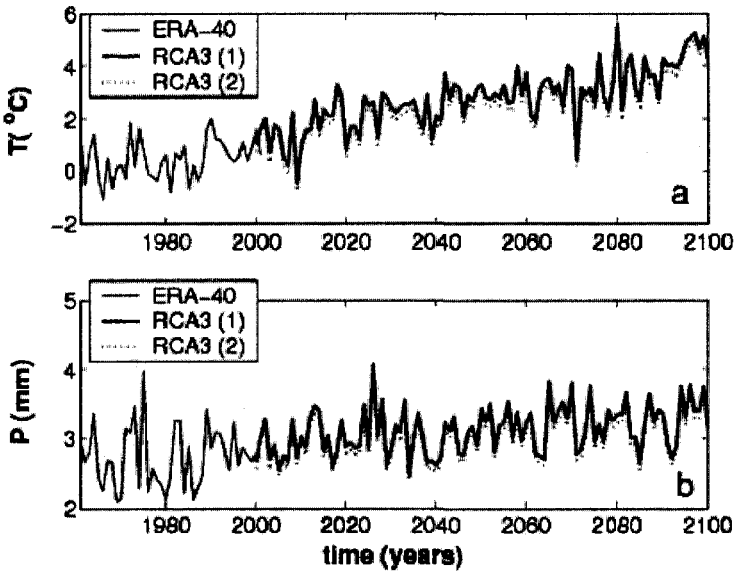

Figure 3.4. Annual time series of (a) temperature and (b) precipitation, derived from downscaling RCA3 output using two different baseline periods: (1) 41-year period: 1961-2001, and (2) 2-year period: 2000-2001.

For precipitation, the local scaling method simply multiplies the large-scale simulated precipitation at each local grid point by a seasonal scale factor [*Widmann et al.*, 2003]. Since changes in precipitation over the year show no obvious seasonal cycle but a more random distribution, we scale precipitation equally throughout the year. Thus, the future series $P_i(t)$ is generated by:

$$P_i(t) = P_{i,c}(t)\frac{\overline{P_{ERA}}}{\overline{P_c}}, \qquad i = 1,\ldots,12 \tag{3.6}$$

where $P_{i,c}$ is monthly precipitation sum from the climate model from t = 2001 to 2100, $\overline{P_c}$ and $\overline{P_{ERA}}$ are mean precipitation from the climate model and ERA-40, respectively, averaged over the baseline period. Climate models tend to underestimate large amounts of precipitation and overestimate small amounts [*Xu*, 1999]. This is also a characteristic of ERA-40 precipitation when compared to observations from Ritsem station (Figure 3.3). But ERA-40 captures well the temporal variability, what is more crucial than absolute amounts for the type of mass balance

model chosen (Equation 3.4). Figure 3.4 illustrates the annual time series of temperature and precipitation derived from downscaling the RCA3 model with different baseline periods. Since the differences in the series resulting from the baseline periods 1961-2001, 1971-2001, 1981-2001 and 1991-2001 are too small to be distinguished in the figure, only one of these series is presented while the series derived from 2-year baseline period 2000-2001 shows notable differences.

Volume changes

In response to prolonged mass balance changes, glacier area and volume will change. These changes may be approximated by volume-area scaling [*Bahr et al.*, 1997; *Van de Wal et al.*, 2001]. Glacier volume change, ΔV, is estimated by:

$$\Delta V(t) = b_n(t)A(t), \tag{3.7}$$

where b_n is the modeled future annual net mass balance and A is the area of the glacier. Volume V is related to area A by the empirical relation:

$$V(t) = k\,[A(t)]^{\gamma}, \tag{3.8}$$

where γ=1.375 was obtained by *Bahr* [1997] using theoretical considerations and the constant k=0.0633 $km^{3-2\gamma}$ is derived from Storglaciären's initial volume $V(t=2001)$= 0.3 km^3 and the initial area $A(t=2001)$=3.1 km^2. After each mass balance year a new volume is computed from which a new glacier area is derived. For comparison, we also perform runs with glacier area kept constant.

Static mass balance sensitivity

Modeled future mass balances are used to estimate static mass balance sensitivities due to temperature (*db/dT*) and precipitation (*db/dP*) changes. The concept of mass balance sensitivity [e.g. *Braithwaite et al.*, 2002] has been widely used in predicting glacier changes [*Gregory and Oerlemans*, 1998; *Oerlemans et al.*, 1998, 2005]. We derive static mass balance sensitivities in the 21st century by calculating time series of *db/dT* and *db/dP* based on the difference between 20-year running averages of mass balances, temperature and precipitation, and corresponding averages over a fixed 20-year reference period (2001-2020):

$$\frac{db}{dT} = \frac{\sum_{t=t_0+1}^{t_0+20} b_n(t) - \sum_{t=2001}^{2020} b_n(t)}{\sum_{t=t_0+1}^{t_0+20} T(t) - \sum_{t=2001}^{2020} T(t)}, \tag{3.9}$$

$$\frac{db}{dP} = \frac{\frac{1}{20}\sum_{t=t_0+1}^{t_0+20} b_n(t) - \frac{1}{20}\sum_{t=2001}^{2020} b_n(t)}{\left(\frac{\sum_{t=t_0+1}^{t_0+1} P(t)}{\sum_{t=2001}^{2020} P(t)} - 1\right) 100}, \tag{3.10}$$

with t_0 = 2001,..., 2080, where mass balance, temperature and sums of precipitation are averaged for consecutive 20-year intervals starting from 2001.

As mass balance sensitivity to temperature change (*db/dT*) is not independent of precipitation change, and vice versa, additional estimates of sensitivities are calculated to separate both climate signals in the modeled mass balance change. This is done by calculating *db/dT* from mass balance predictions where climate model temperature predictions are included but the precipitation is held constant in time, i.e. equal to monthly averaged ERA-40 precipitation over the period 1961-2001. Analogously, *db/dP* is computed from a model run including climate model precipitation predictions, while holding temperature steady, i.e. the seasonal cycle is assumed equal to the averaged cycle from ERA-40 over the period 1961-2001.

In contrast to dynamic sensitivities, static sensitivities neglect time-dependent geometry changes and other dynamic and non-linear effects. Although glacier area changes are computed (Equation 3.8), this has no bearing on the modeled mass balance according to Equations (3.3) and (3.4). Hence, sensitivities according to Equations (3.9) and (3.10) are static rather than dynamic. In addition, the mass balance model was calibrated for a period of roughly constant glacier area. Therefore, the mass balance record and the derived regression coefficients in the mass balance model reflect climate forcing but neglect the effect of area changes [*Elsberg et al.*, 2001; *Harrison et al.*, 2005].

3.6 Results and discussion

3.6.1 Validation of ERA-40 temperature

Daily, monthly and annual ERA-40 temperature data of all nine grid points correlate well with the corresponding Tarfala data, yielding $r^2>0.8$ for all cases. The data from the grid point north-west from the central grid point shows the highest correlation for daily ($r^2=0.927$), monthly ($r^2=0.980$) and annual averages ($r^2=0.872$), and were thus used in further analysis. R_{ERA} (Equation 3.1) explains more than 70% of the variance in R_{OBS}, and $F(t)$ (Equation 3.2) ranged between 0.7 and 1.4, indicating that observed seasonal variability is well represented by ERA-40. Averaged over the period 1965-2001, daily ERA-40 temperatures are systematically higher than the observations, which is partially due to the 626 m difference in elevation between the grid cell and the weather station (Figure 3.5a). Shifting the ERA-40 series according to an average lapse rate of -0.0062 K m^{-1} yields best agreement with the measurements, although seasonally variable biases are evident (Figure 3.5b). Such derived 'statistical lapse rates' include temperature variations with elevation, horizontal gradients and model bias. Figure 3.6 shows the monthly lapse rates that when applied to the ERA-40 yield the best agreement between ERA-40 and observations (Figure 3.5c). A distinct seasonal cycle is evident; the ERA-40 temperatures require larger reduction with altitude in summer than in winter in order to coincide with the measurements. It must, however, be borne in mind that the seasonal cycle may be due to seasonal variations in both lapse rates and in model bias. The average lapse rate derived from ERA-40 data and annual data from four weather stations amounts -0.0037 K m^{-1} ($r^2=0.76$) and is applied in the mass balance model with method 8.

3.6.2 Validation of ERA-40 precipitation

Regressing daily, monthly and annual precipitation from ERA-40 (all nine grid points) against corresponding data from Ritsem yields the highest correlation for the grid point west from the central grid point with $r_d^2=0.381$, $r_m^2=0.670$ and $r_a^2=0.563$, respectively. Analysis of seasonal averages revealed that correlation was better in autumn (September, October, November, SON) and winter (December, January and February, DJF) than in the remaining seasons ($r_{DJF}^2=0.807$, $r_{MAM}^2=0.748$, $r_{JJA}^2=0.601$, $r_{SON}^2=0.882$). As expected, these correlations are lower than those for temperature. When analyzing inter-annual variability, the highest correlation between R_{OBS} and R_{ERA} was obtained for the winter season ($r_{DJF}^2=0.830$, $0.8<F(t)<1.3$) and the lowest for the summer season ($r_{JJA}^2=0.484$, $0.6<F(t)<1.6$). Based on high correlation for inter-annual variability

we conclude that ERA-40 can be used as a reference for downscaling precipitation (Equation 3.6).

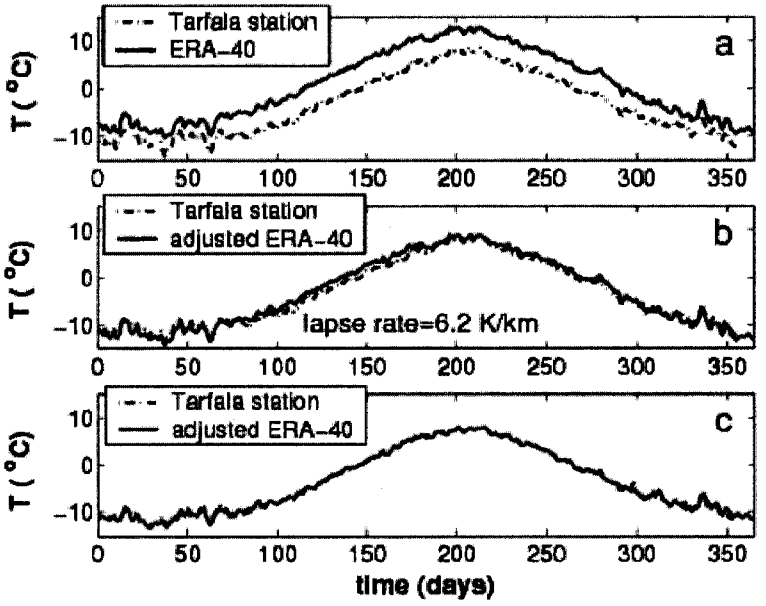

Figure 3.5. Daily air temperatures averaged over the period 1965-2001 from ERA-40 and Tarfala: (a) without adjustment in ERA-40 data, (b) ERA-40 temperatures are lowered by constant lapse rate that yields best agreement with the observations, (c) ERA-40 temperatures are lowered by monthly variable lapse rates (crosses in Figure 3.6).

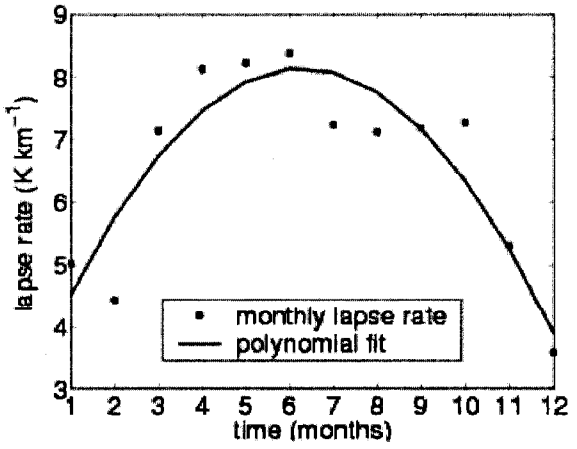

Figure 3.6. Monthly lapse rates (absolute values) derived from ERA-40 and Tarfala station temperatures averaged over the period 1965-2001. The line shows a polynomial fit.

Generally speaking, our analysis above suggests that ERA-40 temperature and precipitation captures measured seasonal and inter-annual variability sufficiently well to be used as input for mass balance modeling of Storglaciären.

3.6.3 Calibration of the mass balance model

Table 3.2 presents the results of the regression analysis between measured and modeled mass balances, as produced by the nine (I-IX) variants of the input to the mass balance model. In most cases correlation is higher for the summer than the winter balance, with r^2 ranging from 0.49 to 0.80 for b_s and 0.28 to 0.73 for b_w. The highest correlations are comparable and even slightly higher than those derived for Storglaciären from model VI using measured data from Ritsem ($r^2(b_s)$=0.87, $r^2(b_w)$=0.65, [*de Woul and Hock*, 2005]).

The most sophisticated method IV, which fits the ERA-40 temperatures to the observed Tarfala temperatures before adjusting it further to the glacier site, does not yield the highest correlation. In fact, all methods except II and III tend to produce very similar correlations regardless of the temperature adjustment to local conditions or whether daily or monthly data are used as input. This aspect is encouraging for use of GCM data for mass balance predictions, since GCM data tend to be most easily accessible with monthly resolution rather than daily. Methods II and III, which exclude any temperature adjustment, yield lower correlation compared with the other methods, emphasizing the importance of adjusting temperature to maximize the correlation between degree-day sums ($\Sigma a_i T_i$) and b_s. This may be considered as a way of tuning the model to achieve the best representation of observed mass balances. However, the tuning is not purely mathematical, because the reduction of temperature in order to achieve better representation of mass balance includes the better representation of temperature at the elevation of the glacier and the locally colder air temperature above the melting glacier surface due to surface cooling [*Braithwaite et al.*, 2002]. Correlations from method I, which also excludes any temperature adjustment, yield correlations that are similar to methods IV to IX probably because only months with high probability for positive temperatures are included for the summer balance, while the spring and fall periods with temperatures closer to freezing point (thus more sensitive to a temperature bias) are excluded. Adjusting ERA-40 temperatures according to a-priori determined lapse rates derived from meteorological observations (method IV and V) does not improve the

performance of the model when compared to the methods VI and VII which do not require any temperature observations. The latter methods apply a lapse rate (≈-0.004 K m^{-1}) derived from tuning the mass balance model. This is surprising considering the bias in ERA-40 temperatures (Figure 3.5a), but also encouraging for ERA-40 driven mass balance modeling in areas where meteorological measurements are not available.

Table 3.2. Explained variance (r^2) between the measured summer mass balances, b_s and positive degree-day sums, $\Sigma a_i T_i$, and between measured winter mass balances, b_w, and annual snow precipitation $\Sigma a_i P_i$,as produced by the nine variants of the input to the mass balance model (see text for explanation) and for three different calibration periods. Letter in brackets correspond to daily (d) or monthly (m) meteorological input of temperature and precipitation. Highest r^2 for each calibration period are bold

Method	1965/66-1980/81		1980/81-2000/01		1965/66-2000/01	
	b_s	b_w	b_s	b_w	b_s	b_w
I (m)	0.640	0.657	0.636	0.650	0.642	0.651
II (m)	0.549	0.462	0.747	0.534	0.566	0.501
III (d)	0.541	0.405	0.623	0.395	0.503	0.393
IV (d)	0.663	0.676	0.765	0.582	**0.681**	0.634
V (m)	0.605	0.611	0.776	**0.705**	0.650	0.646
VI (d)	**0.678**	0.634	0.777	0.654	0.679	0.647
VII (m)	0.621	**0.732**	**0.794**	0.640	0.650	**0.653**
VIII (d)	0.579	0.400	0.790	0.652	0.631	0.546
IX (m)	0.648		0.751		0.625	

Correlations, especially for summer mass balance, tend to be higher for the calibration period 1980/81-2000/01 compared to the preceding period or the total 35-year period. This may be attributed to improved quality in the ERA-40 after the more extensive inclusion of satellite data since 1979. Figure 3.7 illustrates the measured and modeled b_s, b_w and b_n derived using method VII for the period 1980/81-2000/01. Maximum deviation from the measured b_n is ± 0.66 m a^{-1}, which is equivalent to an error of 0.002 km^3 in the estimation of ΔV. This should be kept in mind when considering calculations of future volume changes in the following section.

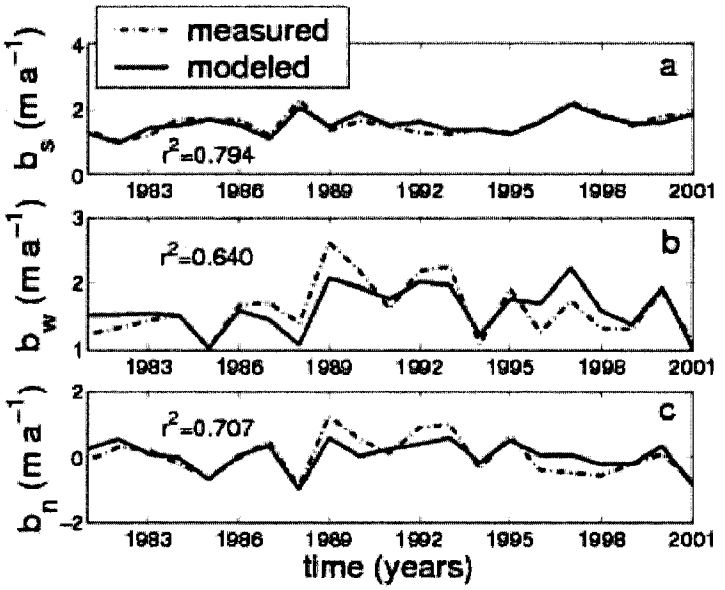

Figure 3.7. Measured and modeled (a) summer mass balance, b_s, (b) winter mass balance, b_w, and (c) net mass balance, b_n. Modeled mass balance is based on method VII of the mass balance model and forced by ERA-40 data using the calibration period 1980/1981-2000/2001.

3.6.4 Mass balance and volume projections until 2100

Sensitivity to mass balance model input

Volume evolution of Storglaciären as predicted by mass balance modeling with eight methods (I-VIII) and climate forcing derived from RCA3 model from 2001 to 2100 are presented in Figure 3.8a. All model variants, except the model using method I, predict a decrease in initial volume by approximately 30% by 2050 and 60% by 2100. This is due to progressively more negative mass balance, especially after 2040, when b_n becomes consistently negative. Method I is an outlier because it calculates melt only in 3 summer months (JJA) while the snow accumulation is equal to all precipitation during the rest of the year. It is therefore unable to capture the prolongation of the melt season associated with future warming and increased probability of precipitation falling as rain from September to May. Albeit achieving comparable correlation coefficients during the calibration period, method I is not suitable for climate change impact studies. Method III produces the largest mass loss because it uses ERA-40 temperatures without any lapse rate adjustment and therefore estimates more days with positive temperatures over the year and hence

more ablation. The differences of modeled volume change by 2100 derived from all methods, excluding methods I and III, are within a range of 10% of initial volume.

Our projection of 30% loss of volume by the middle of the 21st century closely coincides with the loss projected for Storglaciären by a distributed melt model combined with a three-dimensional ice flow model driven by ECHAM4 [*Schneeberger et al.*, 2001]. A 1-dimensional ice-flow model driven by hypothetical warming of 0.02 K per year without change in precipitation projected 20% volume loss by 2050 and 80% loss by 2100 [*Oerlemans et al.*, 1998].

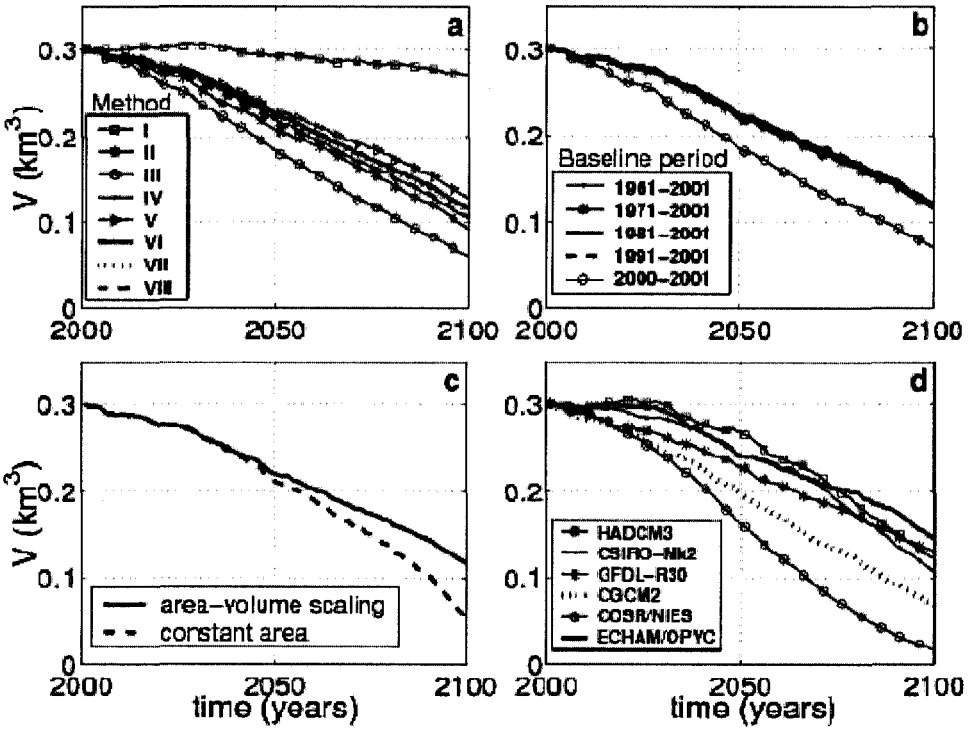

Figure 3.8. Volume projections for Storglaciären in the 21st century derived from: (a) eight methods (I-VIII) of the mass balance model and RCA3 output downscaled with ERA-40 reference climate for the baseline period 1961-2001, (b) method VII applied on the RCA3 output downscaled by use of five different baseline periods, (c) method VII applied on the RCA3, downscaled using the 1961-2001 baseline period, and with volume-area scaling and constant area, (d) method VII applied on the six GCMs which are downscaled using 1961-2001 baseline period. In all projections, unless noted differently, the volume is derived from volume-area scaling.

Sensitivity to choice of reference climate

The effect of the choice of the baseline period in generating the future climate time series on the volume evolution is illustrated in Figure 3.8b which shows the volume evolution estimated by the model with method VII when the five baseline periods are applied to downscale the RCA3. All volume curves, except for the one forced by the climate series derived from the 2000-2001 baseline, are within a range of 3% of initial volume. This is smaller than the difference caused by the choice of the method for the mass balance model. The outlier is explained by lower future sums of precipitation compared to the sums from other baselines (Figure 3.4b), which is immediately reflected in reduced winter mass balance and therefore in enhanced loss of mass. It is obvious that the baseline needs to be properly chosen and include a sufficient number of years to subdue the effect of inter-annual variability. In our case the model is insensitive to the choice of any of the >10 year long baseline periods used.

Sensitivity to the glacier area assumptions

Figure 3.8c presents the volume change derived from the mass balance model (method VII) with volume-area scaling and with constant area in the Equation (3.7). Until the middle of the 21st century there is no substantial difference between the two curves. Thereafter the volume decrease becomes considerably overestimated (by 20% at the end of 2100) if the area reduction is not considered. Results must be considered as rough estimates since feedback between mass balance and area-elevation distribution is neglected (i.e. mass balance becomes less negative as area is removed from low lying high ablation altitudes). The larger volume loss when the glacier area is kept constant is a mathematical consequence of the use of Equation (3.8) when b_n becomes consistently negative.

Sensitivity to choice of climate model

In order to investigate the sensitivity of mass balance and volume predictions to the choice of the GCM, the mass balance model (method VII) is forced by downscaled temperature and precipitation from six GCMs (Figure 3.8d). Table 3.3 contains the trends in temperature and precipitation for annual, winter (DJF) and summer (JJA) means.

All models predict volume losses between 50% (ECHAM) to 90% (CCSR) of the initial value. This is a direct consequence of warming trends in the range of 2.3 to 4.9 K per century, which is

more evident in the winter than in the summer season for most of the models. Positive trends in precipitation contain relative errors of more than 100% in the estimates (Table 3.3) which make the trends insignificant. Even if the trend was real, the increase in the range of 57 to 212 mm a^{-1} per century cannot compensate the increased ablation due to the warming.

Table 3.3. Annual, winter (DJF) and summer (JJA) trends in the climate models for the grid point nearest to Storglaciären. Temperature trends (*T*) are in K per century and precipitation trends (*P*) are in mm a^{-1} per century, while the uncertainties are based on the error from the least squares method by which the slope of the trend is determined

	Trend					
	Annual		Winter (DJF)		Summer (JJA)	
Model	*T*	*P*	*T*	*P*	*T*	*P*
HADCM3	3.24 ± 0.34	57 ± 41	2.77 ± 0.85	34±21	2.72 ± 0.38	49 ± 20
CSIRO-Mk2	3.11 ± 0.18	136 ± 36	2.90 ± 0.32	44 ± 19	3.02 ± 0.17	10 ± 18
GFDL-R30	2.31 ± 0.37	76 ± 43	2.97 ± 0.87	14 ± 17	1.45 ± 0.40	8 ± 29
CGCM2	2.67 ± 0.35	44 ± 45	2.48 ± 0.87	23 ± 20	1.95 ± 0.28	64 ± 26
CCSR/NIES	4.87 ± 0.20	199 ± 59	5.04 ± 0.36	17 ± 21	4.56 ± 0.25	53 ± 35
ECHAM/OPYC3	3.25 ±0.31	212 ± 52	4.62 ± 0.62	92 ± 23	1.97 ± 0.50	7 ± 24
RCA3	2.94 ± 0.26	143 ± 38	4.37 ± 0.61	64 ± 17	2.28 ± 0.31	2 ± 22

The CCSR model predicts the largest mass loss due to its extreme warming trend. CGCM2, although showing trends comparable with other models, predicts smaller loss of volume than CCSR but larger loss in comparison with the other models. This is due to a sudden shift to higher annual temperatures in the period 2001-2010 and higher maximum temperatures in the inter-annual variations after 2060 while lacking any trend in precipitation. HADCM3, due to its higher precipitation and low temperature trend from 2001 to 2020, predicts a small growth of volume in that period. Afterwards the volume decreases due to an increase in temperature. GFDL-R30 follows the volume evolution as in CGCM and CCSR until 2020 when it starts to predict lower mass loss (by 50% at the end of 2100) probably caused by lower slope in temperature trend and, in general, lower minimum temperatures in the inter-annual variability. ECHAM maintains almost the same volume evolution as CSIRO until 2070 when it shifts to the smaller loss of volume because it projects higher sums of precipitation.

An analysis of the differences in temperature and precipitation trends and inter-annual variations predicted by the GCMs shows how the differences are highly reflected in the modeled future mass balance. The range of volume change by the end of 2100 is within 40% of the initial volume. This is the largest range in total sensitivity in this study.

One additional test is performed to show the importance of the downscaling method applied on the GCMs: if the future temperature series are corrected with long-term annually averaged temperature instead of monthly averages ($\overline{T_{i,c}}$, $\overline{T_{i,ERA}}$) over the baseline period, as in Equation (3.5), the mass balance model produces the volume changes presented in Figure 3.9. Results differ considerably from the ones based on monthly averages (Figure 3.8d), especially for the GCMs with markedly different seasonal cycles compared to the ERA-40 data (Figure 3.2). Most notably, CSIRO produces a strong volume increase by 2100 despite a significant warming trend. This is caused by a seasonal temperature cycle with too low amplitude causing underestimation of summer temperatures and ablation.

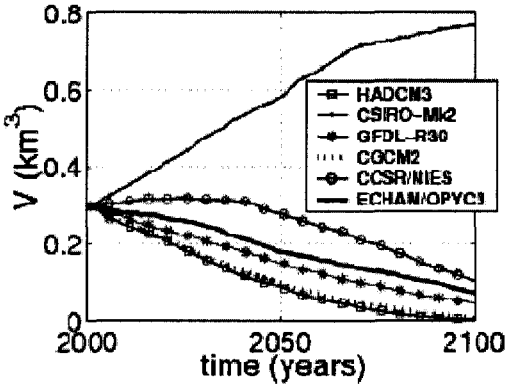

Figure 3.9. Volume projections for Storglaciären in the 21st century, derived from method VII of the mass balance model and forced by output from six GCMs. The temperature bias between GCM and ERA-40 is corrected for by the averaged difference over the baseline period 1961-2001 instead of using seasonally variable values.

Static mass balance sensitivity

Running 20-year relative changes of net mass balance (*db*), temperature (*dT*) and precipitation (*dP*) with respect to the reference period 2001-2020 are presented in Figure 3.10. Mass balance is obtained from method VII of the mass balance model with the climate input from RCA3

downscaled with the baseline period 1961-2001. Temperature change shows constant increase which is due to a linear warming trend, while % precipitation change shows increase with a secondary minimum at the end of the 2020s. Mass balance changes gradually decrease towards more negative values.

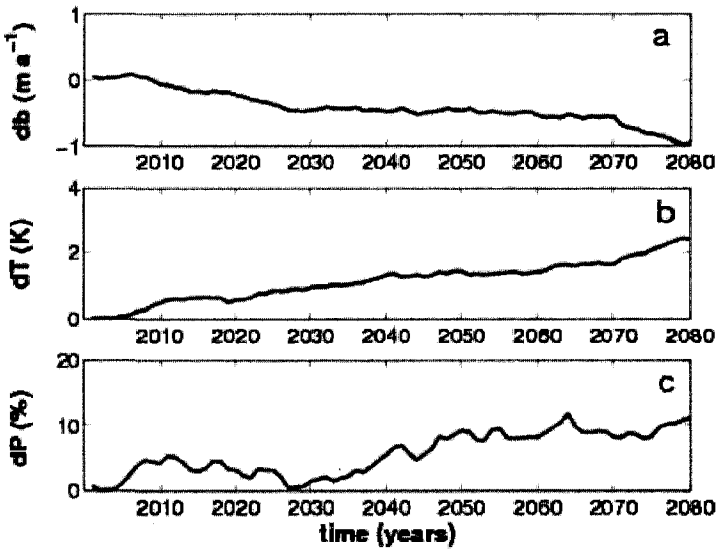

Figure 3.10. Running 20-year relative changes of (a) net mass balance, *db*, (b) air temperature, *dT*, and (c) precipitation, *dP*, with respect to the reference period 2001-2020.

The static mass balance sensitivity due to temperature (*db/dT*) and precipitation (*db/dP*) change is presented in Figure 3.11. Sensitivity to temperature, excluding any precipitation trend, varies around the mean value of -0.48 m a^{-1} K^{-1} with a standard deviation of 0.002 m a^{-1} K^{-1}. The mean value agrees well with -0.46 m a^{-1} K^{-1} derived from a model forced by observational data [*de Woul and Hock*, 2005] where a hypothetical increase of 1 K was applied. Also, the result agrees well with -0.48 m a^{-1} K^{-1} calculated by the degree-day method and local data for Storglaciären [*Braithwaite and Zhang,* 1999]. Sensitivity to precipitation excluding any temperature trend, gives almost a constant value in time: 0.025 m a^{-1} per 1% increase in precipitation. The negative peak occurring around 2030 is due to the drop in *dP* (Figure 3.10). Derived *db/dP* is slightly higher than the 0.015 m a^{-1} per 1% increase in precipitation obtained by *de Woul and Hock*, [2005].

The results show no substantial variation in static mass balance sensitivity. However, the sensitivity to climate forcing is partly incorporated in the correlation coefficients of the mass balance model, which are kept temporally constant in future projections. Therefore, the static sensitivities reflect the linearity of the model and no substantial changes in time are effected given the model assumptions.

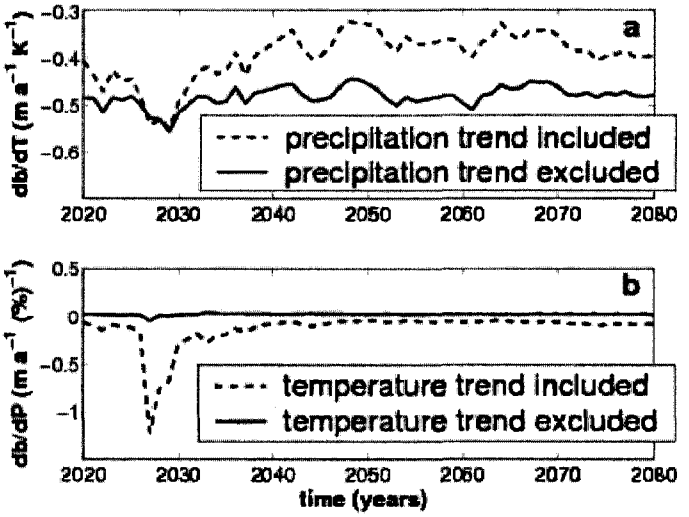

Figure 3.11. Static mass balance sensitivity due to (a) temperature change, *db/dT*, and (b) precipitation change, *db/dP*, calculated from the Equations 3.9 and 3.10.

3.6 Conclusions

We have used ERA-40 in the calibration of a simple mass balance model and for downscaling climate models in order to estimate future volume changes of Storglaciären. Our main findings are:

1. Validation of ERA-40 in the Storglaciären's region showed that ERA-40 temperature explains more than 80% of the variance of observed daily, monthly and annual temperatures at Tarfala Station and that inter-annual variability is captured well. Precipitation from ERA-40 explains, on average, 50% of the variance of observed precipitation sums at Ritsem station and inter-annual variability is captured sufficiently well for use in the mass balance modeling.
2. A mass balance model driven by nine variants of ERA-40 input performs similarly well regardless of temporal resolution of the input data (daily or monthly averages). The model explains 70% of the variance of measured mass balance when the ERA-40 temperatures are reduced by the optimized (tuned) lapse rate between grid point elevation and glacier's ELA.

Fitting ERA-40 temperatures to observations does not improve the performance of the model. Hence, in this case ERA-40 can be used for mass balance modeling independently of meteorological observations.

3. Projections of volume change in the 21st century driven by the B2 emission scenario from statistically downscaled RCA3 and six GCMs outputs result in a volume loss of 50-90% of the glacier's initial volume by end of 2100. Differences in these projections vary within 40% of the initial volume. Each volume projection varies within a range of 20% due to applied volume-area scaling or constant area. The choice of the method in the mass balance modeling, after excluding obvious outliers, corresponds to an uncertainty range of 10% for the volume projection, while the choice of the baseline period for the downscaling method results in 3% uncertainty range. In the range of uncertainties we need to add the uncertainty in the performance of the degree-day model itself: for the period of calibration 30% of the variance of the measured mass balance remains unexplained by the model. Modeled projections are not only highly sensitive to the choice of GCMs but can completely offset the results if seasonal biases in future series are not corrected by the reference climate, i.e. if a proper downscaling method is not applied.
4. The static mass balance sensitivities to future temperature and precipitation change, calculated as running difference between 20-year averages of b_n and averaged b_n over the reference period 2001-2020, show very small variations in time with the mean values of db/dT=-0.48 m a^{-1} K^{-1} and db/dP=0.025 m a^{-1} per 1% precipitation increase.

This sensitivity study showed that the model is capable of predicting future volume changes that are comparable with those derived from more sophisticated models [*Oerlemans et al.*, 1998; *Schneeberger et al.*, 2001] and that the estimated static mass balance sensitivity corresponds well to previous estimates on Storglaciären [*Braithwaite et al.*, 2002; *de Woul and Hock*, 2005]. A possible way of using our results for global assessment of glacier volume change in the 21st century is direct application of the model to other glaciated regions taking advantage of the model's simple data requirements available from ERA-40 reanalysis. However, further study is needed to evaluate how far the calibrated mass balance model for one glacier is transferable to other glaciers, and whether representative sets of model parameters can be found for glaciers in similar environmental settings. Alternatively, a more sophisticated mass balance model based on energy balance calculations [e.g., *Greuell and Konzelmann*, 1994] may be used, but it requires

more inventory and climate data. In the end, one needs to find the balance between model requirements and data availability. At present, air temperature and precipitation are variables that are most readily available and have received most scrutiny in terms of validation and downscaling techniques, and are therefore the best-suited for mass balance projections.

Acknowledgments

This study is a contribution to the CE (Climate and Energy) project funded by Nordic Energy Research (NEFP). Financial support is provided by the Swedish Research Council for Environment, Agricultural Sciences and Spatial Planning FORMAS (project number: 21.4/2003-0387). Gratitude is expressed to the Rossby Centrum at SMHI, particularly to E. Kjellström for providing the RCA3 data, and P. Kållberg and C. Maass (ECMWF) for helping to retrieve ERA-40 data. The weather data and ERA-40 data were received from SMHI and ECMWF, respectively. Comments by C. Tijm-Reijmer, T. Jóhannesson, A. Arendt, an anonymous reviewer, R. Braithwaite and editor R. Anderson have helped to improve the paper.

3.7 References

Adalgeirsdottir, G., T. Jóhannesson, H. Björnsson, F. Pálsson and O. Sigurðsson (2006), The response of Hofsjökull and southern Vatnajökull, Iceland, to climate change, *J. Geophys. Res.*, 111, F03001, doi:10.1029/2005JF000388.

Arendt, A. A., K. A. Echelmeyer, W. D. Harrison, C. S. Lingle, and V. B. Valentine (2002), Rapid wastage of Alaska glaciers and their contribution to rising sea level, *Science, 297*, 382-286.

Bahr, D. B., M. F. Meier, and S. D. Peckham (1997), The physical basis of glacier volume-area scaling, *J. Geophys. Res., 102*(B9), 20355-20362.

Braithwaite, R.J. (1984), Calculations of degree-days for glacier-climate research, *Z. Gletscherkd. Glazialgeol., 20*, 1-8.

Braithwaite, R. J. and Y. Zhang (1999), Modelling changes in glacier mass balance that may occur as a result of climate changes, *Geogr. Ann., 81A*(4), 489-496.

Braithwaite, R. J., Y. Zhang, and S. C. B. Raper (2002), Temperature sensitivity of the mass balance of mountain glaciers and ice caps as a climatological characteristic, *Z. Gletscherkd. Glazialgeol., 38*(1), 35-61.

Church, J. A., J. M. Gregory, P. Huybrechts, M. Kuhn, K. Lambeck, M. T. Nhuan, D. Qin, and P. L. Woodworth (2001), Changes in sea level, in *Climate Change 2001: The Scientific Basis*, edited by J. T. Houghton et al., pp. 639-693, Cambridge Univ. Press, New York.

de Woul, M., and R. Hock (2005), Static mass balance of Arctic glaciers and ice cap using a degree-day approach, *Ann. Glaciol.*, 42, 217-224.

Dyurgerov, M. B., and M. F. Meier (2000), Twentieth century climate change: Evidence from small glaciers, *PNAS, 97*(4), 1406-1411.

Elsberg, D. H., W. H. Harrison, K. A. Echelmeyer and R. M. Krimmel (2001), Quantifying the effects of climate and surface change on glacier mass balance, *J. Glaciol., 47*(159), 649-658.

Giorgi, F., B.C. Hewitson, J. Christensen, M. Hulme, H. Von Storch, P. Whetton, R. L. Jones, L. Mearns, and C. Fu (2001), Regional Climate Information - Evaluation and Projections, in *Climate Change 2001: The Scientific Basis*, edited by J. T. Houghton et al., pp. 583-638, Cambridge Univ. Press, New York.

Gregory, J. M., and J. Oerlemans (1998), Simulated future sea-level rise due to glacier melt based on regionally and seasonally resolved temperature changes, *Nature, 391*(6666), 474-476.

Greuell, W., and T. Konzelmann (1994), Numerical modelling of the energy balance and the englacial temperature of the Greenland ice sheet, Calculations for the ETH-camp location (West Greenland, 1155 m a.s.l.), *Global Planet. Change, 9*(1-2), 91-114.

Hanna, E., P. Valdes, and J. McConnel (2001), Patterns and variations of snow accumulation over Greenland, 1979-98, from ECMWF analysis, and their verification, *J. Clim.,14*, 3521-3535.

Harrison, W. D., D. H. Elsberg, L. H. Cox, and R. S. March (2005), Different mass balance for climatic and hydrologic applications, *J Glaciol., 51*(172), 176.

Hock, R. (2003), Temperature index melt modelling in mountain areas, *J. Hydrol., 282*(1-4), 104-115.

Hock, R., and B. Holmgren (1996), Some aspects of energy balance and ablation of Storglaciären, northern Sweden, *Geogr. Ann., 78A*(2-3), 121-131.

Hock , R., and B. Holmgren (2005), A distributed energy balance model for complex topography and its application to Storglaciären, Sweden, *J. Glaciol., 51*(172), 25-36.

Hock, R., P. Jansson, and L. Braun (2005), Modelling the response of mountain glacier discharge to climate warming, in *Global Change and Mountain Regions - A State of Knowledge Overview, Advances in Global Change Series*, edited by U. M. Huber et al., pp. 243-252, Springer, Dordrecht.

Holmlund, P. (1987), Mass balance of Storglaciären during the 20th century, *Geogr. Ann., 69A*(3-4), 439-447.

Holmlund, P., P. Jansson, and R. Pettersson (2005), An analysis of mass changes of Storglaciären over the last 58 years, *Ann. Glaciol.*, 42, 389-394.

IPCC (2001), Climate Change 2001: The Scientific Basis – Contribution of Working Group 1 to the Third Assessment Report of the Intergovernmental Panel on Climate Change, edited by J. T. Houghton et al., 881 pp., Cambridge Univ. Press, New York.

Kållberg, P. W., A. J. Simmons, S. M. Uppala, and M. Fuentes (2004), The ERA-40 Archive, *ERA-40 Project Report Series, 17*, 31 pp., ECMWF, Reading.

Kjellström, E., L. Bärring, S. Gollvik, U. Hansson, C. Jones, P. Samuelsson, M. Rummukainen, A. Ullerstig, U. Willén and K. Wyser (2005), A 140-year simulation of European climate with the new version of the Rossby Centre regional atmospheric climate model (RCA3), *Reports Meteorology and Climatology*, 108, SMHI, SE-60176 Norrköping.

Krenke, A. N. and V. G. Khodakov (1966): O svyazi poverkhnostnogo tayaniya ledinkov s temperaturoy vozdukha [The relationship between surface ice melting and air temperature], *Mater. Glyatsiol. Issled.*, *12*, 153-164.

Martin, E. (2004), Validation of Alpine snow in ERA-40, *ERA-40 Project Report Series, 14*, 21 pp., ECMWF, Reading.

Meier, M., M. Dyurgerov, and G. J. McCabe (2003), The Health of Glaciers: Recent Changes in Glacier Regime, *Climatic Change, 59*(1-2), 123-135.

New, M., M. Hulme and P. J. Jones (1999), Representing twentieth century space-time climatic variability, Part 1: Development of a 1961-1990 mean monthly terrestrial climatology, *J. Clim.*, 12, 829-856.

Oerlemans, J., B. Anderson, A. Hubbard, Ph. Huybrechts, T. Jóhannesson, W. H. Knap, M. Schmeits, A. P. Stroeven, R. S. W. van de Wal, J. Wallinga, and Z. Zuo (1998), Modelling the response of glaciers to climate warming, *Clim. Dynam., 14*, 267-274.

Oerlemans, J., R. P. Bassford, W. Chapman, J. A. Dowdeswell, A. F. Glazovsky, J.-O. Hagen, K. Melvold, M. de Ruyter de Wildt, and R. S. W. van de Wal (2005), Estimating the contribution from Arctic glaciers to sea-level change in the next hundred years, *Ann. Glaciol., 42*, 230-236.

Pettersson, R., P. Jansson, and H. Blatter (2004), Spatial variability in water content at the cold-temperate transition surface of the polythermal Storglaciaren, Sweden, *J. Geophys. Res., 109*(F2), doi:10.1029/2003JF000110.

Raper, S. C. B. and R. J. Braithwaite (2006), Low sea level rise projections from mountain glaciers and icecaps under global warming, Nature, 439, 311-313, doi: 10.1038/nature04448.

Rasmussen, L. A., and H. Conway (2004), Climate and glacier variability in western North America, *J. Clim., 17*(9), 1804-1815.

Reichert, B. K., L. Bengtsson and J. Oerlemans (2001), Midlatitude forcing mechanisms for glacier mass balance investigated using general circulation models, *J. Clim., 14*(17), 3767-3784.

Salathé, E. P. (2005), Downscaling simulations of future global climate with application to hydrologic modelling, *Int. J. Climatol., 25*, 419-436.

Schneeberger, C., O. Albrecht, H. Blatter, M. Wild, and R. Hock (2001), Modelling the response of glaciers to a doubling in atmospheric CO2: a case study of Storglaciären, northern Sweden, *Clim. Dynam., 17*(11), 825-834.

Simmons, A.J., and J.K. Gibson (2000), The ERA-40 Project Plan, *ERA-40 Project Report Series, 1*, 63 pp., ECMWF, Reading.

Simmons, A.J., P.D. Jones, V. da Costa Bechtold, A. C. M. Beljaars, P. Kallberg, S. Saarinen, S. M. Uppala, P. Viterbo, and N. Wedi (2004), Comparison of trends and low-frequency variability in CRU, ERA-40, and NCEP/NCAR analyses of surface air temperature, *J. Geophys. Res., 109*(24), 1-18, doi:10.1029/2004JD005306.

Vallon, M., C. Vincet and L. Reynauld (1998), Altitudinal gradient of mass-balance sensitivity to climatic change from 18 years of observations on Glacier d'Argentière, France, *J. Glaciol.,44*(146), 93-96.

Van de Wal, R. S. W., and M. Wild (2001), Modelling the response of glaciers to climate change by applying volume-area scaling in combination with a high resolution GCM, *Clim. Dynam., 18*(3-4), 359-366.

Velicogna, I., J. Wahr, E. Hanna, and P. Huybrechts (2005), Short term mass variability in Greenland, from GRACE, *Geophys. Res. Lett., 32*, L05501, doi:10.1029/2004GL021948.

Widmann, M., C. S. Bretherton, and E. P. Salathé Jr. (2003), Statistical precipitation downscaling over the Northwestern United States using numerically simulated precipitation as a predictor, *J. Clim, 16*(5), 799-816.

Wilby, R.L., T. M. L. Wigley, D. Conway, P. D. Jones, B. C. Hewitson, J. Main, and D. S. Wilks (1998), Statistical downscaling of general circulation model output: A comparison of methods, *Water Resour. Res., 34*, 2995-3008.

Xu, C.-Y. (1999), Climate change and hydrologic models: A review of existing gaps and recent research developments, *Water Resour. Manag., 13*, 369-382.

Chapter 4

Volume-area scaling vs flowline modelling in glacier volume projections[1]

4.1 Abstract

Volume-area scaling provides a practical alternative to ice-flow modelling to account for glacier size changes when modelling the future evolutions of glaciers; however, uncertainties remain as to the validity of this approach under non-steady conditions. We address these uncertainties by deriving scaling exponents in volume-area relationship from one-dimensional ice-flow modelling. We generate a set of 37 synthetic steady-state glaciers of different sizes, and then model their volume evolutions due to climate warming and cooling as prescribed by negative and positive mass balance perturbations, respectively, on a century time scale. The scaling exponent derived for the steady-state glaciers (γ=1.56) differs from the exponents derived for the glaciers in transient (non-steady) state by up to 86%. Nevertheless, volume projections employing volume-area scaling are relatively insensitive to these differences in scaling exponents. Volume-area scaling agrees well with the results from ice-flow modelling. In addition, the scaling method is able to simulate the approach of a glacier to a new steady state, if mass-balance elevation feedback is approximated by removing or adding elevation bands at the lowest part of the glacier as the glacier retreats or advances. If area changes are approximated in the mass balance computations in this way, our results indicate that volume-area scaling is a powerful tool for glacier volume projections on multi-century time scales.

4.2 Introduction

Melting glaciers, after ocean thermal expansion, are considered to be the second major contributor to the observed sea level rise in the 20th century [*Church et al.,* 2001; *Dyurgerov and Meier,* 2005). Regarding future climate projections, the glacier contribution is expected to accelerate due to fast response of glaciers to global warming, and many recent and ongoing researches are focused on modelling and quantifying this future contribution [e.g. *Gregory and Oerlemans*, 1998; *van de Wal and Wild,* 2001; *Raper and Braithwaite*, 2006]. However, modelling future glacier contributions carries a variety of uncertainties. This is due to scarcity of glacier inventory and hypsometry data and a large spectrum of uncertainties in modelling and downscaling future climate change, in modelling mass balance and finally in assessing the glacier

[1]Published as Radić, V., R. Hock and J. Oerlemans (2007), Volume-area scaling vs flowline modelling in glacier volume projections, *Ann. Glaciol.*, *46*, 234-240. Reproduced with the permission of the International Glaciological Society.

volume changes. The uncertainties in modelling volume changes are addressed in this paper focusing on the volume-area scaling approach proposed by *Bahr et al.* [1997].

Numerical ice-flow models best account for the physical processes involved, but they need detailed input data on glacier surface and bed geometry and therefore can only be applied on a small number of glaciers. Hence, owing to simplicity, the volume-area scaling approach has widely been used for considering area changes in volume predictions [e.g. *Church et al.*, 2001; *van de Wal and Wild*, 2001; *Radić and Hock*, 2006] or for estimating volumes of existing glaciers [e.g. *Meier and Bahr*, 1996; *Raper and Braithwaite*, 2005]. Volume and area for any glacier in a steady state are related via a power law, however, under non-steady-state conditions the power law relationship may change as the mass balance profiles change [*Bahr et al.*, 1997] posing a problem to employing volume-area scaling in modelling the response of glaciers to future climate warming. Based on some experiments with a numerical ice-flow model, *van de Wal and Wild* [2001] assumed such differences to affect volume predictions of a retreating glacier by not more that 20%. *Pfeffer et al.* [1998] tested the power-law relation by 3D ice-flow modelling of synthetic glaciers in steady states with focus on estimating glacier response times. Their results agreed well with the theory of *Bahr et al.* [1997], but non-steady-state conditions were not investigated.

In this study we apply a one-dimensional ice-flow model to numerically generated synthetic glaciers in order to investigate the volume-area power law relationships for both steady-state and non-steady-state conditions. The main objectives are: (1) to determine and compare the relationships for steady-state and non-steady-state conditions in order to test the validity of the power law relationship for non-steady-state conditions, and (2) to compare volume projections derived from volume-area scaling with those derived from the ice-flow modelling.

Using synthetic glaciers has the advantage that it easily allows to model a large number of glaciers under defined and controlled conditions, but it must be borne in mind that conclusions on the validity of the volume-scaling approach in comparison with the ice-flow modelling are restricted to the 1-D flowline representation of glaciers as defined in our experiments. In a next step we will elaborate on this paper by considering real glaciers constrained by observational data.

4.3 Theory of volume-area scaling

Several authors [e.g. *Macheret et al.*, 1988; *Chen and Ohmura*, 1990] have suggested that the volume V of valley glaciers is proportional to the surface area A raised to a power of about 1.36. *Bahr et al.* [1997] have shown the physical basis for the power-law relationship by applying exponential relationships between various glacier characteristics such as length x, width w, slope α, shape factor F and mass balance profile $b(x)$. These relationships are reasonable approximations to the behaviour of the ice flow and they include the flow law exponent n, the width scaling exponent q in $[w] \sim [x]^q$, the side drag scaling exponent f in $[F] \sim [x]^f$, the slope scaling exponent r in $[\sin\alpha] \sim [x]^r$ and parameters determining the mass balance profile. The brackets indicate characteristic values which can be assumed as the glacier's mean width, maximum length, total area etc. In geometric scaling analysis [*Bahr et al.*, 1997] the exact choice of characteristic values is not critical because each type of characteristic values is scaled by constants of proportionality. Mass balance profiles of valley glaciers can generally be expressed by:

$$b(x) \approx -c_1 x^m + c_0, \tag{4.1}$$

where c_1 and c_0 are positive constants and $m \approx 2$ [e.g. *Dyurgerov*, 1995; *Bahr et al.*, 1997]. This quadratic balance profile is the dominant term in a polynomial expansion of the actual mass balance. Dimensional analysis of glacier characteristics results in the following relation between $[V]$ and $[A]$:

$$[V] \propto [A]^\gamma, \gamma = \frac{1+m+n(f+r)}{(n+2)(q+1)} + 1, \tag{4.2}$$

where for valley glaciers q=0.6, m=2 and f=0 are suggested by empirical data, and r is either 0 for steep surface slopes or $r=(1-m+n-nf)/2(n+1)$ for shallow slopes. Inserting these values into Equation (4.2) the exponent in volume-area relationship equals γ=1.375 what is in close agreement with the exponent γ=1.36 which has been empirically derived from many Eurasian and Alps glaciers [*Chen and Ohmura*, 1990; *Meier and Bahr*, 1996].

4.4 Methods

Firstly, using a flowline model forced by different mass balance profiles we produce 37 synthetic steady-state glaciers ranging in size from 4 to 58 km^2. Modelled volumes and areas are used to determine the scaling exponent γ in the volume-area relationship from regression analysis. Secondly, non-steady-state conditions are modelled by imposing positive and negative mass balance perturbations on a subset of these synthetic glaciers producing in total 24 volume evolutions for 100 years. For each volume evolution we derive the scaling exponent γ based on the annual transient values of volume and area. Thirdly, we use the volume-area scaling approach to model glacier volume evolutions and compare results to those obtained by the flowline model. Finally, we apply several sensitivity experiments to evaluate the scaling approach when geometry changes are excluded or included in area-averaged net mass balance computations and when the glacier is in non-steady-state condition prior to the mass balance perturbations. We also investigate the sensitivity of results to the choice of the scaling exponent and the sensitivity of results in scenarios where the climate stabilizes after a period of perturbation.

4.4.1 The flowline model

We use the one-dimensional ice-flow model (central flowline along x) by *Oerlemans* [1997]. We consider this model as a good reference for evaluating the scaling approach since the model has proved to perform well in reconstructions of real glacier fluctuations [e.g. *Greuell*, 1989; *Oerlemans*, 1997; *Schlosser*, 1997]. The model equations are generated from the vertically integrated continuity equation, assuming incompressibility of ice, and Euler's equations combined with Glen's flow. From these equations, the prognostic equation for thickness H is derived as:

$$\frac{\partial H}{\partial t} = \frac{-1}{w}\frac{\partial}{\partial x}\left[D\frac{\partial h}{\partial x}\right] + b, \tag{4.3}$$

where b is mass balance rate, w the width of the glacier, h the surface elevation and D the diffusivity which is equal to:

$$D = w(\rho g)^3 H^3 \left(\frac{\partial h}{\partial x}\right)^2 (f_d H^2 + f_s), \tag{4.4}$$

where ρ is ice density and g is acceleration of gravity. Values for deformation parameter f_d=1.9 × 10^{-24} $Pa^{-3}s^{-1}$ and sliding parameter f_s=5.7 × 10^{-20} Pa^{-3} m^2 s^{-1} are taken from *Budd et al.* [1979]. This assumes that the vertical mean ice velocity is entirely determined by the local "driving stress" τ and it has two components: one associated with internal deformation $f_d H\tau$ and one with basal sliding $f_s\tau/H$. The "driving stress" τ is proportional to the ice thickness H and surface slope $\partial h/\partial x$. For further details about the model the reader is referred to *Oerlemans* [1997]. Equation (4.1) is solved on a 100 m resolution along the flowline while time integration is done with a forward explicit scheme which is stable if the time step is sufficiently small (e.g. 0.005 years).

4.4.2 Set of synthetic steady-state glaciers

We apply the flowline model to generate a set of synthetic glaciers defined as slabs of ice with uniform widths lying on a bed with uniform slope (tan α = 0.1). The model is run for 37 choices of mass balance profile $b(x)$ defined by different values of c_1 and c_0 (Equation 4.1), in order to obtain a set of glaciers in steady states with different climate conditions and glacier sizes. We define the mass balance profile as function of elevation $b(h)$ which is then transformed to the function of horizontal position $b(x)$ by fitting a parabolic function. By doing this we estimate the value for parameter c_1 with scaling exponent m=2. An example is shown in Figure 4.1 where the mass balance profile $b(h)$ is approximated by the profile $b(x)$. We consider the glacier in steady state if modelled glacier volume and area remain unchanged over a period of 100 years. In order to get the scaling exponent γ to agree with the theory of power-law relation for valley glaciers we have chosen the following set of exponents: q=0.6, f=0, m=2 and n=3. In the theory the choice of f=0 corresponds to the glaciers with little side drag, i.e. the glaciers with the half-width much larger than the glacier thickness [*Nye*, 1965]. Despite the fact that this may not be a good approximation for valley glaciers, the empirical data from valley glaciers showed that f is expected to be close to zero [*Bahr et al.*, 1997]. Therefore, to achieve $f\approx 0$, we produced synthetic glaciers with large widths relative to their thickness. To obtain q=0.6 we run the flowline model with a-priori determined uniform width and produced a glacier in a steady state. Then the steady-state glacier's length x is used to determine the glacier's width w as:

$$w = c\, x^q, \tag{4.5}$$

where c=10 m^{1-q} is our choice for constant of proportionality. The flowline model is then re-run using the derived width to produce the synthetic steady-state glacier. We leave the value for scaling exponent r undefined a-priory as it is dependent on other scaling exponents and on the steady-state glacier geometry derived from the flowline model.

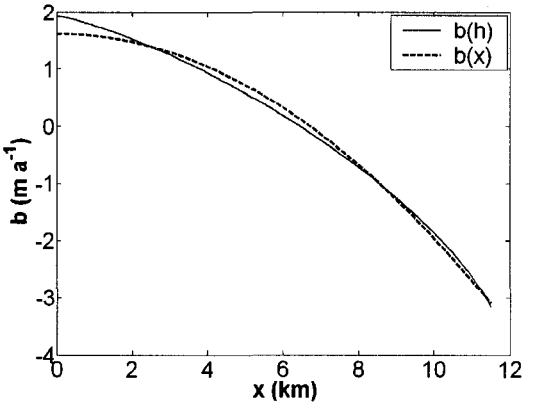

Figure 4.1. Mass balance profile $b(h)=-1.45\times10^{-6}\ h^2 + 0.0085\ h - 9.5$, where h is elevation (m asl), and its approximation with the profile $b(x)= -3.564\times10^{-8}\ x^2 + 1.614$, where x is length along the flowline (m). The profile generated the synthetic glacier with area A=31.64 km^2 and V=4.08 km^3.

4.4.3 Model-derived volume-area relationships

From the 37 synthetic glaciers we obtain a set of values for V and A from which we determine the power-law relationship for steady-state conditions. To investigate volume-area scaling under non-steady-state conditions (transient conditions) we introduce a perturbation db in the mass balance profile on a subset of the 37 synthetic steady-state glaciers:

$$b(x,t) \approx -c_m x^m + c_0 + db(t). \tag{4.6}$$

The magnitude of mass balance perturbation $db(t)$ increases with a constant rate:

$$db(t)=db(0)\ t, \tag{4.7}$$

where t=1,...100. A period of 100 years is chosen because future climate change studies are often focused on a century scale. We chose 3 different initial magnitudes for *db(0)*, corresponding to climate cooling and warming: ± 0.005, ± 0.01 and ± 0.015 m a^{-1}. In total we create 24 volume evolutions of glaciers with different initial sizes (12 responding to climate warming and 12 responding to cooling). We determine a power-law relationship for each of these 24 transient volume and area evolution by linearly regressing on logarithmic axes the modelled annual values of volume and area once the steady-state area has changed.

4.4.4 Volume projections using volume-area scaling

Finally, we investigate how well volume evolutions can be estimated from the volume-area scaling approach by comparing results to those obtained from the flowline model. For each of the 24 volume evolutions produced by the flowline model, we compute corresponding volume evolutions based on the scaling approach. While the flowline model calculates the thickness change for each time step which determines the volume change, in the scaling approach the volume changes are represented by:

$$dV(t) = \bar{b}(t)A(t), \tag{4.8}$$

where $\bar{b}(t)$ is annual area-averaged net mass balance. After the volume change has been calculated at t=0 the glacier's area at the next time step t=1 is calculated by inverting Equation (4.2). The new area at t=1 is used to calculate the mass balance (Equation 4.9) and the volume change at t=1 by using again Equation (4.8) and the calculation is repeated until t=100. Annual area-averaged net mass balance $\bar{b}(t)$ is calculated from the mass balance profile as:

$$\bar{b}(t) = \frac{\sum_{i=1}^{n} b_i(t)a_i(t)}{A(t)}, \tag{4.9}$$

where b_i and a_i are discrete values of mass balance *b(x,t)* and surface area *a(x,t)* for each spatial band (i=1...n) over the glacier length, while A is total surface area. We use two definitions for annual area-averaged net mass balance following *Elsberg et al.* [2001] and *Harrison et al.* [2005]: if $\bar{b}(t)$ is calculated keeping surface area constant in time (equal to initial area *A(t=0)*) the result

is a 'reference-surface' mass balance. If area in Equation (4.9) is updated for each year by volume-area scaling we derive 'conventional' mass balance. Here, we assume that change in total area occurs on the tongue of the glacier, thus the lowest area bands are excluded if total area shrinks or new area bands are included if total area grows. Area bands have the length of 100 m to be equal size as the grid spacing in the flowline model.

For comparison we apply three different methods to calculate volume evolution from Equations (4.8) and (4.9) differing from each other solely in whether or not area changes are included in Equations (4.8) and (4.9):

1. The glacier area A is assumed constant in both Equations (4.8) and (4.9). Hence volume-area scaling is not applied. $\bar{b}(t)$ is calculated as a 'reference surface' mass balance using constant area A and constant number of spatial bands in Equation (4.9).
2. The area A is assumed constant in Equation (4.9) but variable in Equation (4.8), as done e.g. by *Radić and Hock* [2006]. The glacier area is adjusted according to volume-area scaling, i.e. a new area is computed using Equation (4.2) from the volume change obtained by Equation (4.8), but $\bar{b}(t)$ is computed as a 'reference surface' mass balance using constant area (Equation 4.9).
3. Area changes are considered in both Equations (4.8) and (4.9). $\bar{b}(t)$ is calculated as a 'conventional' mass balance meaning that $A(t)$ and number of spatial bands changes in Equation (4.9). Volume-area scaling is applied. This method partially accounts for the feedback between geometry changes and mass balance (e.g. area-averaged mass balance of a valley glacier becomes less negative as the glacier, in its approach to a new steady state, retreats from low-lying high-ablation altitudes to higher and colder altitudes).

We compare the results of each method with the volume evolution derived from the flowline model. To test how sensitive the volume projections are to the choice of scaling exponent in the scaling methods, we use the exponent γ in volume-area relation derived from the 37 steady-state glaciers, the values obtained from the volume evolutions of the non-steady-state glaciers, and γ=1.375 according to the theory of *Bahr et al.* [1997].

4.5 Results and discussion

4.5.1 Volume-area relationship in steady state

Figure 4.2 illustrates the relationship between volume and area plotted on logarithmic axes for all 37 synthetic glaciers in steady states. Glacier areas and volumes span in the range [4.37, 57.88] km^2 and [0.17, 10.29] km^3, respectively. The strong correlation shows that the flowline model produces glacier volumes and areas that follow a power-law relationship. The slope of the regression line corresponds to scaling exponent γ and it equals 1.56 with r^2 of 0.999. Hence, it differs from γ=1.375 derived by *Bahr et al.* [1997] by 14%. However, although theoretically derived, the value by *Bahr et al.* [1997] is largely dependent on empirical data to which their results were adjusted. Since we analyse synthetic glaciers the deviation from empirical results was expected because our synthetic glaciers have largely simplified geometry (e.g. uniform widths) and are created with the flowline model which presents a simplified approximation for glacier dynamics. Below, we aim to answer how significant this deviation is when deriving volume evolutions.

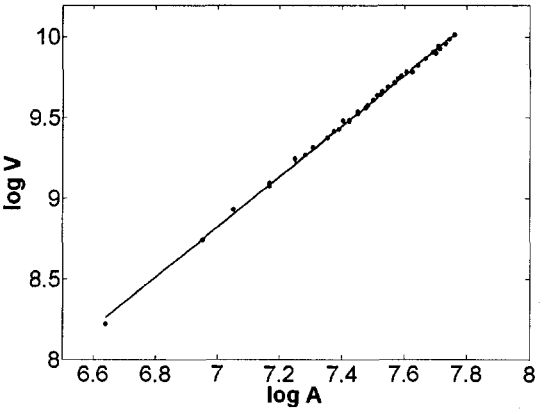

Figure 4.2. Log-log plot of volume V vs area A for 37 synthetic glaciers in steady state with a regression $logV=1.56\ logA - 2.11$ (r^2=0.999).

4.5.2 Volume-area relationship in non-steady state

The ice-flow model produced volumes and areas as a discrete set of values with a time step of one year. While volume changes occur almost immediately after introducing the perturbation *db*, due to discretization, modelled length and surface area remain constant for an initial period of ~30-50 years, depending on the magnitude of perturbation. As an example, Figure 4.3 shows the area

evolution in response to the mass balance perturbation of $b(0)$=-0.015 m a^{-1}.We decided to treat the first 50-year period as a 'discretization spin-up' period and consider the set of V and A in the remaining period as a representative set to derive scaling exponents under non-steady-state conditions. Figure 4.3 illustrates all 24 sets of V and A on logarithmic axes. Scaling exponents are derived for each of the 24 volume evolutions and they span in the range [1.80, 2.90] for γ with corresponding range of [-3.88, -12.01] for k in $logV=\gamma\ logA+k$. Larger values for γ tended to occur for negative mass balance perturbations (warming scenario) compared to positive perturbations (cooling scenario) and γ tended to decrease with increasing initial glacier size. Scaling exponents for our set of test glaciers differ by 21% (γ=1.80) to 86% (γ=2.90) from the scaling exponent derived for the synthetic glaciers in steady states (γ=1.56). One of the possible reasons for this difference is that the glacier's width in the transient state is not scaled with the glacier's length according to Equation (4.5), meaning that the scaling parameter q in width-length relationship may change in time since the glacier's length changes while the width is kept constant. Thus, changes in any of the exponential relationships between glacier characteristics, such as between width and length, modifies the scaling exponent in the volume-area relationship. The significance of this difference in scaling exponent γ is analyzed in the next section.

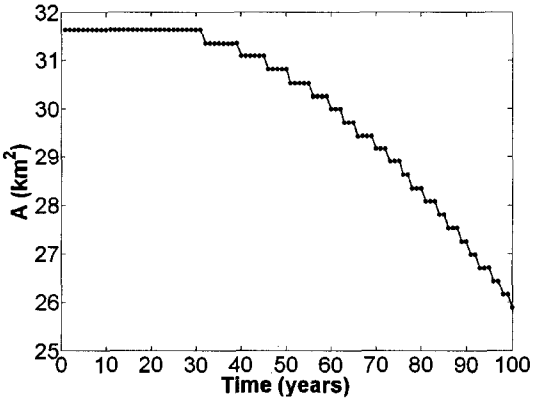

Figure 4.3. Surface area evolution derived from the flowline model as response to the perturbation of $db(0)$=-0.015 m a^{-1}.

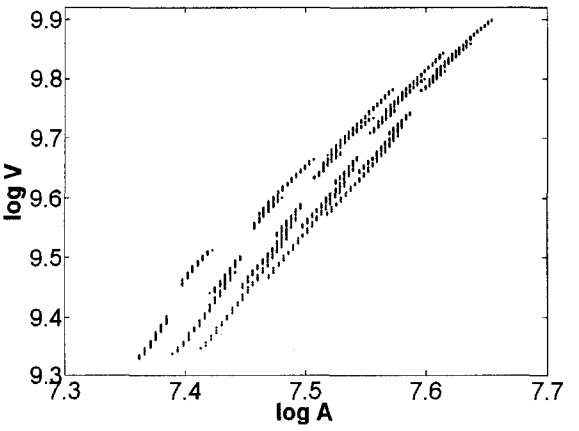

Figure 4.4. Log-log plot of volume vs area for 24 volume (area) evolutions as a response to different mass balance perturbations. Each evolution contains 50 values of V and A. For each evolution we derived a regression $logV=\gamma logA+k$ in order to determine the scaling exponent γ.

4.5.3 Volume evolutions: sensitivity experiments

Figure 4.5 illustrates the results for the total volume change over 100 years projected by the ice-flow model compared to those projected by the scaling approach. Here, we illustrate only two of the 24 evolutions since results in terms of sensitivity to the choice of the method are similar for all evolutions. We choose the largest glacier in the set ($A(0)$=38.92 km^2, $V(0)$=5.77 km^3) responding to the largest perturbation of $db(0)$=±0.015 m a^{-1}. The evolutions are normalized to the initial volumes. In Figure 4.5a we compare three different variants of the scaling approach as described above ((a) the 'reference-surface' mass balance with no volume-area scaling (b) the 'reference surface' mass balance with scaling and (c) the 'conventional' mass balance with scaling). The scaling exponent γ=1.56 as previously derived from the 37 synthetic steady-state glaciers is applied. To optimize initial conditions for each volume evolution the constant of proportionality in the volume-area scaling relationship is derived from the glaciers' initial volume and area instead of using the constants k derived from regression analysis of each evolution (Figure 4.4).

Results based on methods (a) and (b) closely follow the evolution curves from the flowline model in the first ~50 years for both the warming and the cooling scenario, while those from method (c) notably deviate somewhat earlier (Figure 4.5a). However, by the end of the 100-year period the

volume change obtained from method (c) is smallest. Note that the volume response is not symmetrical for positive and negative mass balance perturbation of equal magnitude for the methods (b) and (c) which include scaling. This is due to the exponential character of the volume-area relationship (Equation 4.2). Results from the whole set of 24 evolutions showed that by increasing the magnitude of the mass balance perturbation the sensitivity to the choice of the scaling method increases, i.e. the difference between the projections derived by the flowline model and the scaling methods increases. Also, smaller glaciers in the set ($A < 20$ km^2) are more sensitive to the choice of the scaling method. However, these differences in total volume change over 100 years for the whole set of 24 evolutions are within the range of 12% of initial volume when method (c) is applied and 16% and 23% when methods (a) and (b) are applied, respectively. Thus the smallest differences are produced by method (c). This was expected result since the scaling method (c) is the most sophisticated method of those three taking into account area-changes and considering these in the mass-balance computations.

The next sensitivity test quantifies the uncertainty in volume projections due to different values of scaling exponent γ in volume-area scaling. For this purpose we use the 'conventional' mass balance scaling approach, method (c), but with three different scaling exponents as derived from our 37 steady-state synthetic glaciers, the transient evolutions of the synthetic glaciers and the theoretically derived value by *Bahr et al.* [1997]. Results for the largest glacier in the set are shown in Figure 4.5b. In the total set of 24 evolutions the 100-year volume changes derived by the scaling method with three different scaling exponents differ from each other less than 6%. The difference tends to decrease with decreasing mass balance perturbations or increasing initial glacier size. These results suggest that applying scaling exponents that differ up to 86% yield differences not larger than 6% in derived volume changes on a century time scale. This difference may be considered negligible in comparison to the range of differences due to the choice of the scaling methods and the range of uncertainties due to the approximations in the flowline model and volume-area scaling approach. Additionally, applying the scaling exponent γ derived from each transient evolution of the synthetic glacier produced the volume projections that followed most closely those from the flowline model. This is to be expected since the scaling exponent is calculated directly from the relationship between transient volumes and areas produced by the flowline model.

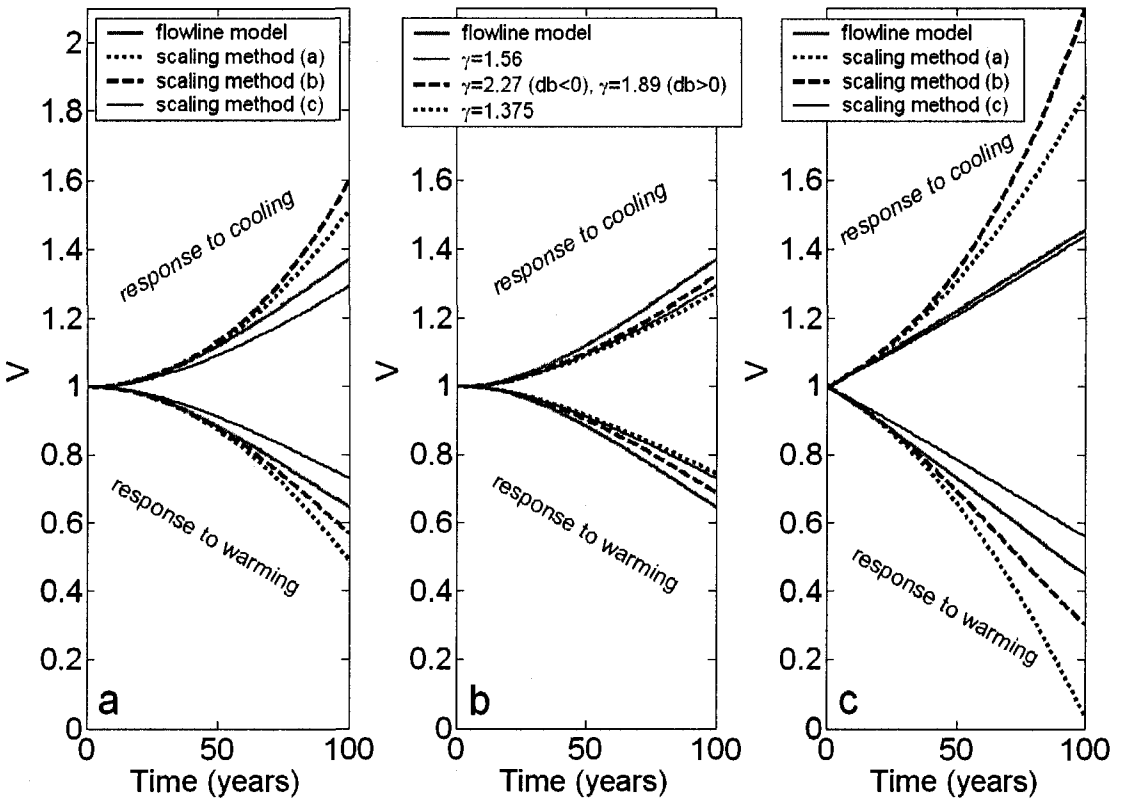

Figure 4.5. Normalized volume evolutions of the largest test glacier responding to the mass balance perturbation of $db(0)$=+0.015 m a^{-1} ('cooling scenario') and $db(0)$=-0.015 m a^{-1} ('warming scenario'). In figure (a) and (c) the three methods correspond to three different ways of calculating area-averaged net mass balance and volume changes: the 'reference-surface' mass balance without volume-area scaling (method a), the 'reference surface' mass balance with scaling (method b) and the 'conventional' mass balance with scaling (method c). Scaling exponent γ=1.56 is used in the volume-area relationship. In figure (b) volume evolutions are derived from scaling method (c) using three different scaling exponents: γ=1.56 derived from our 37 synthetic steady-state glaciers, γ=2.27 (1.89) derived from the transient response to warming (cooling) of this test glacier, and γ=1.375 derived theoretically by *Bahr et al.* [1997]. In figure (c) the test glacier is in non-steady state prior to the mass balance perturbation.

So far we have evaluated the scaling approach for synthetic glaciers that are initially in steady states. In the next sensitivity experiment we compute the volume evolutions for glaciers that are initially in non-steady state, i.e. their mass balance has been negative or positive for several decades prior to the mass balance perturbation. The results for the largest synthetic glacier in the set are shown in Figure 4.5c. Initial mass balance for the glacier with warming scenario is $b(0)$=-0.54 m a^{-1} and it is perturbed with $db(0)$=-0.015 m a^{-1}, while for the cooling scenario the values are $b(0)$=0.55 m a^{-1} and $db(0)$=0.015 m a^{-1}. All scaling methods show a stronger response to the mass balance perturbation compared to the results for glaciers initially in steady state (Figure 4.5a). This is due to the larger magnitude of the initial mass balance perturbation. In addition, deviations between the different projections are much larger. For all 24 evolutions the differences between the 100-year volume changes obtained from the ice-flow model and the volume changes from methods (a) and (b) are up to 47% and 74%, respectively, while the volume changes from method (c) differ up to 16% of initial volume. Thus, method (c) produced the best approximation of 100-year volume evolutions derived from the flowline model for the synthetic glaciers initially in non-steady state. We also assumed different scaling exponents in the scaling method (c), as done above, and derived the 100-year volume changes which differed by less than 12%. As in the experiment above, applying the scaling exponent γ derived from each transient evolution produced the closest volume projection to the one obtained from the flowline model. We expect the volume projections derived from the scaling approach to continue to diverge from those derived by the flowline model if the mass balance perturbation according to Equation (4.7) is applied beyond the period of 100 years. How much they diverge depends on magnitude of mass balance perturbation, initial size of the synthetic glacier and the method for calculating area-averaged mass balance.

Our final sensitivity test evaluates the scaling methods for hypothetic scenarios where the climate stabilizes after the initial period of perturbation. To that end, we derived volume projections for a 300-year period applying a cooling or warming scenario for the first 100 years while afterwards the climate is kept stable. Thus, after an initial period of 100 years with mass balance perturbation, as employed in our previous experiments (Equation 4.7), we continued the evolution for additional 200 years keeping the mass balance perturbation equal to the perturbation at t=100. The results are shown in Figure 4.6 for a cooling and warming scenario applied on the largest glacier in the set. For both scenarios the volume evolutions derived from the flowline model reach

new steady states. This is not the case for the scaling methods (a) and (b) which keep the surface area constant in the calculations of area-averaged mass balance thus excluding the feedback between the mass balance and glacier geometry changes. Only the method with 'conventional' mass balance calculation, method (c), is able to simulate the approach of the glacier to a new steady state. Although the method (c) produces 100-year volume changes which deviate up to 12% from the changes derived by the flowline model, it is the only of those three scaling methods which is capable of simulating the response of area-averaged mass balance to geometry/elevation changes as simulated by the flowline model on a multi-century time scale. For our synthetic glacier with uniform width this feedback is simulated by subtracting (adding) area bands on the tongue of the glacier as glacier retreats (grows) due to warming (cooling).

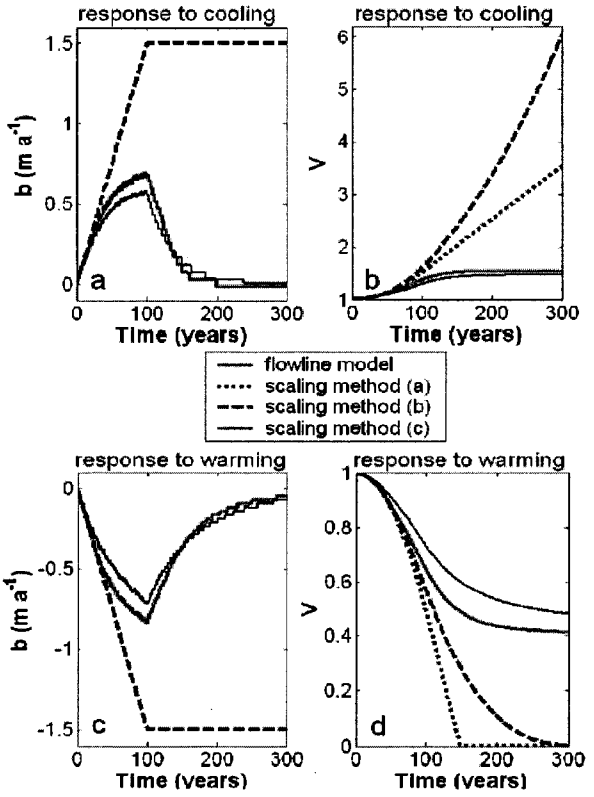

Figure 4.6. Evolution of area-averaged mass balance (a, c) and normalized glacier volume (b, d) derived from the flowline model and from the scaling methods. Initial perturbation is $db(0)$=0.015 m a^{-1} (cooling scenario) and $db(0)$=-0.015 m a^{-1} (warming scenario). Scaling methods (a) and (b) are based on 'reference surface' mass balances and scaling method (c) is based on 'conventional' mass balances as also in the flowline model.

4.6 Conclusions

Scaling exponent γ=1.56 in the volume-area relationship obtained from 37 synthetic steady-state glaciers of different sizes differed from γ=1.375 derived theoretically by *Bahr et al.* [1997] and from the exponents (γ=[1.80, 2.90]) derived for each of 24 investigated glaciers under non-steady-state conditions, i.e. responding to hypothetical mass balance perturbations. Exponents γ were generally larger for negative mass balance perturbations (warming scenarios) than for positive perturbations (cooling scenarios) and γ tended to decrease with increasing initial glacier size. However, the range of differences in scaling exponent by up to 86% is shown to make negligible differences, less than 6%, in 100-year volume changes derived from the scaling approach.

Volume projections on a century time-scale differed within the range of 12%-23% of initial volume from the flow model results depending on the method by which the area-averaged net mass balance is calculated, i.e. whether or not volume-area scaling is applied and area changes obtained from volume-area scaling are included ('conventional' mass balance) or excluded ('reference surface mass balance') in the mass balance computations. The most sophisticated method accounting for area-changes and considering these in the mass-balance computations resulted in the smallest differences (up to 12%) in projected volume changes over 100 years. This method best agreed with the projections by the ice flow model when the glaciers are initially in non-steady state or when the climate is assumed to stabilize after a period of perturbation. In fact, the method is capable of simulating the glacier approaching a new steady state by simulating the feedback between area-averaged mass balance and glacier geometry/elevation changes resulting from retreat or advance of the glacier. This feedback is captured by excluding area from or adding area to the lowest part of the glacier. In contrast, neglect of volume-area scaling and neglect of area-changes in the mass balance computations fails to simulate this feedback and the approach to a new steady state.

Although based on a set of synthetic glaciers of highly simplified geometry, our results are promising for use of volume-area scaling in glacier volume projections provided that the mass balance-elevation feedback is captured by considering area-changes in the mass balance computations. Our approach to add and remove area from the lowest elevation bands of the glacier seems to be able to capture these processes sufficiently well to obtain results comparable

to those from the ice flow model. In a next step we will test the approach on real glaciers with observational records.

Acknowledgements

Financial support for this work is provided by the Swedish Research Council for Environment, Agricultural Sciences and Spatial Planning (project number: 21.4/2003-0387). Regine Hock is Royal Swedish Academy of Science Research Fellow supported by a grant from the Knut Wallenberg Foundation. We are very grateful to S. Raper, R. van de Wal, M. Dyurgerov and two anonymous reviewers for useful comments and suggestions.

4.7 References

Bahr, D. B., M. F. Meier, and S. D. Peckham (1997), The physical basis of glacier volume-area scaling, *J. Geophys. Res., 102*(B9), 20355-20362.

Budd, W. F., P. L. Keage and N. A. Blundy (1979), Empirical studies of ice sliding, *J. Glaciol., 23*(89), 157-170.

Chen, J. and A. Ohmura (1990), Estimation of Alpine glacier water resources and their change since the 1870's, International Association of Hydrological Science Publication 193 (Symposium at Lausanne 1990 – Hydrology in Mountainous Regions. I – Hydrological Measurements; the Water Cycle), 127-135.

Church, J. A., J. Gregory, P. Huybrechts, M. Kuhn, K. Lambeck, M. Nhuan, D. Qin and P. Woodworth (2001), Changes in sea level, in Climate Change 2001: The Scientific Basis. Contribution of Working Group I to the Third Assessment Report of the Intergovernmental Panel on Climate Change, edited by J. Houghton, Y. Ding, D. Griggs, M. Noguer, P. van der Linden, X. Dai, K. Maskell and C. Johnson, 639-684, Cambridge University Press, Cambridge, UK.

Dyurgerov, M. B. (1995), Changes in the 'activity index' of the northern hemisphere glaciers during global warming (abstract), Eos Trans. AGU, 76(46), Fall Meet. Suppl., F208.

Dyurgerov, M. B. and M. F. Meier (2005), Glaciers and the Changing Earth System: a 2004 Snapshot. Occasional Paper 58, Institute of Arctic and Alpine Research, University of Colorado, Boulder, Colorado, 117p.

Elsberg, D. H., W. H. Harrison, K. A. Echelmeyer and R. M. Krimmel (2001), Quantifying the effects of climate and surface change on glacier mass balance, *J. Glaciol., 47*(159), 649-658.

Gregory, J. M. and J. Oerlemans (1998), Simulated future sea-level rise due to glacier melt based on regionally and seasonally resolved temperature changes. *Nature, 391*(6666), 474-476.

Greuell, W. (1989), Glaciers and climate: energy balance studies and numerical modelling of the historical front variations of the Hintereisferner (Austria), Ph.D. thesis, Utrecht University.

Harrison, W. D., D. H. Elsberg, L. H. Cox, and R. S. March (2005), Different mass balance for climatic and hydrologic applications, *J. Glaciol., 51*(172), 176.

Macheret, Y. Y., P. A. Cherkasov and L. I. Bobrova (1988), Tolschina I ob'em lednikov Djungarskogo Alatau po dannym radiozondirovaniya, *Mater. Glyatsiologicheskikh Issled. Khronika Obsuzhdeniya*, (Data of Glaciol. Studies. Chronicles and Discussions), *62*, 59-71.

Meier, M. F. and D. B. Bahr (1996) Counting glaciers: use of scaling methods to estimate the number and size distribution of glaciers of the world, CRREL Spec. Rep., 96-27, 89-94.

Nye, J. F. (1965), The flow of a glacier in a channel of rectangular, elliptic or parabolic cross-section, *J. Glaciol., 5*, 661-690.

Oerlemans, J. (1997), A flowline model for Nigardsbreen, Norway: projection of future glacier length based on dynamical calibration with the historic record, *Ann. Glaciol., 24*, 382-389.

Pfeffer, W. T., C. Sassolas, D. B. Bahr and M. F. Meier (1998), Response time of glaciers as a function of size and mass balance: 2. Numerical experiments, *J. Geophys. Res., 103*(B5), 9783-9789.

Radić, V. and R. Hock (2006), Modelling future glacier mass balance and volume changes using ERA40-reanalysis and climate models –A sensitivity study at Storglaciären, Sweden. *J. Geophys. Res., 111*, F03003, doi:10.1029/2005JF000440.

Raper, S. C. B. and R. J. Braithwaite (2006), Low sea level rise in projections from mountain glaciers and icecaps under global warming, *Nature, 439*, 311-313, doi:10.1038/nature04448.

Raper, S. C. B., and R. J. Braithwaite (2005), The potential for sea level rise: New estimates from glacier and ice cap area and volume distributions. *Geophys. Res. Lett., 32*, L05502, doi: 10.1029/2004GL021981.

Schlosser, E. (1997), Numerical simulation of fluctuations of Hintereisferner, Ötztal Alps, since AD 1850, *Ann. Glaciol., 24*, 199-202.

van de Wal, R. S. W., and M. Wild (2001), Modelling the response of glaciers to climate change by applying volume-area scaling in combination with a high resolution GCM. *Clim. Dynam., 18*(3-4), 359-366.

Chapter 5

Analysis of scaling methods in deriving future volume evolutions of valley glaciers[1]

5.1 Abstract

Volume-area scaling is a common tool for deriving future volume evolutions of valley glaciers and their contribution to sea level rise. We analyze the performance of scaling relationships among glacier's volume, area and length in deriving volume projections in comparison to projections from a one-dimensional ice-flow model. The model is calibrated for six glaciers (Nigardsbreen, Rhonegletscher, South Cascade Glacier, Sofiyskiy Glacier, Midre Lovénbreen and Abramov Glacier). Volume evolutions forced by different hypothetical mass balance perturbations are compared to those obtained from volume-area (V-A), volume-length (V-L) and volume-area-length (V-A-L) scaling. Results show that the scaling methods mostly underestimate the volume losses predicted by the ice-flow model, up to 47% for V-A scaling and up to 18% for V-L scaling by the end of the 100-year simulation period. In general V-L scaling produces closer simulations of volume evolutions derived from the ice-flow model, suggesting that V-L scaling may be a better approach for deriving volume projections than V-A scaling. Sensitivity experiments show that the initial volumes and volume evolutions are highly sensitive to the choice of the scaling constants yielding both over- and underestimation. However, when normalized by initial volume, volume-evolutions are relatively insensitive to the choice of scaling constants especially in the V-L scaling. 100-year volume projections differ within 10% of initial volume when V-A scaling exponent commonly assumed γ=1.375 is varied by -30% to +45% (γ=[0.95, 2.00]) and V-L scaling exponent q=2.2 is varied by -30% to +45% (q=[1.52, 3.20]). This is encouraging for use of scaling methods in glacier volume projections, particularly since scaling exponents may vary between glaciers and the scaling constants are generally unknown.

5.2 Introduction

The importance of glaciers as contributors to the global sea level rise is well recognized [*IPCC*, 2007] and several authors have presented the methods of assessing recent and modeling future glacier wastage on a global scale [e.g. *van de Wal and Wild*, 2001; *Raper and Braithwaite*, 2006; *Meier et al.*, 2007]. Since volume observations are available only for a limited number of glaciers in the world while data on surface areas are far more abundant, a common way to estimate glacier volume is through a scaling relationship between glacier volume and area. *Bahr et al.* [1997]

[1]In press as Radić, V., R. Hock and J. Oerlemans (2008), Analysis of scaling methods in deriving future volume evolutions of valley glaciers, *J. Glaciol.*, *54*(187). Reproduced with the permission of the International Glaciological Society.

derived power-law scaling relationships between the steady-state volume of a glacier and its area and length. Although scaling exponents may change under non-steady state conditions, scaling has commonly been used in future volume projections on a global scale [e.g. *van de Wal and Wild*, 2001; *Raper and Braithwaite*, 2006; *IPCC*, 2007; *Meier et al.*, 2007] since the input data required for more sophisticated approaches are generally not available.

Volume-area scaling improves projections assuming constant glacier area in time [e.g. *ACIA*, 2005]. Keeping the area fixed in time does not allow the glacier to reach new equilibrium in a different climate while the scaling, coupled with mass continuity equation, allows for changes in glacier size. Therefore, scaling accounts for at least some of the feedback between glacier mass balance and geometry as the glacier size and shape adjust to climate change. The area-averaged surface mass balance of a glacier will change as the glacier thins and retreats or thickens and advances until it has reached new equilibrium geometry in response to a steplike climate perturbation, but there are two opposing effects. By lowering the ice surface as the ice thins the glacier is exposed to higher air temperatures resulting in more negative mass balances. However, as the glacier retreats loss of area at predominantly lower altitudes will make the area-averaged mass balance less negative [*Braithwaite and Raper*, 2002]. *Raper et al.* [2000] developed a 'geometric' model including scaling relationships between glacier volume, area and length. This model forced by Global Climate Model (GCM) scenarios reduced the estimated global glacier ablation for the end of the 21 century by about 45% compared to results when the glacier area was kept constant in time, in agreement with the range of 40% to 50% reported by *IPCC* [2007].

Considering the dominance of scaling methods in attempts to estimate the global glacier volumes and future glacier wastage, only little effort has been devoted to a systematic error analysis of the results derived from scaling relationships. For example, *van de Wal and Wild* [2001] compared the scaling method with an ice-flow model for several individual glaciers and reported that a retreating glacier is at any arbitrary time not more than 20% smaller in volume than expected from the volume-area scaling. *Schneeberger et al.* [2003] performed similar comparison between the volume-are scaling and a 2-D ice-flow model for 11 glaciers. Since volume projections by the scaling method were both over- and underestimated depending on how well a particular glacier in their sample fits in the scaling relationship, they concluded that the scaling method should be applicable on a large data set. *Meier et al.* [2007] applied scaling to a global data set and reported

an error in calculating volumes from area values of the order of 25% for global aggregates, but of the order of 50% for individual ice masses. However, none of these studies provide any details how error estimates are derived or a systematic evaluation of the scaling methods.

Pfeffer et al. [1998] used a pseudo 3-D ice-flow model for synthetic glaciers in steady state to test if the scaling relationships in *Bahr et al.* [1997] are derived correctly from the underlying continuum mechanics. Although they confirmed the physical background of the scaling relationships, they did not perform an error analysis nor applied the model on real glaciers. Another study on synthetic glaciers, by *Radić et al.* [2007], compared volume evolutions derived from a scaling method with those derived from a 1-D ice-flow model. Results indicated that the volume projections derived from scaling were relatively insensitive to the assumptions on scaling exponents. In this paper we elaborate on their analysis using a set of real glaciers in order to investigate the uncertainties in modeling future glaciers volume changes from the scaling methods. Our aim is to present a detailed analysis on the performance of scaling relationships between glacier's volume, area and length used for deriving volume projections in comparison to projections from an ice-flow model.

5.3 Methods

A 1-D ice-flow model along a flowline [*Oerlemans*, 1997] is applied to produce volume evolutions which serve as a reference to which volume evolutions derived from the scaling methods are compared. Our procedure can be divided in 4 steps: First, we calibrate the ice-flow model by varying the glacier mass balance profiles to maximize the agreement between both observed and simulated glacier historical length fluctuations and recent glacier surface profile along the flowline. Second, we impose hypothetical mass balance perturbations to the reference mass balance profile, defined as a negative trend in the mass balance rate, and derive 100-year volume evolutions from the ice-flow model. Third, results are compared to the volume evolutions derived from scaling methods using the same mass balance perturbations. We use three different scaling methods: volume-area scaling, volume-length scaling and volume-area-length scaling. Finally, we apply a series of model experiments in order to investigate the sensitivity of volume evolutions to the choice of scaling parameters and to the way mass balance – elevation feedback is incorporated.

5.3.1 Investigated glaciers and data

For this study we selected six glaciers from different geographical locations and climatic regimes and for which the required input data could be retrieved: Nigardsbreen (61.72°N, 7.13°E), an outlet glacier of Jostedalsbreen in southern Norway, Rhonegletscher (46.62° N, 8.40° E) in the center of the Swiss Alps, South Cascade Glacier (48.37°N, 121.05°W) in the North Cascades of Washington State, US, Sofiyskiy (49.78°N, 87.77°E) a continental summer-accumulation-type glacier in the Russian Altai mountains, Midre Lovénbreen (78.88°N, 12.07°E) a polythermal valley glacier in northwest Spitsbergen and Abramov Glacier (39.67°N, 71.50°E) in the Alay Range of Kirghizstan. The surface maps of these glaciers are shown in Figure 5.1.

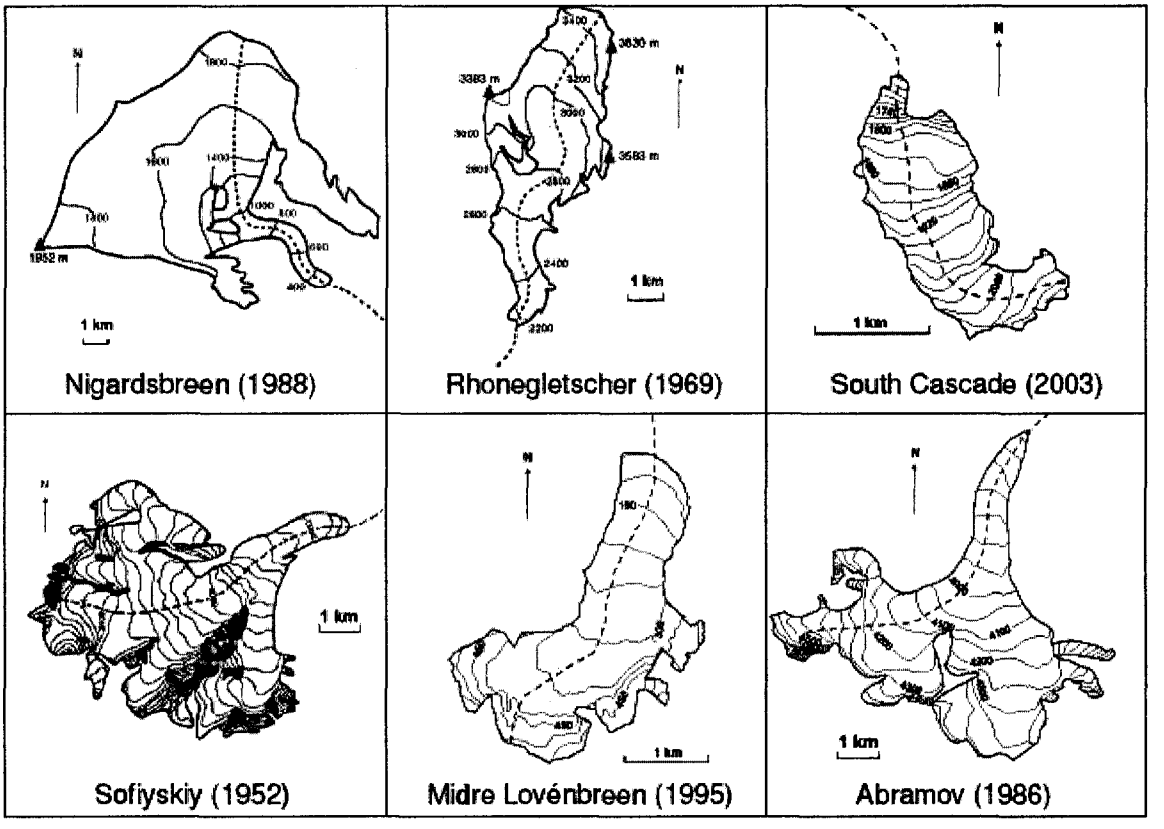

Figure 5.1. Contour maps of the investigated glaciers based on topographic maps. Years refer to the dates of the topographic maps.

To run the ice-flow model, data on bed and surface topography, historical front observations, and mass balance are needed. The ice-flow model has previously been applied to Nigardsbreen [*Oerlemans*, 1997], Rhonegletscher [*Stroeven et al.*, 1989; *Wallinga and van de Wal*, 1998] and Sofiyskiy Glacier [*De Smedt and Pattyn*, 2003] and their input data were available in this study. Unless otherwise stated mass balance data were taken from the reports of World Glacier Monitoring Service (WGMS; e.g. *Haeberli et al.* [2005]) and from the reports of the Norwegian Water Resources and Energy Directorate [e.g. *Kjøllmoen*, 2001]. The digital elevation model (DEM) for the surface of South Cascade Glacier and observations of mass balance profiles were taken from USGS Scientific Investigations Reports [e.g. *Krimmel*, 2002; *Bidlake et al.*, 2004]. The bed topography map was provided by Bob Krimmel (unpublished data) while the historical front observations were compiled in Rasmussen and Conway (2001). The bed topography of Midre Lovénbreen was derived from ground penetrating radar data [*Björnsson et al.*, 1996; J. Moore, unpublished data] while the surface topography maps were compiled by the Norsk Polarinstitut from aerial photographs made from several time periods as explained in *Rippin et al.* [2003]. Interpolated mass balance profiles for Midre Lovénbreen were provided by Jack Kohler (unpublished data). *Kuzmichenok et al.* [1992] produced the bed and surface topography maps for Abramov Glacier while the observed mass balance profiles were compiled in *Pertziger* [1996]. In Table 5.1 we listed, for these six glaciers, the time periods for which the data of length fluctuations and mass balance were available and the years of the surface and bed topography maps used in the calibration of the ice-flow model. Some data on ice velocities were available for Rhone, South Cascade and Sofiyskiy glaciers and used to calibrate the ice-flow model.

5.3.2 Volume evolutions from the ice-flow model

Model description

For each of six glaciers we used the 1-D ice-flow model (central flowline along x) by *Oerlemans* [1997]. The time step was 0.005 year and grid point spacing along the flowline was 100 m. The 3-D geometry was taken into account by parameterization of the cross-sectional geometry at each grid point. The cross-profile has a trapezoidal shape and is described by the valley width at the base, w_b, glacier thickness along the flowline, H, and the angle between valley wall and the vertical, Θ. Values for the width at the glacier's surface, w_s, and for Θ were calculated from topographic maps. The width at the base was parameterized as a function of H:

$$w_b = w_s - 2(\tan\theta)H\,. \tag{5.1}$$

For Sofiyskiy Glacier the surface width derived from the topography map was kept constant in time due to lack of bed topography data. The driving equation for calculating volume evolutions from the model is the continuity equation which, assuming constant ice density, can be written as:

$$\frac{\partial S}{\partial t} = -\frac{\partial(US)}{\partial x} + w_s\dot{b}\,, \tag{5.2}$$

where S is the cross section area of the glacier defined by

$$S = [w_b + (\tan\theta)H]H\,. \tag{5.3}$$

U is the depth-averaged ice velocity and $\dot{b}$ is the specific mass balance rate. U is calculated by [*Budd et al.*, 1979; *Paterson*, 1981]:

$$U = U_d + U_s = f_d H\tau^3 + f_s\frac{\tau^3}{\rho g H}, \tag{5.4}$$

where subscripts d and s refer to internal deformation and basal sliding, respectively, τ is the local "driving stress" which is proportional to the ice thickness H and surface slope $\partial h/\partial x$, ρ is ice density (ρ=0.9 kg m^{-3}) and g acceleration by gravity. The flow parameters f_d and f_s depend on bed conditions, debris content and crystal structure of the basal ice layers but their values are not known accurately. Therefore we used the flow parameters as tuning parameters to achieve the closest match between the observed and the modeled surface profile along the flowline. Substitution of Equations (5.1) and (5.3) into Equation (5.2) yields the prognostic equation for the glacier thickness, H:

$$\frac{\partial H}{\partial t} = -\frac{1}{w_b + 2(\tan\theta)H}\left[[w_b + (\tan\theta)H]\frac{\partial(UH)}{\partial x} + UH\frac{\partial[w_b + (\tan\theta)H]}{\partial x}\right] + \dot{b} \tag{5.5}$$

which we used for deriving volume evolutions.

Dynamical calibration

Following *Oerlemans* [1997] the ice-flow model was calibrated via so-called dynamical calibration. This technique consists of minimizing the difference between modeled and observed historical front variations by experimentally determining a stepped mass-balance variation forcing, thus allowing rough reconstruction of the recent mass-balance history. For a successful calibration it is necessary that the available record of glacier length, L, exceeds the characteristic glacier's response time which is in the order of several decades for our study glaciers [*Oerlemans*, 2001]. For the recent period with available mass balance observations we applied the observed annual net mass balance profiles, $b(h,t)$, as an input to the model. For the prior period, we averaged the observed mass balance profiles over the total period of available observations and described the mean annual mass balance profile by a polynomial function of glacier surface elevation, h. This polynomial function served as a reference annual mass balance profile, $b_{ref}(h)$, in the simulations of the historic front variations. The model was calibrated by introducing a stepped perturbation, $\Delta b(t)$, to a reference mass balance profile so the annual mass balance profile along the flowline is:

$$b(h,t) = b_{ref}(h) + \Delta b(t). \tag{5.6}$$

Table 5.1 contains the periods over which we averaged the mass balance profiles and calculated $b_{ref}(h)$ for each glacier while the reference mass balance profiles are shown in Figure 5.2. The calibration, i.e. tuning of flow parameters f_d and f_s and mass balance perturbations $\Delta b(t)$, is considered successful if the modeled front variations and surface profile at the year of the surface map (Figure 5.1) yield the closest possible match to the observations. Additional control parameters for the dynamical calibration were the observed surface velocities which provided an expected order of magnitude for the modeled vertically averaged velocities. More details on this optimization are given in Oerlemans (1997). For Midre Lovénbreen and Abramov Glacier the flowline model was calibrated to best match the observed and modeled thickness profiles because a long-term record of front variations is missing.

Table 5.1. Observational time periods used in the flowline model for the six glaciers: Nigardsbreen (NIG), Rhonegletscher (RHO), South Cascade Glacier (SCG), Sofiyskiy Glacier (SOF), Midre Lovénbreen (ML) and Abramov Glacier (ABR), flow parameters derived from the dynamical calibration, and modeled values of volume, V, area, A, and length, L, at the end of the calibration periods, i.e. prior to the 100-year mass balance perturbations. b is area-averaged mass balance averaged for each glacier over the period of mass balance observations

Glacier	Observational time periods				Flow parameters		Modeled values			
	length fluctu-ations	mass balance profile	bed topography	surface topography	$f_d \times 10^{-24}$ ($Pa^{-3}s^{-1}$)	$f_s \times 10^{-20}$ ($Pa^{-3}m^2s^{-1}$)	V km^3	A km^2	L km	b m
NIG	1710-2005	1964-2005	/	1988	1.90	5.69	3.93	48.4	10.3	0.04
RHO	1602-1990	1979-1981	/	1969	0.32	1.08	2.68	17.1	9.6	-0.08
SCG	1900-2005	1969-2003	~1977	1980-2003	0.32	0.30	0.16	1.9	3.1	-0.57
SOF	1630-2000	1998-2000	~2000	1952	1.01	3.72	1.31	10.2	7.0	-0.18
ML	/	1968-2005	1990, 1998	1977, 1995	0.63	1.39	0.36	5.0	4.2	-0.55
ABR	1967-1994	1971-1998	1986	1986	0.92	1.08	2.11	20.8	8.6	-1.20

In Figure 5.3 we present the results of the dynamical calibration i.e. the observed and simulated historical glacier lengths and corresponding perturbations in mass balance profile, Δb, as a deviation from the reference mass balance profile, $b_{ref}(h)$. Since we used the same input geometry data for Nigardsbeen, Rhonegletscher and Sofiyskiy Glacier as in the previous studies [*Oerlemans*, 1997; *Wallinga and van de Wal*, 1998; *De Smedt and Pattyn*, 2003] we obtained very similar simulations with almost identical flow parameters. For these three glaciers a good match between the observed and the modeled historical lengths was obtained. For the South Cascade Glacier deviations were large in the first 50 years of the simulation. This was attributed to the lack of reliable bed topography data beyond the current glacier extension and the existence of a lake ~1 km downstream of the current glacier snout into which the glacier was calving in the first half of the 20th century. Therefore we put more emphasis on simulating the length fluctuation

in the last 50 years i.e. to accurately reproduce the recent glacier's retreat. Figure 5.4 presents the observed and simulated thickness profiles for all six glaciers at the year of the surface map (Figure 5.1). Although the match between observed and modeled surface profiles was not entirely satisfying those were the best results with respect to optimal agreement between both modeled and observed glacier length fluctuations. The flow parameters obtained through the calibration are listed in Table 5.1 with the modeled volume, area, and length at the end of the calibrating period including the area-averaged mass balance for the reference mass balance profile $b_{ref}(h)$. The modeled A and L were within ±20% and ±15% of those reported in the glacier inventory by World Glacier Monitoring Service (WGMS; e.g. *Haeberli et al.*, [2005]), respectively.

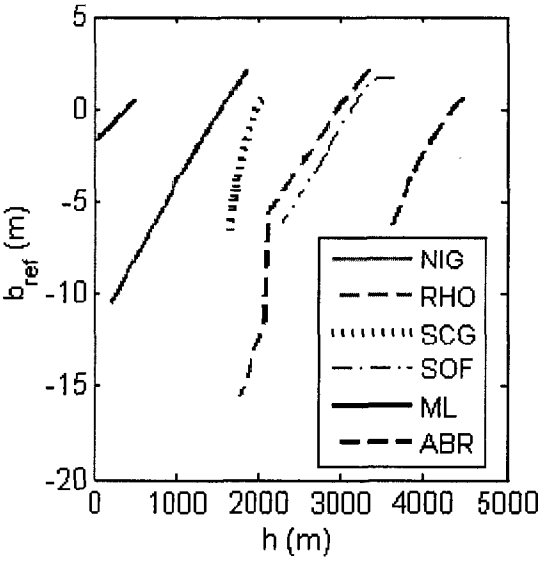

Figure 5.2. Reference mass balance profiles, $b_{ref}(h)$, for Nigardsbreen (NIG), Rhonegletscher (RHO), South Cascade Glacier (SCG), Sofiyskiy Glacier (SOF), Midre Lovénbreen (ML) and Abramov Glacier (ABR).

Volume projections

The last year of the dynamical calibration is the initial year of volume projections forced by hypothetical mass-balance perturbations (see last year in column "length fluctuations" in Table 5.1). At the initial year ($t=0$) with the corresponding glacier volume $V(t=0)$ we introduced a hypothetical trend-like mass balance scenario in the flowline model by perturbing the annual mass balance profile according to Equation (5.6). The magnitude of future mass balance profile perturbation, Δb, increases with a constant rate:

$$\Delta b(t) = \Delta b(0)t\,, \tag{5.7}$$

where t=1,...100 years. A period of 100 years was chosen because future climate change studies are often focused on a century scale. Following *Radić et al.* [2007] we chose 3 different rates of mass balance profile perturbation, $\Delta b(0)$, equal to -0.005 ma^{-1}, -0.010 ma^{-1} and -0.015 ma^{-1} which are applied on all six glaciers, and correspond to perturbations of -0.5 m, -1.0 m and -1.5 m, respectively, after 100 years. Hence, we did not consider glacier response to real climatic changes which differ from glacier to glacier but we "homogenized" the response. Thus, we assumed a climate change scenario which produces identical changes in the mass balance profiles of all six glaciers.

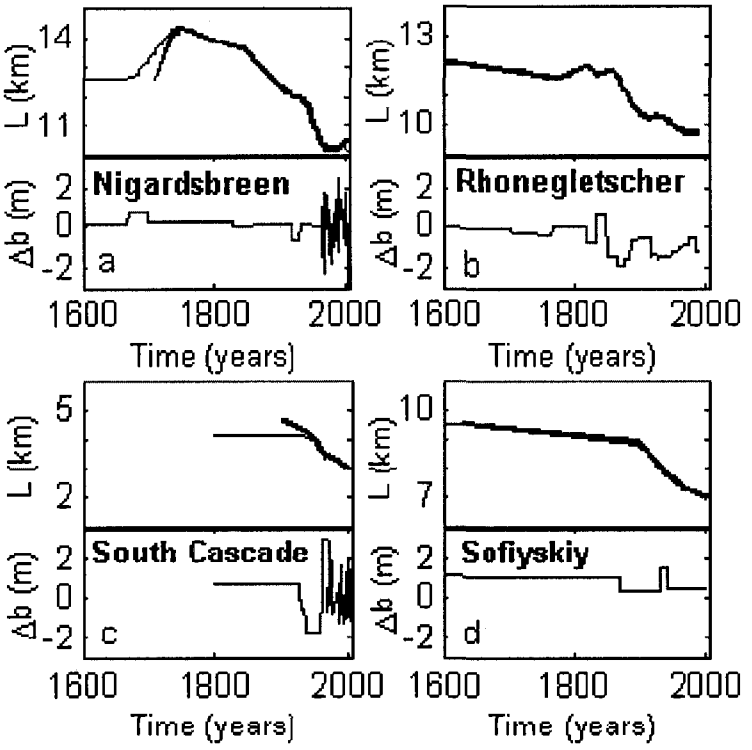

Figure 5.3. Results of the dynamic calibration for four glaciers. The observed (solid thick line) and modeled (solid thin line) length fluctuations are presented in the upper graph for each glacier while the lower graphs show the reconstructed perturbations in the mass balance profiles, Δb, derived from the dynamical calibration (Equation 5.6).

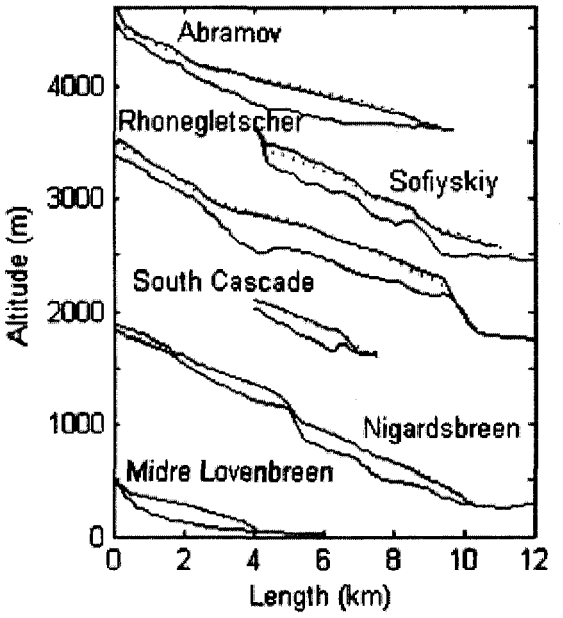

Figure 5.4. Observed (solid line) and modeled (dashed line) surface elevations and bed along the flowline. The dates for the observed surface profiles are the same as in Figure 5.1.

Although the dynamical calibration gives one of many possible solutions for the tuning parameters it creates a glacier's state that corresponds to the state of response to recent climate forcing. This implies that a steady-state assumption is not needed, i.e. the glacier may be in non-steady state prior to application of the mass balance perturbation for the 100-year projections. Thus the flowline model allows the glacier to have a 'memory'.

5.3.3 Volume evolutions from the scaling methods

Scaling relationships

Since the required input data for ice-flow modeling seldom are available alternative methods have been developed to account for glacier geometry changes in volume projections. A commonly used approach is based on scaling relationships between glacier characteristics such as volume, area, length, width and mean thickness. Using models that assume perfect plasticity, *Oerlemans* [2001] investigated the relationships between thickness, length, slope, mass balance gradient and response times for glaciers and ice caps. Initially, the scaling exponents in the volume-area and

the width-length relationships were derived from glacier inventory data [e.g. *Macheret et al.*, 1988; *Chen and Ohmura*, 1990]. The relationships were investigated by *Bahr* [1997a] and *Bahr et al.* [1997] and shown to be based on a theoretical analysis of glacier dynamics and glacier geometry. A volume, V, of a valley glacier without calving and without hanging or discontinuous longitudinal profiles is related to its surface area, A, and its length, L, via a power law:

$$V = c_a A^{\gamma}, \tag{5.8}$$

$$V = c_l L^{q}. \tag{5.9}$$

According to *Bahr et al.* [1997] the scaling exponents are γ=1.375 and q=2.2 while c_a and c_l are the constants of proportionality. These two relationships are equivalent provided that width-length scaling is applied such that the characteristic (average) width, $[w]$, is proportional to $L^{0.6}$. Based on glacier inventory data and measured volumes through radio echo-soundings [e.g. *Macheret and Zhuravlev*, 1982], *Chen and Ohmura* [1990] found average values of γ=1.357 and c_a=0.2055 $m^{3-2\gamma}$ for 63 mountain glaciers. Values ranged between 1.15 and 1.52 for γ and between 0.12 and 0.22 $m^{3-2\gamma}$ for c_a for different regions. Using probability density function for c_a, derived from volume and surface area data for 144 glaciers around the world, *Bahr* [1997b] found the mean of the distribution to be 0.191 $m^{3-2\gamma}$ and the standard deviation to be 0.073 $m^{3-2\gamma}$, where γ=1.375. Corresponding values for the constant c_l in Equation (5.9) could not be found in the literature.

Volume projections

We applied the scaling relationships in order to derive volume evolutions for our six glaciers forced by the same hypothetical climate scenario as applied in the flowline modeling. The input data were the initial volume, area and length of the glacier or at least one of these characteristics since the scaling enables us to derive one characteristic from another. Additionally, the mass balance profile and the area-elevation distribution were required. Thus, starting from t=0 and applying the same mass balance profile perturbations, Δb, to the annual mass balance profile, $b(h,t)$, as above, we calculated the volume change at any year t as:

$$\Delta V(t) = \sum_{i=1}^{n} b_i(t) a_i(t) \cdot \tag{5.10}$$

This is the discretized mass continuity equation with constant ice density where $b_i(t)$ is the annual specific mass balance of the i-th elevation band which corresponds to $b(h,t)$, while $a_i(t)$ is the area of the i-th band and n the total number of bands. Elevation bands were equally spaced (100 m) along the flowline (x-axis) to correspond to the elevation bands in the ice-flow model. For each elevation band we know its length along the flowline, elevation and area. The sum of all the area bands is equal to the total surface area $A(t)$:

$$A(t) = \sum_{i=1}^{n} a_i(t) \cdot \tag{5.11}$$

Based on the mass balance obtained from Equation (5.6) for any year t a new volume at t+1 was calculated as:

$$V(t+1) = V(t) + \Delta V(t) \cdot \tag{5.12}$$

We applied three different methods for determining the glacier's area and the number of bands, n, via the scaling relationships: (1) volume-area scaling, (2) volume-length scaling and (3) "volume-area-length" scaling which combines (1) and (2).

(1) Volume-area (V-A) scaling

The volume-area relationship (Equation 5.8) was used to derive the glacier's area for year t+1:

$$A(t+1) = \left(\frac{V(t+1)}{c_a} \right)^{\frac{1}{\gamma}} \cdot \tag{5.13}$$

We assumed that the glacier area-elevation distribution remains constant and any change in area occurs only at the glacier's front. Elevation bands were subtracted (if the glacier retreated) or added (if the glacier advanced) at the glacier front. We derived the new number of bands, n, from Equation (5.11). *Radić et al.* [2007] applied this method for volume evolution of synthetic

glaciers with simplified geometry and showed that the mass-balance/area-elevation feedback is captured well when compared with the results from the flowline model.

(2) Volume-length (V-L) scaling

The procedure is analogous to (1) but the changes in the number of elevation bands n and the area are driven by the changes in glacier length which are calculated via the volume-length scaling (Equation 5.9). Thus, for year t+1 the length is equal to:

$$L(t+1) = \left(\frac{V(t+1)}{c_l} \right)^{\frac{1}{q}}. \tag{5.14}$$

Knowing the distance of each elevation band along the flowline and calculating the glacier's length for each time step of one year we derived the total number of elevation bands and the total glacier area from Equation (5.11). Thus the distribution of the new area with elevation was dictated by the volume-length scaling instead of the volume-area scaling. We adjusted the length according to V-L scaling, but kept the glacier's width for each elevation band constant in time instead of adjusting it according to length-width scaling, thus allowing the scaling exponents in the V-A relationship (Equation 5.8) to change in time.

(3) Volume-area-length (V-A-L) scaling

We applied both Equations (5.13) and (5.14) in such a way that the number of bands, n, was calculated from the volume-length scaling while the changes in total area were derived from the volume-area scaling. This was achieved by assuming that the initial shape of the glacier area-elevation distribution remains constant in time (Figure 5.5). A normalized area-elevation distribution is:

$$a_{N,i} = \frac{a_i(t=0)}{A(t=0)} \quad i=1...n \tag{5.15}$$

and when multiplied by the calculated area $A(t)$ Equation (5.15) gives the area-elevation distribution for each year t. As in the previous methods, the maximum altitude of the glacier remained constant. However, in contrast to the methods which assumed all area changes to occur

exclusively at the glacier snout, V-A-L scaling removes or adds area along the entire length of the glacier. This approach may in extreme cases lead to increase in area of individual elevation bands although the glacier becomes shorter. It also decreases area in the highest elevation bands of the glacier, where area would rarely change especially for glaciers with large vertical extent and accumulation area. Nevertheless, this method is similar to the geometric model of *Raper et al.* [2000] which has been used to estimate the contribution to sea-level rise from all mountain glaciers and ice caps [*Raper and Braithwaite*, 2006]. Their geometric model calculates the terminus position from area-length scaling but approximates the area-altitude distribution with a triangle defined by maximum area at mean altitude and zero-area at minimum and maximum altitude, while we preserve the actual shape of the initial area-elevation distribution through normalization of the distribution (Figure 5.5).

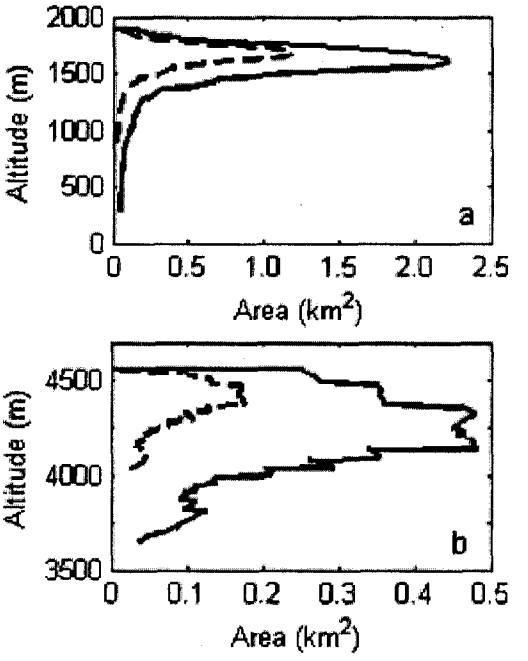

Figure 5.5. Modeled area-elevation distribution prior to future mass balance perturbations (solid line) and after 100-year of the mass balance perturbations (dashed line) for (a) Nigardsbreen and (b) Abramov Glacier.

5.3.4 Sensitivity experiments

Scaling parameters

Since we used γ=1.375 and q=2.2 in the scaling relationships as proposed in *Bahr et al.* [1997] we tested the sensitivity of glacier volume evolutions to the choice of γ and q by varying their values. For each experiment the constants of proportionality c_a and c_l were derived from the initial glacier volume area and length for year t=0, as obtained from the flowline model. Since these constants differ for each glacier our second sensitivity experiment was to apply mean scaling constants, c_a and c_l, in the scaling methods and compare the derived volume evolutions with those produced by the flowline model.

Mass balance/glacier thickness feedback

Changes in mass balance cause changes in surface area and thickness with feedbacks on surface mass balance. We aimed to quantify the importance of the mass-balance/thickness feedback both in the flowline model and in the scaling methods in comparison to the mass-balance feedback due to changes in area-elevation distribution. Since the ice-flow model is one dimensional the changes in thickness along the flowline are assumed uniform across the width of the glacier. First we tested the importance of the mass balance/thickness feedback in the flowline model by excluding the thickness feedback mechanism from the projections. After the dynamical calibration have been finalized, the glacier thickness was kept constant for computation of the mass balance $b(h,t)$.

The scaling methods as applied here include feedback due to changes in area-elevation distribution but lack the mass-balance/thickness feedback, i.e. the glacier area may change, but the thickness along the glacier profile does not. A simple way of introducing this feedback into the scaling approach was to compute the mean glacier thickness, H_m, for each year t:

$$H_m(t) = \frac{V(t)}{A(t)} \tag{5.16}$$

and derive the mean thickness change, ΔH, between two consecutive years. Assuming that the change in H_m is equal to the change in thickness along the flowline we calculated a surface profile, $h(x)$, for year $t+1$ by adding ΔH to the surface profile for year t. Thus derived surface

profiles for each t were used to calculate the mass balance profile $b(h,t)$ as a polynomial function of glacier surface elevation, h, along the flowline.

5.4 Results and discussion

5.4.1 Scaling methods

Figure 5.6 illustrates the normalized volume evolutions ($V(t)$ divided by $V(0)$ for each year t) derived from the ice-flow model and the three scaling methods for all six glaciers. We show the evolutions derived only for $\Delta b(0)$=-0.015 ma^{-1} but the results in terms of differences from the flowline model are similar for all three mass balance perturbations. In Table 5.2 we list the differences between 100-year volume change projected by the flowline model and the scaling methods, given in percentages of the initial volume for all three perturbations. It must be borne in mind that the 1-D ice-flow model along the flowline of the glacier is highly parameterized and a simplified representation of reality. For example, the model's parameterizations may be introducing the scaling relationships between the glacier's characteristics that are inconsistent with those considered in *Bahr et al.* [1997]. Hence, the scaling exponents in V-A and V-L relationships may differ from the theoretical ones. For example, valley glaciers will have scaling exponents γ=1.375 and q=2.2 if, among the other assumptions, the characteristic glacier width is linearly related to the characteristic glacier thickness [*Bahr,* 1997a]. This linearity may not result in the flowline model where the combination of width parameterization (Equation 5.1) and the change in the valley width w_s along the flowline dictate the characteristic width-thickness scaling relationship. Nevertheless, the good agreement between model results and observations in the calibration period provide some confidence in the performance of the model.

All projections show considerable volume losses by the end of the 100-year period. As expected, the glaciers with more negative initial area-averaged mass balance as calculated from the reference mass balance profile, b_{ref} (Table 5.1), lost a larger portion of their initial volume than those closer to zero mass balances. However, the scaling methods underestimate the total volume loss projected from the flowline model for most of the glaciers. This underestimation varies up to 47% (for Nigardsbreen, $\Delta b(0)$=-0.015 ma^{-1}) for V-A scaling, up to 18% (for South Cascade, $\Delta b(0)$=-0.005 ma^{-1}) for V-L scaling and up to 32% (for Abramov, $\Delta b(0)$=-0.005 ma^{-1}) for V-A-L scaling. Part of the systematic underestimation by the scaling methods may be attributed to the initial state of the glaciers prior to the perturbations. Most of the glaciers experienced negative

mass balances and were in non-steady state prior to the perturbation. While the dynamic calibration of the ice model accounts for this state, scaling does not, since it includes no memory of the previous mass balance history. Furthermore, while the dynamics in the ice-flow model are governed by Glen's flow law, the scaling methods assume perfect plasticity i.e. the assumption that dynamical changes in glacier geometry are instantaneous. As climate changes, the values of scaling constants, c_a and c_l, which we assume constant in time, may actually be expected to evolve through time as the glacier has to change its flow regime in response to resulting mass changes. Nevertheless, our results show that volume-length scaling gives the closest match to the evolutions from the flowline model. Thus, application of V-L scaling in order to derive the changes in area-elevation distribution which then dictate the volume change according to mass continuity (Equation 5.10) is superior to volume-area scaling when compared to normalized volume evolutions derived from the flowline model.

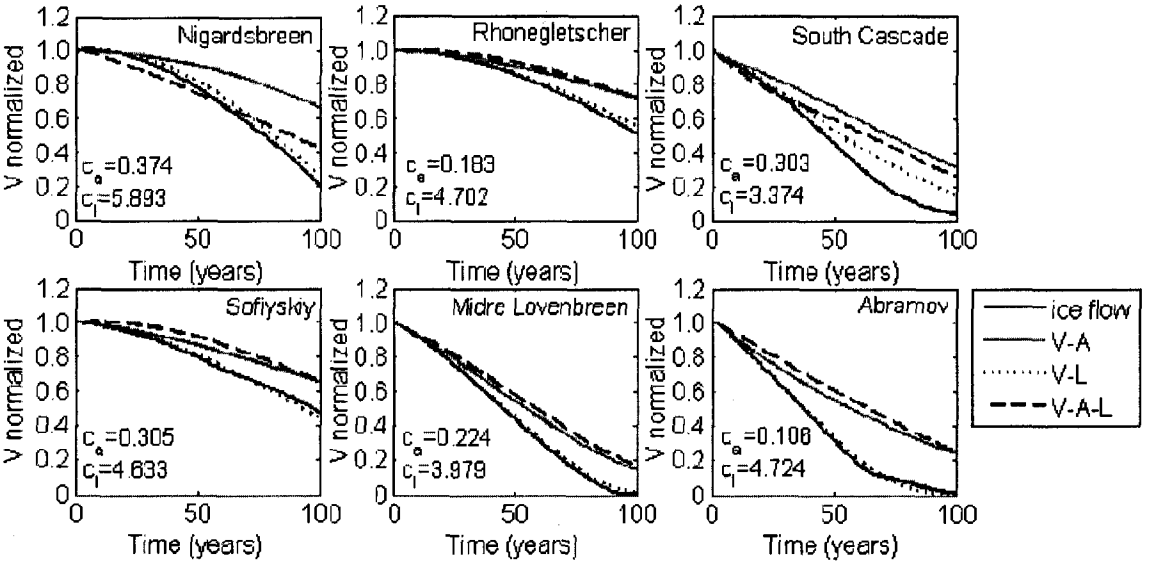

Figure 5.6. Future volume evolutions (normalized by initial volume at t=0) for six glaciers, forced by a perturbation in mass balance profile of $\Delta b(0)$=-0.015 ma^{-1}, as projected from the flowline model (solid black line), V-A scaling, V-L scaling and V-A-L scaling. The values for scaling constants, c_a [m$^{3-2\gamma}$] and c_l [m^{3-q}], derived from the glacier volume, area and length at t=0 are specified for each glacier. The scaling exponents are assumed γ=1.375 and q=2.2 according to *Bahr et al.* [1997].

Since the width of the glacier in the flowline model is parameterized for each elevation band as a function of thickness (Equation 5.1) the area in each elevation band is allowed to shrink or grow along the cross section. However, the glacier length shrinks only when the thickness in the lowest elevation band reaches zero. Therefore, the flowline model allows the glacier to have a thin terminus with relatively large terminus area. Considering these characteristics of the flowline model the lower performance of V-A and V-A-L scaling compared to V-L scaling is attributed to the following considerations:

- In V-A and V-L scaling changes in surface area occur only at the glacier snout. However, in the V-A scaling the lost area (ΔA) is subtracted from the glacier's front along the flowline, reducing the length of the glacier i.e. removing the lower lying elevation bands which have most negative specific mass balance (ablation area). Since this removal of low-lying area occurs faster than in the flowline model and in the V-L scaling it leads to less negative mass balances when integrated over the entire glacier (Equation 5.10), and hence to reduced volume losses with time. Integrating over 100 years the projected volume change becomes progressively less in comparison to V-L scaling and to the flowline model.
- By applying V-A-L scaling we allow for area changes to occur along the entire glacier's length. The retreat of glacier is simulated by the V-L scaling while the total area is calculated from the V-A scaling. Since the shape of the area-elevation distribution is preserved (Figure 5.5), a certain amount of area is lost in each elevation band along the flowline. This means that V-A-L can not simulate the maximum reduction of the thickness and area at the glacier terminus as it occurs in the flowline model. Since the volume changes in V-A-L are computed with consistently smaller area in elevation bands than in the flowline model the V-A-L scaling underestimates the modeled volume loss (Equation 5.10) over the 100-year period compared with the flowline model.

Although the projected 100-year volume did not differ more than a few percents depending on whether V-A or V-A-L scaling method was applied, the performance of these methods depends on the glacier's area-elevation distribution. Therefore, for Nigardsbreen, a glacier with long narrow tongue (Figure 5.5) and large accumulation area, the V-A scaling yielded the largest underestimation of the volume loss compared to the flow model results. Considering that the physical basis for the scaling relationships is explained for valley glaciers [*Bahr et al.*, 1997] Nigardsbreen as an outlet glacier of Jostedalsbreen is not a representative for a valley glacier but

more an outlier in our sample. Another glacier for which the scaling methods derived large differences from the flowline model is South Cascade Glacier. This might be due to problems we encountered during the dynamical calibration for this glacier yielding the future projections to be highly sensitive to the tuning parameters in the flowline model.

5.4.2 Sensitivity to scaling exponents

The first sensitivity experiment involved varying the scaling exponents, γ and q, in the V-A and V-L relationships for our six glaciers to analyze the sensitivity of volume evolutions to these scaling exponents. We investigated how much the scaling exponents can be decreased (increased) so that the scaling methods project 100-year volume changes that are 10% and 20% smaller (larger) than the 'reference' volume change. Here, the 'reference' volume projections are those derived from the scaling method with γ=1.375 and q=2.2 as proposed in *Bahr et al.* [1997]. Reducing γ in the V-A scaling to γ=0.95 or increasing it to γ=2.00 underestimates and overestimates the reference loss by less than 10%, respectively. Further decrease to γ=0.65 and increase to γ=2.95 results in projections of volume loss that are within 20% of the volume loss projected by the 'reference' scaling.

For V-L scaling assuming $1.52 \leq q \leq 3.20$ results in volume projections that differ from the 'reference' volume change by less than 10%. The range is $1.04 \leq q \leq 4.72$ if a 20% difference is tolerated. Additionally, the results show that the volume evolutions for glaciers that lost almost their entire volume over the 100-year period (South Cascade, Midre Lovénbreen and Abramov) are more sensitive to variations in the scaling exponents than the other glaciers in our set.

Our sensitivity experiments show that by decreasing the scaling exponents γ and q by 30% (50%) or increasing them by 45% (110%) from the theoretically derived values by *Bahr et al.* [1997] the projections of 100-year volume change differ less than 10% (20%). Thus by applying the range of γ=[1.15 1.52] which was reported by *Chen and Ohmura* [1990] we derive 100-year volume projections which differ less than 5% from the 'reference' projections. Similar analysis performed on synthetic glaciers with V-A scaling [*Radić et al.*, 2007] showed that the range of γ from 1.80 to 2.90 in the V-A scaling yielded differences of <6% in 100-year volume changes derived from the V-A scaling with γ=1.56. Hence, we conclude that the normalized volume evolutions are relatively insensitive to the choice of scaling exponents. However, one should keep in mind that

the scaling relationships, especially V-A scaling, will be affected if the geometry parameterizations in the ice-flow model have large inconsistencies with the geometry of valley glaciers considered in *Bahr et al.* [1997].

5.4.3 Sensitivity to scaling constants

So far we always calculated c_a and c_l (Equations 5.8 and 5.9) from the initial volume, area and length for each glacier assuming γ=1.375 and q=2.2. In Figure 5.6 we present the values of these constants. *Chen and Ohmura* [1990] found c_a=0.2055 $m^{3-2\gamma}$ and *Raper and Braithwaite* [2006] applied their value for assessing global glacier wastages.

For comparison we apply the constant c_a from *Chen and Ohmura* [1990] to derive volume evolutions based on V-A scaling. Since values for the constant in V-L scaling, c_l, could not be found in the literature we use the mean c_l calculated from our six glaciers (c_l=4.5507 m^{3-q}). When these constants are used to calculate initial volume at t=0 from Equations (5.8) and (5.9), initial volume differ from the modeled ones by up to 57% for V-A scaling and by up to 35% for V-L scaling. This supports the statement by *Meier et al.* [2007] that the error in calculating volumes from areas via V-A scaling is of the order of 50% for individual ice masses. However, the 100-year volume projections derived from the scaling methods show a scatter of underestimation and overestimation from the projections derived by the flowline model (Figure 5.7). Statistically this scatter might reduce the errors in total volume projections if the scaling is applied on a large sample of glaciers (e.g. on a global scale). However, quantification of errors is difficult since it depends on how any particular glacier fits into the V-A scaling with an assumed constant c_a.

Even though initial volumes are both under- and overestimated (Figure 5.7), when normalized, V-A scaling consistently underestimates the glaciers wastage at the end of the 100-year projection by 9% to 59% (Table 5.2) compared to the flowline model, while V-L yields slight underestimation or a close match (Figure 5.8). Applying the scaling constant c_l averaged over all glaciers in the V-L scaling yields projected 100-year volume changes that are only in the order of a few percent different from the projections using c_l derived for each glacier individually. Hence, the results are rather insensitive to the choice of c_l which is encouraging for use of V-L scaling in glacier volume projections, especially combined with the finding of generally good performance of the method when compared to the ice-flow model projections.

When deriving scaling constants c_l and c_a from values of V, A and L, one should keep in mind that the scaling constants are related through the Equations (5.8) and (5.9) by:

$$c_l = c_a \frac{A^\gamma}{L^q}. \tag{5.17}$$

Hence, varying c_a by a certain amount is equivalent to varying c_l by a much larger amount since (A^γ/L^q) is of the order of magnitude 10-1000. If this is not considered it will appear that c_l is ~10-1000 less sensitive than c_a.

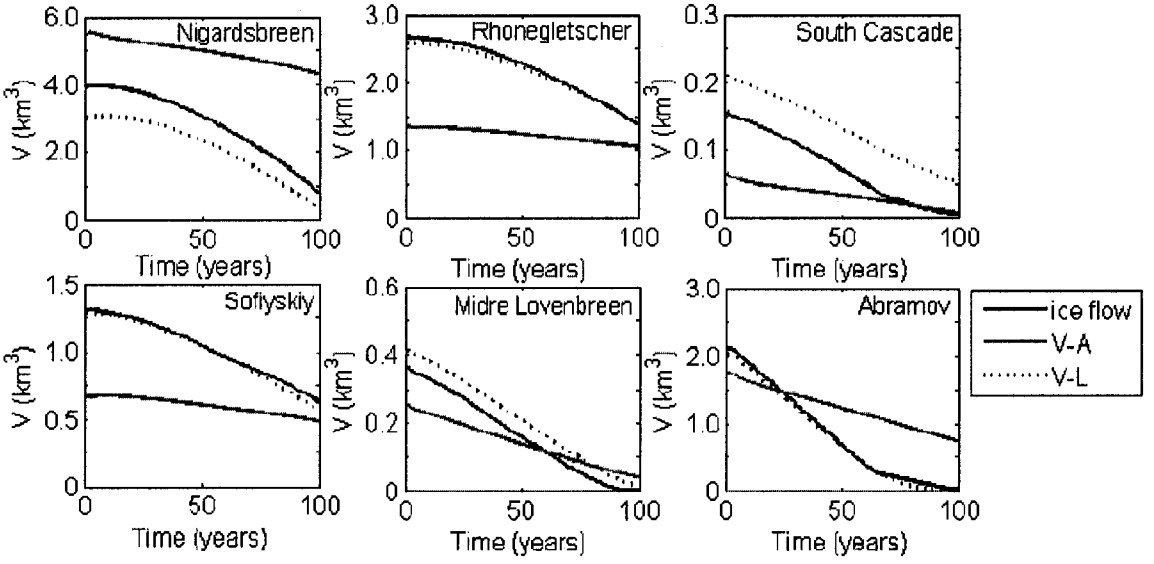

Figure 5.7. Same as Figure 5.6 except that absolute volumes are shown and scaling constant c_a=0.2055 $m^{3-2\gamma}$ [*Chen and Ohmura*, 1990] and c_l=4.5507 m^{3-q} are used.

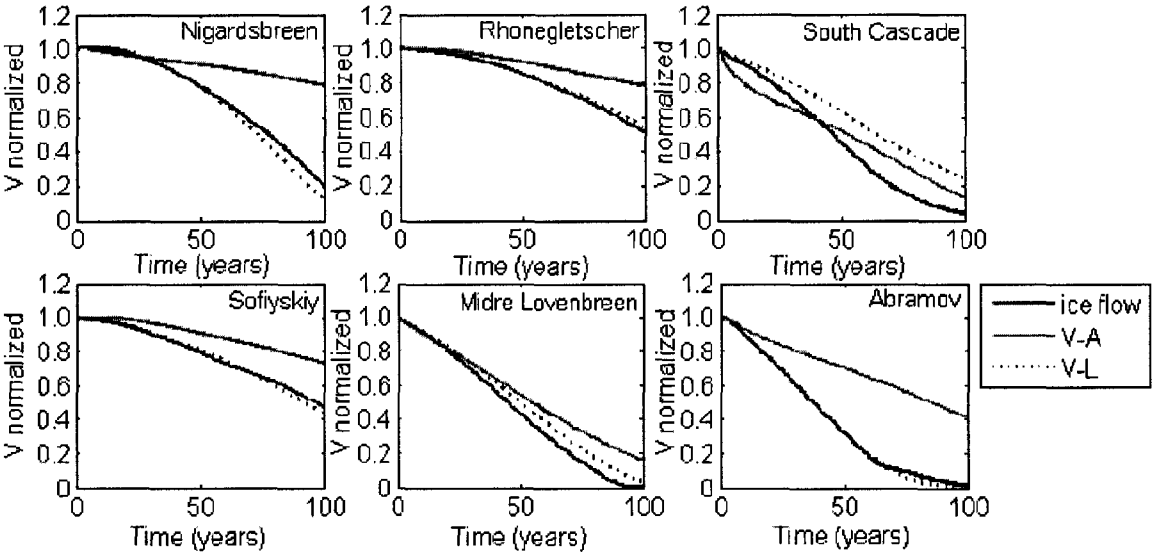

Figure 5.8. Same as Figure 5.7 except that volumes are normalized by initial volumes at t=0.

5.4.4 Mass balance/thickness feedback

Our final sensitivity experiment is to analyze the importance of mass-balance/thickness feedback. When the changes in glacier thickness along the flowline are excluded from the mass balance calculations in the flowline model, the projected 100-year volume loss is underestimated (Table 5.2). According to our results the feedback mechanism in the flowline model contributes to the volume loss 2% to 14% of the initial volume while the glacier loses 50% to 100% of its volume. Thus the mass balance/thickness feedback is small for these six glaciers. However, the importance of this feedback depends strongly on the bed slope [*Oerlemans*, 2001]. Therefore, this analysis may yield different results if applied on large glaciers which lie on much smaller slopes.

Secondly, we include our simple feedback scheme in the scaling methods to test whether this can improve the match between the volume evolutions derived from the scaling methods and the flowline model. The differences in the projected volumes between the flowline model and the V-L scaling method are listed in Table 5.2. Our simple mechanism in the V-L scaling method increases the glacier's wastage but not more than a few percents. When the scheme of the feedback mechanism is introduced in the V-A and the V-A-L scaling the wastage is even less increased (by less than 1% of the initial volume).

Table 5.2. Differences between 100-year volume changes projected from the flowline model and those obtained from the scaling method (V-A, V-L, V-A-L, V-A(c_a), V-L(c_l) and V-L(h)) expressed in percentages (%) of the initial volume for each glacier. If the differences are positive (negative) the scaling method underestimates (overestimates) the volume loss projected from the flowline model. The projections are performed with three perturbations in mass balance profile, Δb. In all cases the scaling exponents are equal to γ=1.375 and q=2.2 [*Bahr et al.*, 1997] while the scaling constants are given in Figure 5.6. V-A(c_a) and V-L(c_l) are the scaling methods with scaling constants equal to c_a=0.2055 $m^{3-2\gamma}$ [*Chen and Ohmura*, 1990] and c_f=4.5507 m^{3-q}. The column Vmod shows how much the volume loss projected by the flowline model differs from the flowline model results when the mass balance/thickness feedback is excluded. V-L(h) shows the difference to the flowline model if the scheme for mass balance/thickness feedback is included in the scaling method

Glacier	Δb(0)=-0.005 ma^{-1}			Δb(0)=-0.01 ma^{-1}			Δb(0)=-0.015 ma^{-1}			Δb(0)=-0.015 ma^{-1}			
	V-A	V-L	V-A-L	V-A	V-L	V-A-L	V-A	V-L	V-A-L	V-A(c_a)	V-L(c_l)	Vmod	V-L(h)
NIG	17	2	-5	32	2	7	47	6	23	59	-8	14	1
RHO	8	0	11	14	2	16	21	5	21	27	4	9	2
SCG	37	18	31	33	15	27	28	11	22	9	21	7	8
SOF	9	-2	15	12	4	15	18	-3	18	25	-4	7	-7
ML	21	5	26	20	4	24	14	1	17	16	3	3	0
ABR	27	-7	32	25	-4	28	23	-1	24	40	-1	2	-3

Our approach must be considered as a first approximation since the glacier thickness change is assumed uniform over the profile (Equation 5.16). One might apply a more complex scheme of the thickness change as, for example, by parameterizing the thickness change along the flowline [*Jóhannesson et al.*, 1989]. Such a parameterization takes into account that the change in the ice thickness is not uniformly distributed but more pronounced at the glacier tongue. However, in order to derive volume evolution from the discretized mass continuity (Equation 5.10) it would require thickness data along the flowline. Since we analyze the scaling methods which are applicable for global estimates, simplicity in the data input is more important than the complexity of the feedback scheme. Considering that the mass balance/thickness feedback is small for these six glaciers, the V-L scaling is shown to simulate sufficiently well the feedback between the mass-balance and area change as simulated in the flowline model.

5.5 Conclusions

We provide a detailed analysis of scaling methods as a possible tool for deriving glacier volume evolutions on a global scale. Using 100-year volume evolutions from the flowline model as reference we compare the performance of three different scaling methods for six valley glaciers assuming identical hypothetical trend-like negative mass balance perturbations of -0.005 ma^{-1}, -0.010 ma^{-1} and -0.015 ma^{-1}. For all six glaciers, the scaling methods mostly underestimate the 100-year normalized volume losses obtained from the flowline model. Nevertheless, the volume evolutions derived from the volume-length (V-L) scaling provide the best match to the evolutions derived from the flowline model. This scaling method projects volume loss by the end of a 100-year period deviating up to 18% of initial volume from the modeled projections, while volume-area (V-A) and volume-area-length (V-A-L) produced maximum differences of 47% and 32%, respectively. Thus the underestimation of the total volume loss is ~20% larger if the V-A scaling is applied instead of the V-L scaling. Although both the V-A and V-L scaling are derived from the exact same continuum mechanics, our results suggest that the V-L scaling may be a better practical tool for assessing future volume changes. However, more glaciers need to be analyzed to ascertain these results, especially considering that our six glaciers are rather small, and, hence not a representative sample of the mountain glaciers and ice caps that are major contributors to sea level [e.g. *Arendt et al.*, 2002; *Rignot et al.*, 2003]. Nevertheless, lack of data is still a major obstacle for extending this sensitivity analysis to large glacier systems and ice caps. Additionally, the validity of scaling methods should be further investigated by comparing their performance with 2-D and 3-D ice-flow models which account for cross-sectional thickness and geometry changes in a more sophisticated way.

Although the application of volume-length scaling in modeling volume changes might be more accurate than volume-area scaling, it might be less practical considering that gathering glacier area data is relatively simple while gathering data for glacier length along the flowline is more difficult. Nevertheless, potential application of volume-length scaling combined with use of glacier length records in extracting past temperature variations on a century time-scale [*Oerlemans*, 2005] emphasize the need to continue or expand monitoring of glacier length fluctuations. Volume-length scaling has also been applied in reconstructing the historical glacier contribution to sea level rise [*Oerlemans et al.*, 2007].

As expected, initial volumes and volumes of 100-year projections of individual glaciers are highly sensitive to the choice of the scaling constants especially in the V-A scaling yielding both over- and underestimation of volumes. However, when normalized by initial volume, volume evolutions are relatively insensitive to the choice of scaling exponents and constants. Varying γ=1.375 and q=2.2 (Bahr et al., 1997) by -30% (-50%) and +45% (+110%) yields a difference in 100-year volume projections by less than ±10% (±20%). This is encouraging for use of scaling methods in global volume projections since scaling constants are unknown for most glaciers and the scaling exponents may vary with changing glacier geometry.

Acknowledgments

Financial support for this work is provided by the Swedish Research Council for Environment, Agricultural Sciences and Spatial Planning (project number: 21.4/2003-0387). Regine Hock is Royal Swedish Academy of Science Research Fellow supported by a grant from the Knut Wallenberg Foundation. We are grateful to R. van de Wal and B. De Smedt for providing the input geometry data needed for the flowline model of Nigardsbreen and Sofiyskiy Glacier. We thank W. R. Bidlake and I. Willis for providing digitized data of surface and bed topography for South Cascade Glacier and Midre Lovénbreen. Furthermore, we are grateful to L. A. Rasmussen for the information on historical fluctuations of South Cascade Glacier, and to L. N. Braun for providing the surface and bed topography maps of Abramov Glacier. Comments by W. D. Harrison, L. A. Rasmussen, A. A. Arendt, M. Truffer and M. de Woul have helped to improve the paper. Special thanks to Editor H. Rott and to A. Fountain and D. B. Bahr whose helpful reviews clarified many points in the text.

5.6 References

ACIA (2005), Impacts of a Warming Arctic: Arctic Climate Impact Assessment, Cambridge University Press.

Arendt, A. A., K. A. Echelmeyer, W. D. Harrison, C. S. Lingle and V. B. Valentine (2002), Rapid wastage of Alaska glaciers and their contribution to rising sea level, *Science, 297*(5580), 382-386.

Bahr, D. B. (1997a), Width and length scaling of glaciers, *J. Glaciol., 43*(145), 557-562.

Bahr, D. B. (1997b), Global distributions of glacier properties: A stochastic scaling paradigm, *Water Resour. Res., 33*(7), 1669-1679.

Bahr, D. B., M. F. Meier and S. D. Peckham (1997), The physical basis of glacier volume-area scaling, *J. Geophys. Res.*, *102*(B9), 20355-20362.

Bidlake, W. R., E. G. Josberger and M. E. Savoca (2004), Water, ice, and meteorological measurements at South Cascade Glacier, Washington, balance year 2002, USGS Scientific Investigations Report 2004-5089.

Björnsson, H., Y. Gjessing, S.-E. Hamran, J.O. Hagen, O. Liestöl, F. Palsson, and B. Erlingsson (1996), The thermal regime of sub-polar glaciers mapped by multi-frequency radio-echo sounding, *J. Glaciol.*, *42*(140), 23-32.

Braithwaite, R. J. and S. C. B. Raper (2002), Glaciers and their contribution to sea level change, *Phys. Chem. Earth*, *27*, 1445-1454.

Budd, W. F., P. L. Keage and N. A. Blundy (1979), Empirical studies of ice sliding, *J. Glaciol.*, *23*(89), 157-170.

Chen, J. and A. Ohmura (1990), Estimation of Alpine glacier water resources and their change since the 1870's, International Association of Hydrological Science Publication 193 (Symposium at Lausanne 1990 – Hydrology in Mountainous Regions. I – Hydrological Measurements; the Water Cycle) 127-135.

De Smedt, B. and F. Pattyn (2003), Numerical modelling of historical front variations and dynamic response of Sofiyskiy glacier, Altai mountains, Russia, *Ann. Glaciol.*, *37*, 143-149.

Haeberli, W., M. Zemp, M. Hoelzle, R. Frauenfelder and A. Kääb (2005), Fluctuations of Glaciers, 1995-2000 (Vol. VIII), International Commission on Snow and Ice of International Association of Hydrological Sciences/UNESCO, Paris. [http://www.geo.unizh.ch/wgms.]

IPCC (2007), Climate Change 2007: The Physical Science Basis. Contribution of working Group I to the Fourth Assessment Report of the Intergovernmental Panel on Climate Change [Solomon, S. and 7 others, (eds.)], Cambridge University Press, Cambridge, UK, 996 pp.

Jóhannesson, T., C. Raymond and E. Waddington (1989), Time-scale for adjustment of glaciers to changes in mass balance, *J. Glaciol.*, *35*(121), 355-369.

Kjøllmoen, B., *ed.* (2001), Glaciological investigations in Norway in 2000, Report No. 2, ISSN 1502-3540, 122p.

Krimmel, R. M. (2002), Water, ice, and meteorological measurements at South Cascade Glacier, Washington, 2000-2001 balance years, USGS Water-Resources Investigations Report 02-4165.

Kuzmichenok, V., E. Vasilenko, Y. Macheret and M. Moskalevsky (1992), Ice thickness and bedrock topography of Abramov Glacier by data of low-frequency sounding, *Data of Glaciological Studies*, *75*, 92-97.

Macheret, Yu. Ya. and A. B. Zhuravlev (1982), Radio echo-sounding of Svalbard glaciers, *J. Glaciol.*, *28*(99), 295-314.

Macheret, Yu., P. A. Cherkasov and L. I. Bobtova (1988), Tolshchina I ob'yem lednikov Dzhungarskogo Alatau po dannym aeroradiozondirovaniya [The thickness and volume of Dzhungarskiy Alatau glaciers from airborne radio-echo sounding data], *Mater. Glyatsiol. Issled.*, *62*, 59-70.

Meier, M. F., M. B. Dyurgerov, U. K. Rick, S. O'Neel, W. T. Pfeffer, R. S. Anderson, S. P. Anderson and A. F. Glazovsky (2007), Glaciers dominate eustatic sea-level rise in the 21st century, *Science,* doi: 10.1126/science.1143906.

Oerlemans, J. (1997), A flowline model for Nigardsbreen, Norway: projection of future glacier length based on dynamical calibration with the historic record, *Ann. Glaciol.*, *24*, 382-389.

Oerlemans, J. (2001), Glaciers and climate change, A. A. Balkema Publishers, Lisse. 148 p.

Oerlemans, J. (2005), Extracting a climate signal from 169 glacier records, *Science*, *308*, 675-677.

Oerlemans, J., M. B. Dyurgerov and R. S. W. Van de Wal (2007), Reconstructing the glacier contribution to sea-level rise back to 1850, *The Cryosphere*, *1*, 59-65.

Paterson, W. S. B. (1994), The physics of glaciers, Third edition. Oxford, etc., Elsevier.

Pertziger, F. I., *ed.* (1996), Abramov glacier data reference book: climate, runoff, mass balance, Technical University, Munich.

Pfeffer, W. T., D. B. Bahr, and C. Sassolas (1998), Response Time of Glaciers as a Function of Size and Mass Balance: II. Numerical Experiments, *J. Geophys. Res.*, *103*(B5), 9783-9789.

Radić, V., R. Hock and J. Oerlemans (2007), Volume-area scaling vs flowline modelling in glacier volume projections, *Ann. Glaciol.*, *46*, 234-240.

Raper, S. C. B., O. Brown and R. J. Braithwaite (2000), A geometric glacier model for sea-level change calculations, *J. Glaciol.*, *46*(154), 357-368.

Raper, S. C. B. and R. J. Braithwaite (2006), Low sea level rise in projections from mountain glaciers and icecaps under global warming, *Nature*, *439*, 311-313, doi:10.1038/nature04448.

Rasmussen, L. A. and H. Conway (2001), Estimating South Cascade Glacier (Washington, U.S.A.) mass balance from a distant radiosonde and comparison with Blue Glacier, *J. Glaciol.*, *47*(159), 579-588.

Rignot, E., A. Rivera, G. Casassa (2003), Contribution of the Patagonia icefields of South America to sea level rise, *Science*, *302*(5644), 434-437.

Rippin, D., I. Willis, N. Arnold, A. Hodson, J. Moore, J. Kohler and H. Björnsson (2003), Changes in geometry and subglacial drainage of Midre Lovénbreen, Svalbard, determined from digital elevation models, *Earth Surf. Process. Landforms, 28*, 273-298.

Schneeberger, C., H. Blatter, A. Abe-Ouchi and M. Wild (2003), Modelling changes in the mass balance of glaciers of the northern hemisphere for a transient 2 x CO2 scenario, *J. Hydrol.*, *282*, 145-163.

Stroeven, A., R. van de Wal and J. Oerlemans, (1989), Historic front variations of the Rhone Glacier: simulation with an ice flow model, In Oerlemans, J., ed. Glacier fluctuations and climatic change. Dordrecht, etc., Kluwer Academic Publishers, 391-405.

van de Wal, R. S. W. and M. Wild (2001), Modelling the response of glaciers to climate change by applying volume-area scaling in combination with a high resolution GCM, *Clim. Dynam.*, *18*(3-4), 359-366.

Wallinga, J. and R. S. W van de Wal (1998), Sensitivity of Rhonegletscher, Switzerland, to climate change: experiments with a one-dimensional flowline model, *J. Glaciol.*, *44*(147), 383-393.

Chapter 6

Conclusions

21st century sea level rise from the melt of all mountain glaciers and ice caps, excluding those around Antarctica and Greenland ice sheets, is projected to range from 0.039 m to 0.150 m according to temperature and precipitation scenarios from four GCMs. This result is within the range of projections in *IPCC* [2007] although our projection of 0.150 m SLE, as derived from one GCM, is on the upper bound even for the projections which include glaciers surrounding Antarctica and Greenland. Thus, the projections are highly sensitive to the choice of GCM. Furthermore, this study showed the full range of complexities of modeling future volume changes of glaciers starting from local scale, i.e. modeling volume changes for one valley glacier, to regional and global scale assessments. The large range of complexities is due to many sources of uncertainties that were investigated in each chapter through a series of sensitivity tests and case studies. Nevertheless, not all uncertainties could be quantified. Below I summarize the main sources of uncertainties in modeling glacier volume changes, both those quantified in this thesis and those remaining to be resolved:

- Incomplete world glacier inventory data (glacier area, volume)

The lack of precise knowledge of ice volume constrains the estimates of the potential and projected sea level rise from the melt of glaciers. Any progress in this field is hampered without a complete glacier inventory database.

- Lack of observational data on recent global volume changes

Observations of recent volume changes exist for less than 1% of the mountain glaciers and ice caps in the world. Since large glaciers and ice caps carry the most weight in sea level estimates (Chapter 2) it is important to observe their recent mass changes. Thus, more mass–balance monitoring (in situ and from space) is needed on large glaciers (> 100 km^2), especially on those that are peripheral to the large ice sheets.

- Uncertainties in GCM output which force the glacier models

Although GCMs have experienced tremendous improvement in the simulation of detailed atmospheric and ocean features during the last decade, many unresolved problems and uncertainties still remain. Forcing the glacier models with an ensemble of GCMs provides a large range of possible projections of individual glacier volume changes (Chapter 3) and global volume changes (Chapter 2). For both, individual and global assessments of volume changes, the choice of GCM forcing glacier models is shown to be the largest source of quantified uncertainties in the projections. According to the ensemble of four GCMs the difference in global volume projections is 0.11 m sea level equivalent for 2001-2100 (Chapter 2).

- Downscaling global climate projections from GCM to local glacier scale

Glacier models for global assessments of volume changes are forced with statistically downscaled GCM output. Glacier volume projections depend on the methods of statistical downscaling whose success in the performance may differ on spatial and temporal scale. For a temperature-index mass balance model, applied on a valley glacier (Storglaciären, Sweden), we showed that correction of the seasonal temperature cycle in GCM is crucial (Chapter 3). Nevertheless, different mass balance models may profit from different statistical downscaling. Ideally, glacier volume changes should be fully coupled in regional climate models (RCMs). If this is not the case then glacier models should be forced by the output of RCM that implement further dynamical downscaling methods (e.g. orographic precipitation model, *Smith and Barstad*, [2004]). Thus, global volume changes should be assessed by modeling volume changes region by region.

- Modeling glacier mass balance (surface balance, internal accumulation, calving)

Temperature-index models are applied for global assessment due to their low data requirements readily available on global scale. A simple regression degree-day model applied on Storglaciären explains 70% of variance in measured specific surface mass balance (Chapter 3). The degree-day model (Chapter 2) explained 50% of variance when applied on 44 glaciers (median r^2 in the sample). Nevertheless, the performance of degree-day models is insufficient for glaciers whose melt is not governed by positive degree days. In these cases a full energy mass balance model can derive different cumulative mass balance over the same period of time (e.g. *Hock et al.*, [2007]). Furthermore, the performance of degree-day models has a high dependence on temperature input such as temperature reanalysis data (e.g. ERA-40 reanalysis, Chapters 2 and 3) used for model

calibration and initialization of global specific mass balance. Uniformly applied bias correction of ERA-40 temperatures, in order to simulate the local temperatures on a mountain glacier or ice cap, is a major source of uncertainty in the assessment of global volume changes (Chapter 2): if the bias correction parameter is changed by ±4% from its original value the global mean specific mass balance for 1961-1990 differs by ±0.1 mm yr^{-1} sea level equivalent or ±40% of its original value. Furthermore, in the assessments of global mass budgets internal accumulation is parameterized in a simple way (Chapter 2) while parameterization of calving is not at all included. Both processes need better treatment in the global estimates and should be objectives of future work.

- Coupling mass balance with glacier geometry changes (glacier dynamics)

Scaling relationships between glacier volume, area and length [*Bahr et al.*, 1997], when coupled with the mass continuity equation, provide sufficient first approximation of interrelated changes in glacier geometry and surface mass balance in glacier volume projections (Chapters 4 and 5). Comparison of ice flow modeling vs. scaling methods for six glaciers (Chapter 5) shows that the scaling methods mostly underestimate the volume losses predicted by the ice flow model, up to 47% for volume-area scaling and up to 18% for volume-length scaling. Applying these results with 'back-on-the-envelope calculation' for global volume projections of 0.15 m sea level equivalent (Chapter 2) gives uncertainty of ~0.05 m for 2001-2100. Sensitivity to the scaling exponents in the volume-area and volume-length relationship is shown to be low in volume evolutions of numerically generated synthetic glaciers (Chapter 4) and six mountain glaciers (Chapter 5). Sensitivity to the scaling constant in global volume changes could not be adequately quantified due to undersampling (Chapter 2). However, when normalized by initial volume, volume evolutions of six mountain glaciers are relatively insensitive to the choice of scaling constants (Chapter 5). Nevertheless, more glaciers need to be analyzed to ascertain these results, especially considering that our six study glaciers are rather small, and, hence not a representative sample of the mountain glaciers and ice caps that are the major contributors to sea level. Ideally, as a long term goal, instead of using scaling or other methods which approximate glacier dynamics one should turn to coupling the mass balance model with an ice flow model for each glacier. This goal depends o availability of glacier inventory and digital elevation model data.

- Spatial extrapolation of volume projections

In the absence of complete world glacier inventory the estimates on total area, volume and number of mountain glaciers and ice caps are derived from assumed regional glacier size distributions, based on percolation theory [*Meier and Bahr*, 1996], and a scaling relationship between individual glacier volume and area [*Bahr et al.*, 1997]. I upscaled the projected volume changes of a small number of glaciers with known area to the total volume changes in the region (Chapter 2). This is done by assuming that the mean volume change in the size bin of each regional distribution is the representative volume change in the size bin (Chapter 2). However, this choice of upscaling method has many degrees of freedom, meaning that any alternative assumption can derive global volume projections to differ by up to ~0.1 m sea level equivalent for 2001-2100. This reflects the complexity in upscaling volume changes (spatial extrapolation of volume projections) due to nonlinearity of the glacier response to climate forcing and sensitivity to climate scenarios in each region.

- Conversion of global volume changes to sea level changes

Total volume changes of all mountain glaciers and ice caps are converted to sea level equivalents (glacier volume change divided by current ocean area of 362×10^6 km^2), thus it is assumed that all melt finds its way directly into the oceans. The uncertainty due to this assumption can not be quantified and requires better understanding of processes driving glacier runoff to the ocean and incorporating them into land surface models. However, this stage is still under development.

6.1 References

Bahr, D. B., M. F. Meier and S. D. Peckham (1997), The physical basis of glacier volume-area scaling, *J. Geophys. Res., 102*, 20355-20362.

Hock, R., V. Radić, M. de Woul (2007), Climate sensitivity of Storglaciären – An intercomparison of mass balance models using ERA-40 reanalysis and regional climate model data, *Ann. Glaciol., 46,* 342-348.

IPCC (2007), Climate Change 2007: The Physical Science Basis. Contribution of working Group I to the Fourth Assessment Report of the Intergovernmental Panel on Climate Change [Solomon, S. and 7 others, (eds.)], Cambridge University Press, Cambridge, UK, 996 pp.

Meier, M. F. and D. B. Bahr (1996), Counting glaciers: use of scaling methods to estimate the number and size distribution of the glaciers in the world, *CRREL Special Report,* 96-27, U.S. Army, Hanover, New Hampshire.

Smith, R. B., and I. Barstad (2004), A linear theory of orographic precipitation, *J. Atmos. Sci.*, *61*, 1377-1391.